Alejandro Garcés Ruiz

Design, Operation and Control of Series-Connected Power Converters for Offshore Wind Parks

NTNU – Trondheim
Norwegian University of
Science and Technology

Acknowledgments

M^Y fist debt of thanks goes to my supervisor Professor Marta Molinas at the Department of Electric Power Systems Engineering at Norwegian University of Science and Technology. Her support in technical aspects as well as her assistance in writing reports have added considerably to my research experience.

I would also thank to Professor Jun-itchi Itoh from Nagaoka University of Technology in Japan, for allowing a short stay in his laboratory where I learnt about experimental work with matrix converters.

I am also grateful to Professor Pedro Rodriguez and his research team from Polytechnic University of Catalunya in Spain for inviting to his laboratory where I tested some of my ideas about reactive power compensation and active filtering.

Special thanks to all my friends at the Department of Electric Power Engineering for their assistance and support. Often casual technical discussions became in enlightening solutions to some of my problems in simulations and experiments.

I would also like to thanks Stewart Clark at the Norwegian University of Science and Technology for editing this thesis.

Abstract

O FFSHORE wind farms need to develop technologies that fulfill three main objectives: Efficiency, power density and reliability. The purpose of this thesis is to study an HVDC transmission system based on series connection of the turbines which theoretically meet these three objectives. A new topology of matrix converter operated at high frequency is proposed. This converter is studied using different modulation algorithms. Simulation and experimental results demonstrated that the converter can be operated as a current source converter with high efficiency. An optimal control based on a linear quadratic regulator is proposed to control the matrix converter as well as the converter placed on shore. Results demonstrated the high performance of this type of control and its simplicity for implementation. An stationary state study based on non-linear programming and Montecarlo simulation was carried out to determine the performance of the concept for long-term operation. Series connection is an efficient technology if and only if the differences in the effective wind velocity are small. This aspect limits the number of wind turbines that can be connected in series, since a numerous number of turbines will lead to high covariances in the distribution of the wind. A complementary study about active filter and reactive power compensation was carried out using an optimization-based algorithm.

Contents

1
Introduction

The purpose of this introductory chapter is to provide a short overview of the the thesis and present their main objectives, scope and contributions.

WIND energy is one of the key technologies to mitigate climate change and the dependency on fossil fuel in the industrialized countries. Wind turbines generate energy with zero emissions and low environmental impact. The last aspect is especially important under the new international treaties like the Kyoto Protocol and Project Europe 2030. In comparison with other energy resources, wind is one of the most environmental friendly technologies. Wind energy does not use water during operation, this is a definite advantage taking into account that even a thermal electric plants require water as working fluid. In addition, wind farms have zero emission during operation, and their impact on ecosystems is very small in comparison with a hydro power or thermal electricity.

Wind energy is a growing market with more than 159 GW installed around the world [1]. Wind farms placed on land are a common element in the landscape in countries like Germany and the Netherlands. This means that the technology and its market are mature. Nevertheless it is still an active research field. Most efforts are aimed to increase the rating and efficiency of the wind turbines and the integration with the grid. Perhaps the most important research challenges are related to the wind farms placed offshore. Although they have indeed some potential advantages over on-land wind farms, there are also many problems that must to be solved. Offshore wind farms lead to high power/energy capability but transmitting the power from offshore to land is a great challenge. AC is an efficient solution for overhead

transmission lines with distances below 100 km. For cables, this breaking point is reduced to only 40 km due to its high capacitive effect [2]. Consequently, HVDC transmission is the most cost-effective technology for offshore wind parks[3].

There are many opportunities to create innovative and customized solutions in offshore wind technology. One of these solutions is the series connection of wind turbines which is selected as the main area of study in this thesis. Consequently, power electronics and the control of the converters must be designed accordingly. Thus a high frequency link based on matrix converter is proposed for offshore turbines. The matrix converter is a technology that has demonstrated to be efficient and reliable for applications where high level of power density is required. Both reliability and power density come from not needing of electrolytic capacitors. The converter is operated at high frequency in order to reduce the size of passive elements such as transformer and filters. An HVDC transmission system based on PWM-CSC technology is proposed for integrating the wind park to the grid. Optimal control of the converters is also studied in this thesis in order to increase the efficiency and controllability of the converters.

1.1 Objectives

1.1.1 General

The main objective of the project is to investigate the concept of series connection of offshore wind farms and the operational capabilities the reduced matrix converter for wind energy application.

1.1.2 Specifics

- To identify challenges and opportunities of series connection for offshore applications.

- To develop an optimal modulation of the converter considering minimum losses.

- To apply an optimal control strategy for controlling the converters.

- To determine the operation features of series connection for long-term operation considering the stochastic behaviour of the wind and the physical constrains of the system.

- To make a prof of concept by an experimental prototype.

1.2   State of the art

In recent years, there has been an increasing interest in new DC grid configurations for offshore wind parks [4]. Some of these configurations apply similar concepts as distribution networks with radial feeders and several stages of conversion at different voltage levels [5, 6]. However, a conventional radial feeder is different than a DC offshore grid, since in the first case the voltage level is raised using conventional transformers while in the second case the voltage level is raised using power electronic converters. Each of these stages of conversion implies an increasing in the investment and operative cost due to the expensive support platforms and the high operational losses.
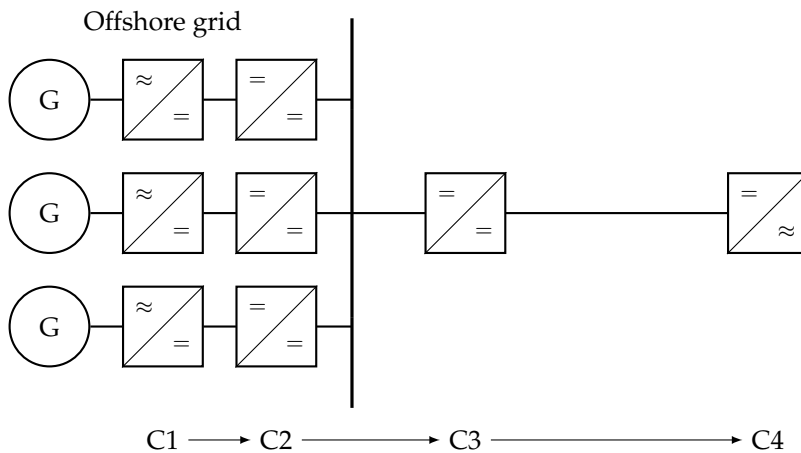
Figure 1.1: Two step-up DC grid proposed by Meyer in [7]

Figure 1.1 shows a DC grid proposed by C.Meyer in [7]. This grid topology presents four stages of conversion labeled as C1 to C4. The first stage of conversion (C1) is required for controlling the generators. The second and third stage of conversion (C2 and C3) are step-up DC/DC converters. The last stage of conversion (C4) is the on-shore converter for grid integration of the wind farm. Other two alternatives of parallel connection are achieved by eliminating the stage C2 or the stage C3. These two options are named centralized converter concept and disperse converter concept respectively. A new type of DC/DC converter with a three-phase high frequency transformer was also proposed in Meyer's work. The centralized converter concept was the most efficient solution with that type of DC/DC converter.

Another option, also studied by Meyer, is the dispersed converter concept with series connection. This topology is schematically represented in Figure 1.2. In that work it was found that series connection leads to the lowest grid losses. However, the total losses are not competitive with a DC parallel connections due to the losses in the converters. As a consequence of that, the efficiency of the converter must be

Offshore grid
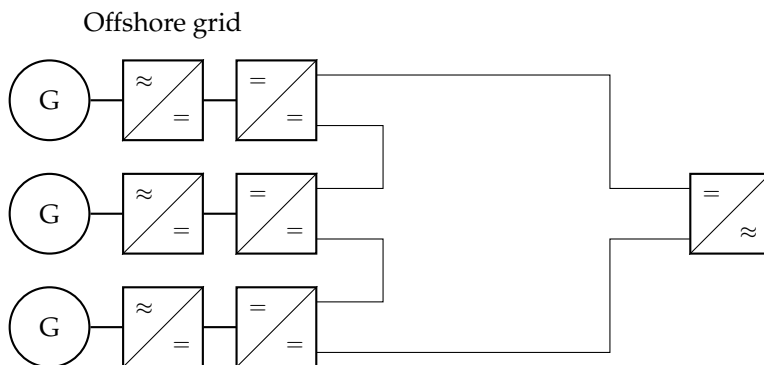
Figure 1.2: Dispersed converter concept with series connection presented in [7]

improved in order to make series connection a practical alternative.

Series connection has been also presented by S.Lunberg in [8] and by L.Max in [9]. Here, other type of DC/DC converter was investigated with the objective to increase the efficiency of the system. Other topologies of DC/DC converters have been proposed in [10].

Mogstad presented in [11] a topology based on matrix converter. The topology was developed with three stages of conversion: AC/AC - transformer - AC/DC. In that work the converter was operated as voltage source with a simple carrier based modulation. The AC/DC converter was an H-bridge and the generator an asynchronous machine. Features such as losses, control and operation of the converter were not analyzed in that work. Therefore results were not conclusive about the advantages of series connection and matrix converter for offshore applications.

From the point of view of the converter, some studies have been developed using three-phase matrix converters [12, 13, 14]. Such a converter of up to 1 MW has been reported in [15]. A three-phase matrix converter with internal high frequency transformer was presented in [16]. This type of converter is suitable for wind energy applications with AC grids. An AC-DC converter with reduced matrix converter was presented in [17] for UPS applications (Uninterrupible power system). That converter is based on voltage source operation exclusively. A topology of a matrix converter with a medium frequency transformer was applied successfully for traction applications in [18]. In [19] a topology of a reduced matrix converter with a medium/high frequency link was presented. The wind turbines are interconnected in the high frequency stage and a platform is required for supporting the AC/DC converter. Modular approaches of matrix converter have been proposed for wind energy applications [20, 21]. Matrix converters with a neutral point can also be used in wind park applications [22]. One of the most important research fields is the new topologies of matrix converters [23, 24]. Different configurations of multilevel matrix converters have been proposed [25]. In [26] a multilevel matrix converter is presented. The multilevel characteristic is achieved by using H-bridge cells as bidi-

rectional switches. Multilevel indirect matrix converters have also been proposed [27, 28, 29].

Controlling offshore wind farms is an important research problem. In [30] an offshore wind farm based on DC bus concept is presented. The control of the DC voltage during faults is one of the main problems in this type of parallel configuration. The system uses voltage source converters and is controlled by using fuzzy logic.

An HVDC system based on PWM-CSC and series connection was proposed in [31]. That work was mainly focused in the control strategy of the system. There are few works related to PWM-CSC for HVDC transmission.

1.3   Main contributions

The main contributions of this thesis are:

- Series connection: most of the studies of series connection of wind turbines used voltage source converter and DC/DC converters. Other studies presented line commutated converters. This thesis presents a new approach with a combination of a high frequency link and a pulse width modulated current source converters. Current source converters are more convenient for series connection since the shared variable is the current. The entire operation of the park changes when this type of converters are used. It requires a coordinated control in order to guarantee optimal operation. Such optimal coordinated control was also developed in this thesis [32].

- Matrix converter: a new topology of matrix converter was proposed for wind energy applications. This topology eliminates one stage of conversion in comparison with previous works presented by Meyer, Max and Lunberg. In those works the energy conversion system consists of four stages: AC/DC - DC/AC - transformer - AC/DC. By using matrix converter the two first stages are replaced by a single converter. The proposed converter is called reduced matrix converter in order to differentiate it from three-phase matrix converter and single-phase matrix converter. In the proposed topology the input is a three-phase sinusoidal waveform and the output is a single-phase square waveform. Different modulation algorithms were developed for the matrix converter. Two types of operation were studied: voltage source and current source. An optimal modulation from the point of view of the losses was implemented [33].

- Control: optimal control theory was applied in the generation system as well as in the on-land converter. Despite being a classic control theory, to the knowledge of the author, it has not been proposed before for offshore wind power applications [34].

- Stochastic analysis of series connection. A Montecarlo simulation and an optimal load flow were developed for series connection. This simulation refines the results obtained before about series connection. It was found that series connection leads to low utilization factor for high standard deviation of the wind velocities. It means series connection is an efficient alternative whenever the wind velocities are the same in all the turbines [35].

- Active filtering. Although active filtering was not an objective of this thesis, a compensation algorithm based on mathematical optimization was implemented. This algorithm is general enough to be considered in different applications[36].

1.4 Scope

The research in this thesis was developed considering two main paradigms: series connection and matrix converter. Both of them pose significant new challenges for grid integration of offshore wind farms. Of course it is impossible to solve all these challenges in just one PhD thesis. Therefore, it is focused on three main tasks:

- Optimal control and operation of the system

- Converter design

- Modulation

The general approach of the project consists on a theoretical investigation, which is complemented with an experimental prototype. Series connection is investigated from the power electronics and power systems point of view. Different types of numerical simulations are considered including time domain analysis, Montecarlo simulation and non-linear optimization. The experimental set-up is presented as prof of concept of the modulation strategy. Losses are also investigated by using numerical simulations. Designing the high frequency transformer as well as the isolation coordination of the entire park was left for future investigations.

1.5 Research results

The first analysis of losses of the proposed topology was presented in [37]. In that stage of the research the topology of the converter and its modulation was the same presented by Mosgtad in [38]. After that, different topologies of high frequency links with asynchronous generators were investigated [39]. The asynchronous generator was controlled using flux oriented theory and classic PI controllers. A modified

space vector modulation for the reduced matrix converter was proposed in [40]. Carrier based modulation and space vector modulation were compared according to the total losses without considering the clamp circuit or the leakage inductance of the high frequency transformer.

In all the aforementioned cases, the converter was operated as a voltage source converter. However, series connection requires converters operated as current source because the current is the shared variable in the circuit. Therefore, two new types of modulation were developed for current source operation [41]. A comparison between voltage source and current source operation was presented in [42, 43]. Some details about the commutation process and the influence of the parasitic capacitances of the transformer were presented in [44]. The complete comparison of modulation strategies was summarized in [33].

The asynchronous machine was replaced by a permanent magnet synchronous generator. The reason behind this decision was the power density and efficiency of the entire system. A full bridge diode rectifier is enough for AC to DC conversion since the machine does not require to be magnetized.

The optimal control of each converter as well as the coordinated control of the entire wind park were the next challenge [45]. Controlling the machine as well as the on-land converter posse big challenges for current source converters which cannot be performed by classic PI controllers. Therefore, an optimal linear regulator control was designed [34]. Optimal control strategies are not common in power electronic applications. In this thesis it is demonstrated its advantages. The operation of the entire park was studied taking into account the stochastic model of the wind [32]. An optimization algorithm based on non-linear programming is used in conjunction with a Montecarlo simulation [46]. This studied demonstrated some possible disadvantages of the series connection whether the differences in the wind velocity are high.

On the other hand, a work about reactive power compensation using mathematical optimization was also developed during the investigation [47, 36]. An active filter can be placed in the on-land converter in order to reduce the harmonic contents. Since this work was not directly connected with the main objectives of the thesis, it is presented as an appendix.

Other applications of matrix converter and PWM-CSC were studied although they were not into the main objectives of the thesis. Series connection with the proposed conversion system were studied in [48] for wave energy applications. An electronic transformer based in matrix converter for smart grids applications was proposed in [49]. In addition, a series connection of wind turbines for small power applications was presented in [50]. The results for this application are particularly promising since isolation is not a concern in such a low power applications.

1.5.1 List of publications

The publications results of this project are:

Journal papers:

- A. Garces, M. Molinas. "A Study of Efficiency in a Reduced Matrix Converter for Offshore Wind Farms". *IEEE Transaction on Industrial Electronics*. vol 59 N 1. Jan 2012. ISSN 0278-0046. Reference [33]

- A. Garces, M. Molinas. "Coordinated Control of Series Connected Offshore Wind Park based on Matrix Converters". *Wind Energy*. Wiley. DOI: 10.1002-we.507. Reference [32]

- A. Garces, M. Molinas, P. Rodriguez. "A Generalized Compensation Theory for Active Filters based on Mathematical Optimization in ABC Frame". Electric Power Systems Research. Vol 90-1012. Elsevier. Reference [36].

- A. Garces, M. Molinas. "Optimal Control for PWM-CSC based HVDC with Series Connected Offshore Wind Turbines". Submitted to IEEE Transaction on Industrial Electronics. Reference [34].

- R. Torres, A. Garces, M. Molinas, T. Underland. "Hybrid HVDC Based on PWM Current-Sourced Converter and Line-Commutated Converter for Offshore Wind Farm Integration". *Submitted to IEEE Transactions on Industrial Electronics*.

Full papers in conferences with oral presentation:

- A. Garces, M. Molinas. "Electrical Conversion System for Offshore Wind Turbines based on High Frequency AC link". *Proc of IX International Conference and Exhibition of Renewal Energy and Ecological Vehicles EVER2009*. Monaco, Monaco. March 2009. Reference [37].

- A. Garces, M. Molinas. "Cluster Interconnection of Offshore Wind Farms Using a Direct High Frequency Link". *Proc of 8th International Workshop on Large-Scale Integration of Wind Power into Power Systems as well as on Transmission Networks for Offshore Wind Farms*. Bremen, Germany. October 2009. Reference [39]

- A. Garces, M. Molinas. "Comparative Investigation of Losses in a Reduced Matrix Converter for Offshore Wind Turbines". *5th IET International Conference on Power Electronics, Machines and Drives (PEMD 2010). IET conference publications*. Brihton, UK. 2010. Reference [40]

- A. Garces, M. Molinas. "High Frequency Wind Energy Conversion from the Ocean". *Proc. of IEEE International Power Electronics Conference ECCE ASIE IPEC 2010*. Sapporo, Japan. 2010. Reference [44]

- A. Garces, M. Molinas. "Impact of Operation Principle on the Losses of a Reduced Matrix Converter for Offshore Wind Parks". *Proc. of IEEE International Symposium on Industrial Electronics ISIE 2010*. Bari, Italy. 2010. Reference [42]

- M. Roed, A. Garces, M. Molinas. "Operation Features of a Reduced Matrix Converter for Offshore Wind Power". *Proc. of IEEE International Symposium on Industrial Electronics ISIE 2010*. Bari, Italy. 2010. Reference [43]

- A. Garces, M. Molinas. "Reduced Matrix Converter Operated as Current Source Converter for Offshore Wind Farms". *Proc. of 14th International Power Electronics and Motion Control Conference*. Ohrid, Macedonia. 2010. Reference [41].

- A. Garces, E. Tedechi, M. Molinas. "Power Collection Array for Improved Wave Farm Output Based on Reduced Matrix Converters". *Proc. of IEEE 12th Workshop on Control and Modeling for Power Electronics (COMPEL)*. USA. 2010. Reference [48]

- A. Garces, M. Molinas. "Optimal Control of a Reduced Matrix Converter for Offshore Wind Parks". *Proc. of Powertech 2011*. Trondheim, Norway. 2011. Reference [45].

- A. Garces, M. Molinas. "A Flexible and Optimal Power Theory for Reactive Power Compensation in ABC Frame". *Proc. of Powertech 2011*. Trondheim, Norway. 2011. Reference [47]

- A. Garces, M. Molinas. "A Control Strategy for Series Connected Offshore Wind Turbines". *Proc. of 9th IEEE International Conference on Power Electronics and Drives Systems*. Singapour. 2011. Reference [51]

- R. Torres, A. Garces, M. Molinas, T. Underland. "Hybrid HVDC Based on PWM Current-Sourced Converter and Line-Commutated Converter for Offshore Wind Farm Integration". *Proc. of IEEE Asia-Pacific Power and Energy Engineering Conference APPEEC2012*. Shanghai, China. 2012. Reference [52]

- S. Sanchez, A. Garces, M. Molinas. "A Current-Coupled Topology for Grid Integration of Wind Turbines in Micro-Grids" *Proc of. IEEE Power and Energy Society Transmission and Distribution Conference and Exposition*. Orlando-Florida. USA. 2012. Reference [50].

- A. Garces, A. Trejos. "A voltage regulator based on matrix converter for smart grid applications". *Proc of. IEEE PES Conference on Innovative Smart Grid Technologies (ISGT Latin America)*. Medellin Colombia, Oct 2011. Reference [49].

- A. Garces, M. Molinas. "Optimal operation of series connected turbines for offshore wind parks". *Proc of. IEEE 12th conference on probabilistic methods applied to power systems PMAPS*. Istanbul, Turkey 2012. Reference [35].

- A. Garces, M. Molinas. "Modulation Features of a high-frequency conversion system for wind farm applications". *Proc of IEEE 3rd international symposium on power electronics for distributed generation systems.* Denmark Jun 2012.

- A. Rodrigez, E. Bueno, F. Rodriguez, A. Garces, M. Molinas. "Analysis and performance comparison of different power conditioning systems for SMES-based energy systems in wind turbines". *Proc of IEEE 3rd international symposium on power electronics for distributed generation systems.* Denmark Jun 2012.

Book chapters:

- A. Garces. et all "Power system issues for wave energy". *Submitted to IET*.

Poster presentations.

- A. Garces. M. Molinas. "Reduced Matrix Converter for Offshore Wind Farm Applications". *Poster presentation in Wind Power R&D Seminar Deep Sea and Wind. 2010* Trondheim. 2010.

- S.Sanchez, A. Garces, M. Molinas. "A Current-Coupled Topology for Grid Integration of Wind Turbines in Micro-Grids". *Poster presentation in NTNU-India Week. Trondheim 2011.*

- A. Garces, M. Molinas. "Series Connection of Offshore Wind Turbines". *Poster presentation in Wind Power R&D seminar deep Sea and Wind. 2011* Trondheim. 2011.

1.6   Layout of the thesis

The thesis is organized as follow:

In Chapter 2 a discussion about the advantages and challenges of series connection is presented. Each element of the system is briefly described. The mathematical model of the elements is also presented.

In Chapter 3 the proposed high frequency link is studied in detail. Different modulation strategies are studied and compared from the total losses point of view. Details of the converter such as protection, semiconductor devices and the topology itself are presented in this chapter.

Chapter 4 studies the optimal control strategy for both the high frequency link and the PWM-CSC placed on-land. Since both type of converters have similar models, the general conclusion of one can be applied to other other. A linear quadratic regulator is used in the inner loop of the matrix converter as well as the PWM-CSC.

Chapter 5 presents some details about the operation of the entire park. An optimal power flow based on a non-linear programming method is presented. Long

term studies based on Montecarlo simulation show some limitations of series connection when the number of series connected turbines is big and the wind velocities are not homogeneous between turbines.

Chapter 6 presents conclusions and future research needs.

Three appendixes complements the thesis. Appendix A summarize the main results from the investigation about non-active power compensation. However an active filter can be placed in any part of the park to reduce the harmonic distortion, this research is more general and can be applied to any grid. This work is not connected directly with the other chapter of the thesis.

Appendix B describes the parameters used in the simulations as well as in the experimental set-up.

Finnally, Appendix C presents the models for the wind in short and long term simulations. The short term model was used for dynamic simulations while the long term model was used for the Montecarlo simulation.

2

Overview of the Concept

This chapter presents a discussion about the advantages and challenges of series connection from the system point of view. A theoretical analysis is presented which demonstrates that series connection not only prevents the need for offshore platforms but also increases the efficiency of the offshore grid. Each element of the proposed system as well as its mathematical model are briefly described.

HIGH voltage direct current transmission (HVDC) is required in deep sea offshore wind farms. The wind turbines offshore can be integrated by either an AC or a DC grid. Efficiency and investment cost could be reduced by using offshore DC grids and in particular series connected DC grid. However, this approach poses a paradigm shift. Power systems have been for years designed and operated in a parallel AC network and a great amount of knowledge has been achieved in this type of grids. Many technological challenges must overcame for making series connection and DC grids a feasible solutions.

Designing efficient and light converters is one of this challenges. Converters in a DC grid do not imply increased investment cost, since they are also required in AC offshore grids. An AC/DC converter is required for the HVDC transmission, but converters are also required in each generator to operate at variable speed in order obtain maximum energy extraction from the wind.

Double fed induction generators are the most common alternative for wind farms in AC grids. The reason behind that is the reduction of size of the con-

verter. A converter with only 30 % of the nominal power of the generator is required in double fed induction generators. However, in DC grids this is not an advantage since another full converter is required for grid integration. Therefore, squirrel cage induction generators or permanent magnet synchronous generators are the most suitable technology. The selection of the type of generator will be discussed later in this chapter. The model of each element in the conversion chain will be also part of the discussion in this chapter, as well as the type of DC grid topologies.

2.1 Offshore wind facilities

Offshore wind farms have demonstrated advantages over conventional land-based wind facilities to meet the increasing electricity demand in a sustainable way. Some of the advantages of offshore wind energy are [53]:

- Less visual and auditory contamination. One of the most frequent complains from people who live close to any wind farm, is the visual impact of the turbines and the noise generated by them. Wind farms could therefore affect the natural and cultural landscape which is one of the most complex problems from the social point of view. It seems clear that off-shore wind farms are a solution to this problem since the distance of the turbines to shore is long enough to the cities.

- Reduced user conflicts. When a wind farm is built, surrounding land must used in order to locate the turbines, substations and transmission lines. Off-shore wind farms will reduce ostensibly these costs.

- More power capacity [54]. Mountains and elements such as trees and buildings create turbulence that have effect on the wind velocity. Therefore, wind velocities offshore are higher and more constant than wind velocities on land.

- Short distances to high density energy demand. Large urban agglomerations have a high density demand for energy in the centres of cities which in many cases are on the shore. Due to the large area occupied by the city itself, on-land wind farms must be placed far away from the centre. Therefore, even if the distance from the offshore wind turbine is high, will often be less than the distance to places where it is possible to install an on-land wind farm.

- Opportunity for new and customized technologies. Each large challenge is in fact an opportunity for new technologies such as innovative designs of power electronic converters as well as grid topologies and control strategies.

- Large wind turbines. On-land wind turbines have a limited rating not only because the technology itself but also because of the constraints related to airplane routes and visual impact. Therefore, offshore wind farms are more suitable places for wind turbines with high power ratings.

- Shorter distances between turbines. Wind turbines must be placed considering the possible interference between turbines and the mountains. This interference creates air turbulences which decrease the usable energy. In some land-based settings, this requires turbines to be separated by as much as 10 rotor diameters from each other. In offshore wind farms this distance can be shortened to as little as four diameters.

Despite of its clear advantages, offshore wind energy has many challenges. One of the most important of them is the transmission of the power from offshore to the main grid. The higher the distance to shore, the better the wind conditions. Therefore, long distances are expected in offshore wind facilities. The most efficient alternative for such long distances is HVDC transmission. Moreover, the offshore grid must be optimized. A DC grid is therefore seen as a suitable option since each turbine must have a power electronic converter anyway. These converters are used to control the rotational speed of the machine in order to obtain maximum power extraction from the wind.

In any electric grid, the transmitted power is given by a product between the voltage and the current and the transmission losses are given by resistance times the square of the current. It is obvious that the higher the voltage is the lower the transmission losses are. However, generators and loads have limited voltage ratings. Therefore, several stages of convention are required in order to increase the generated voltage. These stages of conversion are done by transformers in AC grids or DC/DC converters in DC grids. The DC/DC converters are increasing their efficiency in order to become a competitive technology. Transformers are perhaps the most efficient of the electric machines and even a DC/DC converter for power applications require a transformer inside.

2.2 Requirements of offshore wind farms

Offshore wind farms have to deal with new challenges which must be faced to make them a feasible alternative:

- Size and weight reduction: increasing the power density is an important objective since each component placed offshore represents high investment and operative costs. The fist phase of cost is due to the construction of platforms to support the electric components while the second is related to maintenance because of the transportation of spare parts from shore.

- Efficiency: long distances are expected in offshore wind farms since, as was outlined above, the longer the distance from shore, the higher and more constant the generated power is. Therefore, losses must be minimized not only in the converters but also in the transmission lines.

- Reliability: Maintenance and replacement of components represent high transport costs. Accordingly, the reliability of the components themselves must be optimized.
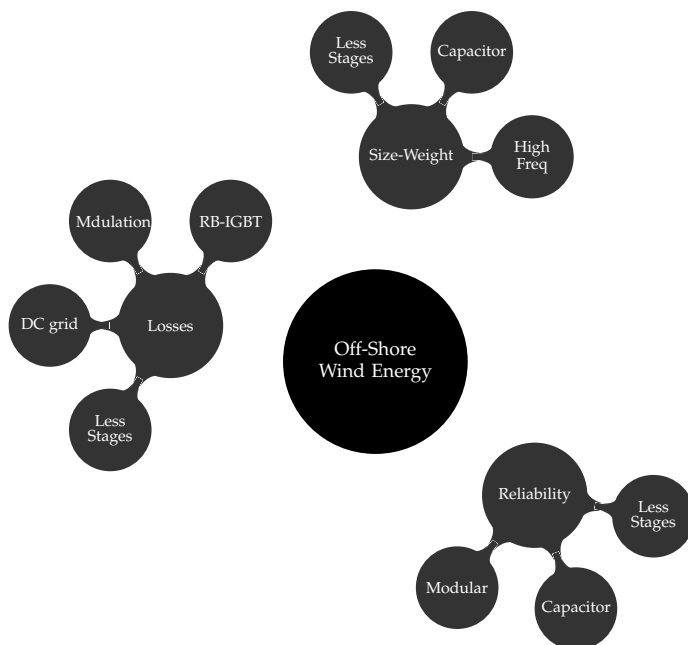
Figure 2.1: Mind map of the three main objectives for offshore grids

These three aspects are shown schematically in Figure 2.1 and are linked to investment and operational cost. Each of these aspects are related to a solution strategy. A solution with high power density means a reduction in the size and weight of equipment and therefore a reduction in investment cost. Losses reduction can be achieved with new semiconductor technologies such as reverse blocking insulated gate bipolar transistors (RB-IGBT), with optimal modulation and control of the converters, and with an optimal design of the DC grid. On the other hand, size and weight can be optimized using high switching frequencies, eliminating bulky elements such as electrolytic capacitors and using topologies with less stages of conversion. Finally, reliability can be improved by eliminating elements and by using modular approaches with less stages of conversion as will be showed later in this chapter.

Series connection of wind turbines in conjunction with an efficient topology of converters are a potential solution for all these challenges. Parallel DC grids require intermediate step-up DC/DC convention in order to achieve the high voltage required for efficient transmission. These DC/DC converters usually include bulky step-up transformers. In the proposed DC grids the high voltage required for HVDC transmission is achieved by connecting the wind turbines in series. Therefore, in-

termediate step-up transformer is not required. As consequence of that, expensive support platforms are not required either. The current of the offshore grid is the same current of the transmission line reducing the total losses.

Another consequence of the series connection is the control strategy. The current must be controlled in order to maintain the system stable. This control could be performed by the offshore wind turbines or by the on-land converter. The first option would require drop controls and could reduce the efficiency of the entire system. The second option is therefore easier and more efficient. For that reason, a current source converter must be placed on-land. A pulse-width-modulated current source converter (PWM-CSC) arises as the most convenient solution although a line commutated converter is also a possible alternative. Line commutated converters are erroneously called current source converters. However, a line commutated converter does not have full control of the current in the three-phase side. Therefore, the term current source converter should be reserved for PWM-CSC. However this technology is as old as the voltage source converters, it is not used for HVDC applications. There is a knowledge barrier between voltage source converters and current sources converters rather than a technological barrier. As will be discussed in the Chapter 4, PWM-CSC has some advantages from the control point of view.

2.3 Offshore grid: AC vs DC topology
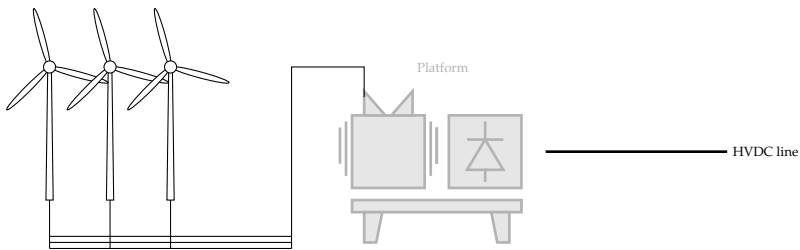
Figure 2.2: Schematic representation of an offshore wind farm with an AC grid

An offshore AC grid is depicted in Figure 2.2. In this concept, the offshore turbines are connected in a conventional three-phase grid which in turns is connected to the HVDC transmission system. Usually, this type of grid is designed with radial suppliers similar to radial feeders in a distribution system. All operative offshore wind farms installed in the world have been built with an AC offshore grid [55]. The reason behind that is the accumulated knowledge about this technology. AC is a well known and reliable technology. However, a DC grid could be a more efficient solution since it increases the utilization of cables offshore [7, 56]. In AC systems with ideal sinusoidal waveforms, cables must carry both active and reactive power. Needless to say transmission operators are mainly interested in the active power which is the one that produces useful work. Reactive power is a flowing power that

appears because of an energetic interchange between electric and magnetic fields in each one of the phases of a three-phase system. Consequently a DC grid is potentially more efficient from the transmission point of view. Power electronic converters are required in both AC and DC grids for controlling the rotational speed and achieve maximum power extraction from the wind.

2.4 Series vs parallel DC grid

In order to transmit power from offshore to land, it is required to increase the voltage level to reduce the current and therefore the transmission losses. This can be done in two ways: using a step-up transformer or by connecting the wind turbines in series. The first alternative implies parallel connection, as shown in Figure 2.3.
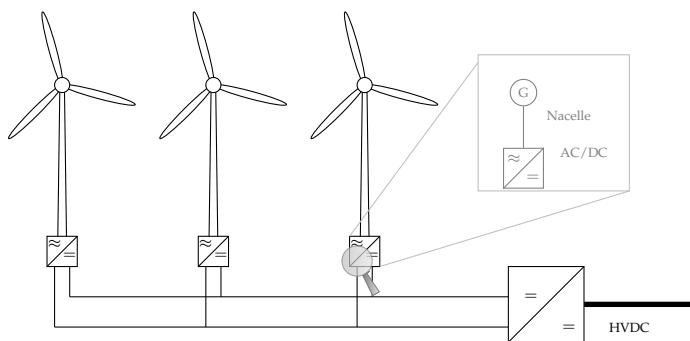
Figure 2.3: Schematic representation of an offshore wind farm with parallel DC grid

The concept is very similar to conventional approaches. The wind turbines are connected in radial suppliers which in turn are connected to a centralized DC/DC converter. An offshore platform is required to support this converter. Most of the designs of DC/DC converters for power systems applications require an internal step-up transformer [7, 9]. To increase the power density in this type of converters is perhaps the most important challenge for this topology.

The second alternative is depicted in Figure 2.4. This grid topology can achieve a high voltage level, suitable for power transmission, without using a step-up transformer or any additional converter. A support platform is not not required. Therefore, investment cost are significantly reduced. In addition, series connection reduces the transmission losses in the offshore grid.

To understand the loss reduction in series connection, let us assume an ideal offshore grid composed of N turbines at the same distance. For parallel operation, with all turbines at nominal voltage and power, the grid losses are given by Equation 2.1
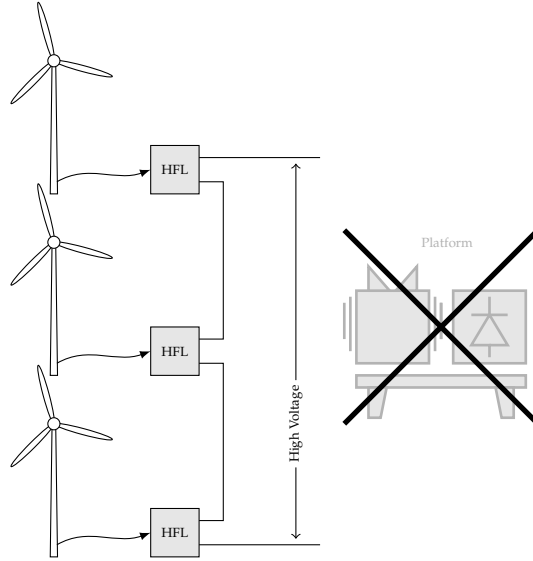
Figure 2.4: Schematic representation of an offshore wind farm with a series grid

$$P_{L(parallel)} = \sum_{k=1}^{N} R_{parallel} \cdot \left(k \cdot \frac{P_{nom}}{V_{nom}} \right)^2 \qquad (2.1)$$

where $R_{parallel}$ is the resistance in one fragment of the conductor, and P_{nom}, V_{nom} are the nominal power and voltage of each turbine. The index k represents the number of the turbine in the sequence starting from the farthest position respect to the centralized platform.

For series connection, the current in each fragment of the supplier is the same and the total losses are given by Equation 2.2.

$$P_{L(series)} = \sum_{k=1}^{N} R_{series} \cdot \left(\frac{P_{nom}}{V_{nom}} \right)^2 \qquad (2.2)$$

Therefore, the losses relation between series and parallel connection is function of the number of turbines as shown in equation 2.3.

$$\frac{P_{L(parallel)}}{P_{L(series)}} = \frac{R_{parallel}}{R_{series}} \cdot \left(\frac{N^2}{3} + \frac{N}{2} + \frac{1}{6} \right) \qquad (2.3)$$

Due to the fact that parallel connection carries more current, $R_{parallel}$ is in general lower than R_{series}. However the total effect of the loss reduction increases

quadratically with the number of series connected wind turbines. For the same type of cable, there is no doubt that series connection reduces the transmission losses. For different types of cables, series connection reduces the transmission losses as the number of series connected turbines increases.
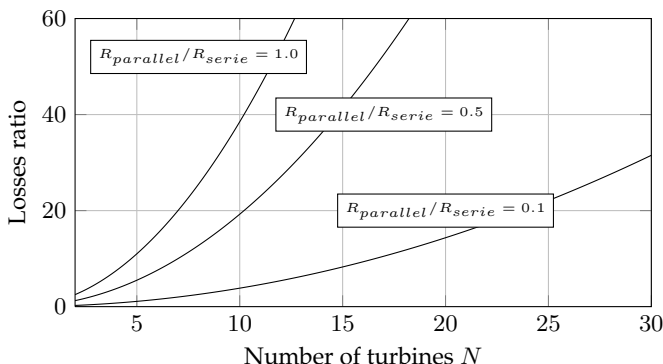
Figure 2.5: Losses ratio between series and parallel connection for different resistance ratio and different number of turbines

Figure 2.5 illustrates the losses ratio in per-unit for different values of resistance and different number of turbines. Notice the fast growth in the power ratio even for a low resistance ratio. For example, losses in a parallel connection are almost 40 times larger than losses in a series connection, for just 30 turbines and a cable resistance that is 10 times higher. Of course this is a simplified analysis since the losses in the converters were not taken into account. More details about series connection can be found in reference [32].

2.5 Challenges of series connection

The reduction of transmission losses in the offshore grid and the elimination of expensive platform support, are the most clear advantages of series connection. However, it presents some technical challenges which need to be faced. For example, variation in the wind velocity could cause variations in the output power and therefore in the output voltage. Consequently, a wide voltage variation capability and coordinated control are required.

On the other hand, insulation in the nacelle of the turbine is a practical problem. Some authors have presented advances in this issue but it is still an open research field [57, 58, 59]. In addition common mode voltage can create undesired currents which results in additional losses. The voltage between the neutral point of each generator and earth will increase as the number of series connected wind turbines increases. Therefore, the required isolation level of each turbine will be different.

In [57] Jovcic proposes some possible solutions to the isolation problem namely:

- Insulating generator windings with respect to generator frame. In this case, each generator requires a high isolation level. It is claimed that this type of high isolation is technically possible although expensive.

- Insulating the nacelle with respect to the tower. This solution was also proposed in [58] and [59]. A portion of the tower can be constructed with an insulating material.

- An insulation transformer can be installed as in the case of low power switch-mode power supplies.

Control of the converters must guarantee a fast response and stable behaviour. Converters offshore must be designed taking into account not only efficiency but also power density. Bulky elements lead to additional operative cost related with the transportation of replacement parts. Therefore, the size and weight of converters, generators and passive elements must be reduced. For that reason, a high frequency link is proposed in this thesis. High frequency reduces the size and weight of passive elements such as transformers and passive filters. This issue will be briefly discussed in next section and will be explained in detail in next chapter.

2.6 The proposed high frequency link

In general, offshore wind turbines require efficient and light power electronic converters. For the case of series connection, a new conversion system is required. The proposed high frequency link is shown in Figure 2.6. It consists on a reduced matrix converter (RMC) which transforms the three-phase voltages and currents in a square wave, high frequency single phase output. A high frequency transformer is used for galvanic isolation and to raise the output voltage. Finally a full-bridge diode rectifier is used as an AC/DC converter to connect the conversion system with the output DC grid. Other topologies of high frequency link are possible. A complete study of these alternatives was presented in [39].

A permanent-magnet synchronous machine is used as a generator in the proposed conversion system. The reason behind this is the high efficiency and power density of the permanent-magnet synchronous generators and their relation with the proposed high frequency link. A permanent magnet machine does not require initial magnetization. Therefore, the AC/DC converter in the high frequency link can be a full-bridge diode rectifier. High frequency is used in order to reduce the size and weight of the inductive elements like the transformer and filters. In addition, this will improve the controllability of the generator since it reduces the delay time of the control. The generator is controlled by the RMC which transforms three-phase sinusoidal voltage/current wave form to a square - high frequency voltage/current
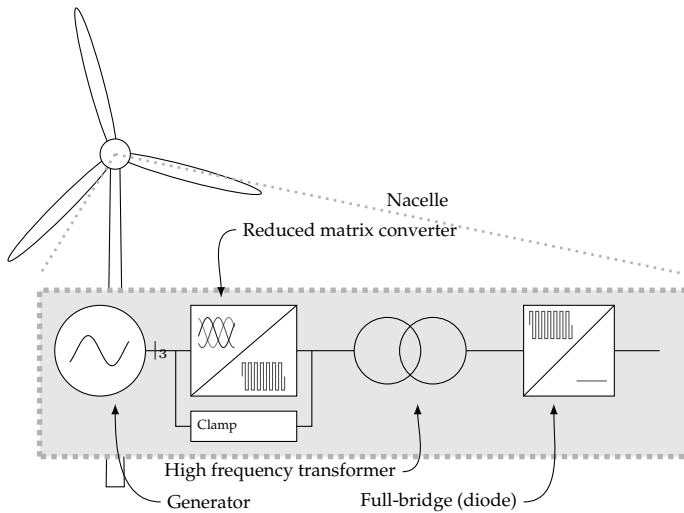
Figure 2.6: Proposed high frequency link based on reduced matrix converter

wave form. The modulation of this converter and details such as the protection scheme will be presented in next chapter. The high frequency transformer is used for isolation purposes and can be designed to raise the voltage level to reduce transmission losses.

2.6.1   High frequency transformer

A single-phase high frequency high power transformer is suggested both for galvanic isolation and to raise the output voltage. Instantaneous power in single-phase transformers oscillates when it comes to a sinusoidal wave form. However, this transformer is operated with a square wave waveform. Therefore, the instantaneous power is constant since it comes from a three-phase balanced voltage source.

It is well known that the volume and weight of a transformer decreases as the operative frequency increases. However, a small size makes the cooling of the electrical parts difficult [60, 61]. Losses in a transformer consist mainly of copper and core losses. At high frequency, copper losses are strongly dependent on the leakage flux and are mainly due to eddy current effect in the conductors, i.e. skin and proximity effects. Core losses change according to the material, the operative frequency, flux density and waveform; Steinmetz is used to calculate core losses:

$$P_{core} = K_{wf} \cdot K_{mt} \cdot f^{\alpha} \cdot B^{\beta} \cdot V_g \tag{2.4}$$

where K_{wf} is a factor which depends on the voltage wave form, K_{mt},α and β

are constant that depend on the core material, f is the frequency, B is the flux and V_g is the volume of the core. Notice that after the converter and transformer have been designed, the frequency, material and volume are all fixed values. Therefore, for operative studies core losses can be modelled as a resistance in the conventional model of the transformer. The same can be said for windings losses.

Unlike a standard transformer, a high frequency transformer must be optimized for the particular operation and waveform. The waveform has an influence on the constant K_{wf} which is related with core losses. The use of new materials is a key factor to improve efficiency [62, 63]. Some investigations have demonstrated that it is possible to build such a high frequency transformer for high power ratings [64]. For example, in [65] a nanocrystalline high frequency transformer of 2.8 [MVA] has been reported.

In [66] it was demonstrated that a three-phase transformer has little benefit in power density compared to a single-phase transformer. Therefore, a single phase topology is plenty justified. Designing of the transformer is beyond the objectives of this thesis. Interested readers are referred to [7] and [67] for designing of three-phase high frequency transformers, [9] for a similar concept in single phase transformers and [68] for a complete analysis about the use of nanocrystalline materials.

2.6.2 Permanent magnet synchronous generator

A permanent magnet synchronous machine (PMSG) is used as the generator. This type of generator has many advantages for wind power applications for small and high power levels [69, 70]. According to [13] it presents advantages such as:

- Flexibility in design allows for smaller and lighter designs.

- Lower maintenance cost and operating costs, bearings last longer.

- No significant losses generated in the rotor.

- In comparison to an asynchronous generator, a PMSG does not consume reactive power. Therefore, the power electronic converter does not require bidirectional power capability.

These advantages fit with the main objectives initially presented for offshore wind farms. In addition, this machine does not require a gear box if it is designed appropriately with high number of poles, and a soft start can be achieved due to the magnetization provided by the permanent magnets.

2.6.3 The wind turbine

A simplified model that shows the relation between wind velocity, generated power and rotational speed is described in Equation 2.5.

$$P_m = \frac{1}{2} \cdot \rho \cdot C_p(\lambda, \beta) \cdot A_\omega \cdot V_\omega^3 \qquad (2.5)$$

where P_m is the output mechanical power, A_ω is the rotor swept area and V_ω is the wind velocity. C_p is the power coefficient which depends on the tip speed ratio λ and the blade pitch angle β. The tip speed ratio is defined as shown in Equation 2.6.

$$\lambda = \frac{\omega_m}{V_w} \cdot \left(\frac{\Phi}{2} \right) \qquad (2.6)$$

According to [71] a general numerical approximation for the power coefficient C_p can be used since there are only small differences between commercial wind turbines. This approximation is given by Equation 2.7.

$$C_p(\lambda, \beta) = 0.5 \left(\frac{116}{\lambda_i} - 0.4\beta - 5 \right) \cdot e^{\frac{-21}{\lambda_i}} + 0.01 \cdot \lambda \qquad (2.7)$$

with

$$\lambda_i = \frac{1}{\frac{1}{\lambda + 0.08 \cdot \beta} - \frac{0.035}{\beta^3 + 1}} \qquad (2.8)$$

In order to analyze the operation of the wind turbine, let us re-define Equation 2.5 in per unit representation:

$$P_{m(pu)} = C_{p(pu)} \cdot V_{\omega(pu)}^3 \qquad (2.9)$$

where $P_{m(BASE)}$ is the nominal power generated by the wind turbine at nominal wind velocity $V_{\omega(BASE)}$. At nominal conditions, $C_{p(pu)} = 1$ and hence the available power only depends on the wind velocity V_w. However, the power coefficient $C_{p(pu)}$ changes for other wind velocities due to the control actions over the pitch angle and the rotational speed. There are two main operative conditions: $V_{w(pu)} > 1$ and $V_{w(pu)} < 1$.

In the first case, the available power is higher than nominal. Therefore, the pitch angle β is controlled in order to reduce C_p and maintain the generated power in

1 pu. Figure 2.7 illustrates the performance coefficient for different values of pitch angle and tip speed ratio. The higher the pitch angle the lower the performance coefficient. In general, the maximum rate of change in the pitch angle (β) is low ($\approx 8^o/s$). Therefore, the pitch angle can be considered as a constant for the speed control.
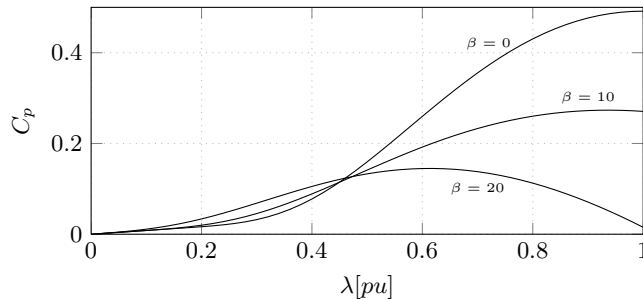
Figure 2.7: Performance coefficient vs tip ratio for different values of β ($\lambda_{opt} = 1[pu]$)

In the second case (low wind velocity) the available power is less than nominal. Therefore, the value of C_p must be as high as possible in order to obtain maximum extraction of power from the wind. This condition is shown in Figure 2.7 for $\beta = 0$ and $\lambda_{pu} = 1$. The rotational speed is controlled by the converter in order to maintain $\lambda = \lambda_{opt}$. Therefore, in per unit representation rotational speed is directly proportional to the wind velocity ($\omega_{m(pu)} = V_{w(pu)}$).

For higher wind velocities the power is maintained constant in its nominal value. However, in series connection this point is not always feasible and sometimes the power must be set on a smaller value to avoid over-voltages in some turbines and under-voltages in the others. This problem will be treated in detail in Chapter 5. In addition, there are two operative limits (cut-in and cut-out) given by the wind velocity. The cut-in velocity is the minimum wind velocity at which the wind turbine generates usable power while the cut-out velocity is the maximum feasible wind velocity.

2.7 Modular approach

The proposed conversion topology can be implemented as a modular solution using multiple generators per turbine. This approach is schematically represented in Figure 2.8. The conceptual presentation of this type of configuration has been studied in [72] from the mechanical point of view. This kind of drive-train presents some advantages over the conventional configurations, such as the increase of reliability and efficiency as well as the reduction of gear box mass.

Maintenance can be done without disconnecting the turbine. Just the gener-

35
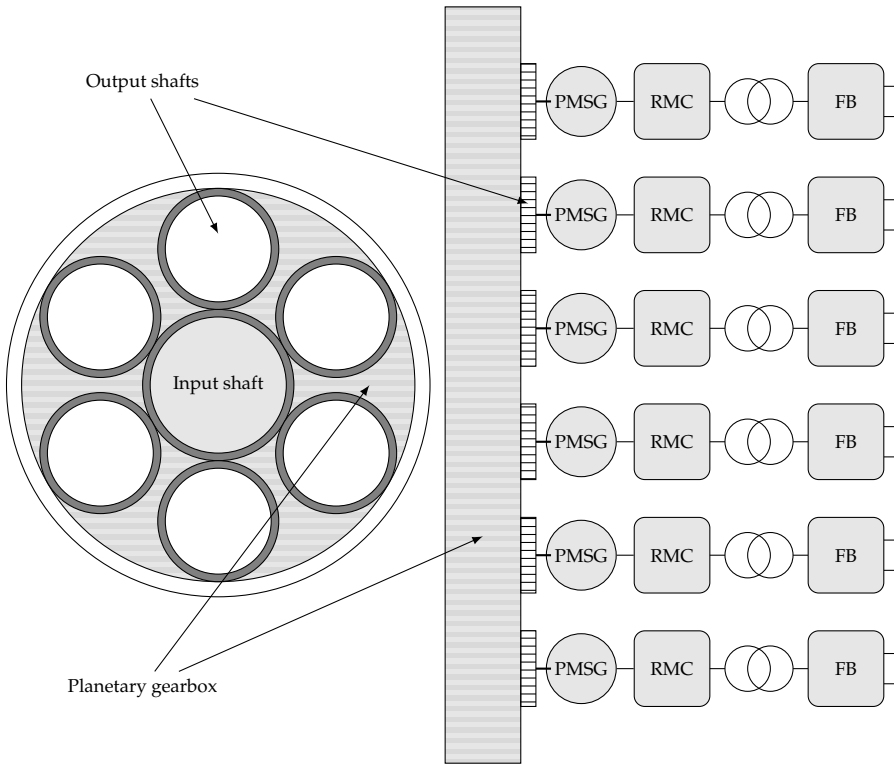
Figure 2.8: Possible modular approach with multiple drive-train

ator/converter under maintenance needs to be disconnected. Modular approach does not increase the complexity of the speed control, since all the generators in one turbine operate at the same speed. In case of short circuit in one module (for example in one high frequency transformer), the other turbines must supply a reduced power to the grid. In that case the speed of the turbine must be adjusted to this new operation point. An hybrid approach between synchronous and asynchronous generator can be used to exploit the advantages of both technologies. Interested reader are referrer to [73] for more details about this concept. Other similar concepts based on multiple generators are presented in [74] and [75]

2.8 The on shore converter

Most of the studies on HVDC and offshore wind farms have been only carried out with classic voltage source converters or line commutated converters. However, far too little attention has been paid to pulse-width modulated current source converters. This converter is shown in Fig. 2.9. It has some advantages compared to voltage
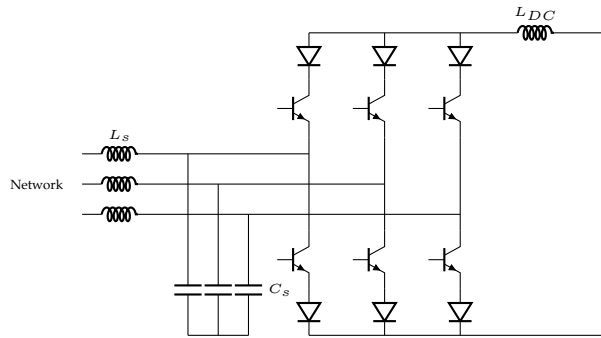
Figure 2.9: Pulse width modulated current source converter

source converters for series connection, namely [76, 77]:

- The DC current is controlled directly by the converter. This is especially important for the proposed series connection where the current must be controlled in order to obtain stable operation. A line commutated converter could control directly this current but its performance is inferior. The voltage could be reduced to almost zero without affecting the controllability of the converter. In a voltage source converter, a low voltage in the DC link significantly affects the stability of the controls.

- The three-phase voltage can be controlled in just one control loop. Therefore, the response of the complete system is expected to be fast. This issue will be discussed in Chapter 4.

- The output voltage presents low harmonic distortion. In addition, power factor can be directly compensated [78].

- PWM-CSC presents better performance in weak grids compared with VSCs.

In a wind park connected in series, the current must be maintained at the same level in all the turbines. This condition is physically imposed by the topology itself. However, the control must be consistent with this constraint, otherwise the entire system could become instable. Therefore, the on-land converter must maintain the constant DC current. A PWM-CSC converter is the selected option at this stage. The complete system for three series connected turbines is depicted in Figure 2.10.

PWM-CSCs are being used in motor drive applications at high power levels [79, 80]. It can also be used in StatComs [81], super conducting energy storage [82] and wind turbines [31]. Other topologies of current source converter can be used for series connection of offshore wind farms. In this work a PWM-CSC is selected although a line commutated converter is also a feasible option. The main disadvantage of a line commutated converter is the harmonic distortion in the AC grid and

37
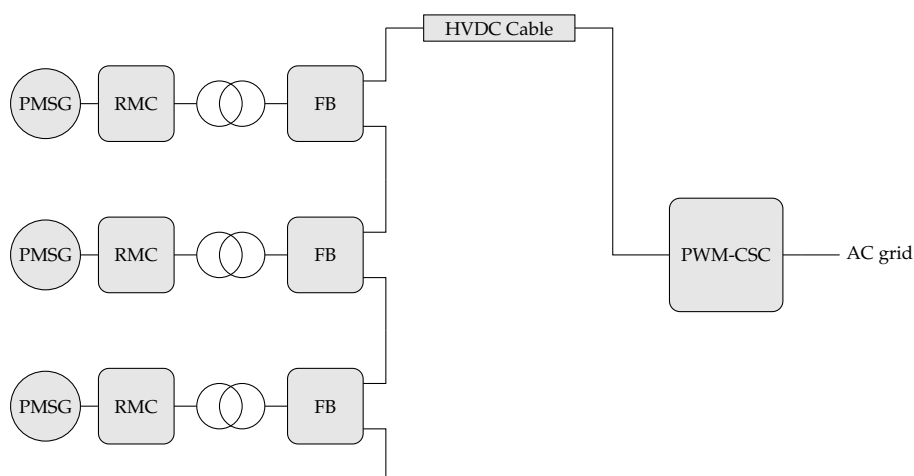
Figure 2.10: HVDC system based on CSC and series connection

the probability of having failure commutation during a contingency. In addition, active and/or passive filters are required in order to reduce the harmonic distortion. A compensation theory based on mathematical optimization is presented in Appendix A.

2.9 Protection

Protection of the entire HVDC system is an important task. Classic HVDC systems based on line commutated converters function well with DC faults. However, they deal with failure commutation for AC faults. Conversely, HVDC light systems based on a voltage source converter have poor performance for DC faults but good enough performance in the case of AC faults. Problems during faults in HVDC systems can be solved by suitable control strategies or by using a DC circuit breaker.

Design of DC circuit breakers is still an open research problem. In [83] and [84] some ideas about DC circuit breakers have been proposed. Losses in a solid state circuit breaker are the main practical issues, since they are higher than in a conventional mechanical breaker. Hybrid solutions appears to be an efficient solution [7]. DC circuit breakers deal with new challenges compared with conventional AC breakers. One of the major differences between AC and DC breakers is the absence of natural current zero crossings in a DC system.

Failure commutation is not a problem in the proposed HVDC system since it is based on forced commutated converters. In addition, it has a good performance in DC faults since it is a CSC. A current source converter presents less problems during a DC short circuit since the voltage can change drastically. In VSC-based systems,
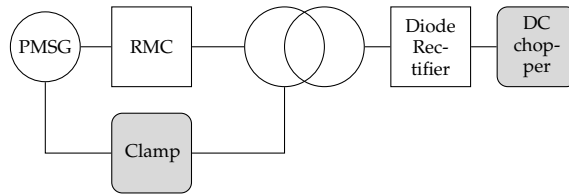
Figure 2.11: Additional elements for protection of the system (in grey)

the HVDC breaker has to be able to interrupt the current quickly, as was stated before. However since series connection is basically a CSC this is not a requirement.

Some additional protection schemes are required in the proposed topology as shown in Figure 2.11. In the matrix converter, a clamp circuit is required in order to avoid over-voltages and over currents in the transformer [85, 86, 87]. Some types of modulation are prone to over-voltages due to the fast frequency and the parasitic capacitances in the circuit. This will be discussed in the next chapter.

Moreover, a DC chopper is placed in the output of each turbine in order to create damping resistance during the start up of the entire system and for over voltage protection. Over voltage can be produced by a difference in the wind velocity between series connected turbines and during a fault in one turbine. Therefore, this DC chopper acts only during transients. For stationary state, the coordinated control will define the appropriate set points of power and current to guarantee minimal losses. This will be discussed in the Chapter 5.

3

Proposed Energy Conversion System

This chapter presents the proposed high frequency link and its modulation using four strategies. A comparison from the losses point of view is performed. Details of the converter such as protection, semiconductor devices and the topology itself are also presented in this chapter.

SERIES connection requires a highly efficient conversion system in each turbine. Otherwise, the efficiency gained due to the topology can be lost in converters. Making the decision about the power electronic converter is mainly related to the type of machine that is used. There are many standard configurations for wind generators. One of the most popular is the double fed induction generator. The reason behind its popularity, specially in on-land wind parks, is the reduced size of the converter. The converter required in a double fed induction generator is only 30 % the rating of the machine. A converter is required in a wind generator for wind speed control. However, a double fed induction generator is not the most efficient topology for DC grids since an additional full converter is required at the output to achieve DC voltage. Needless to say DC machines have not improved enough in efficiency to be competitive with AC machines. Therefore, the options are limited to synchronous or asynchronous generators.

An asynchronous generator can be used with a conversion system as shown in Figure 3.1(a). This configuration was proposed in [9] and [88]. It consists of four stages of conversion AC/DC-DC/AC-Transformer-AC/DC. Since the transformer is in the middle of two controlled converters, the voltage waveforms and the frequency can be different from sinusoidal. In this case, a square medium frequency

41
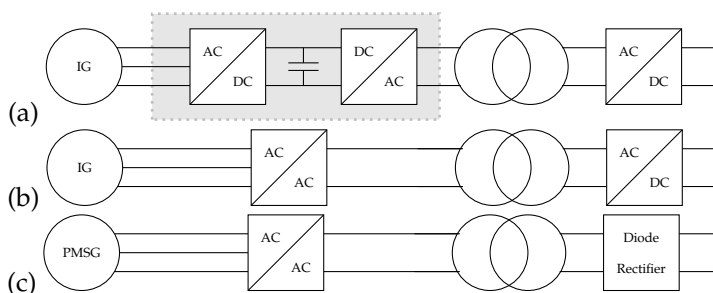
Figure 3.1: Three possible configurations suitable for series connection of wind generators. (a) Asynchronous generator with back to back converter, (b) asynchronous generator with a high frequency link based on matrix converter, (c) Permanent magnet synchronous generator with proposed high frequency link

waveform is used. Consequently, the power density can be improved. A second option with reduced stages of convention was proposed in [89] and is shown in Figure 3.1(b). The main advantage of this configuration is the two first stages of conversion are replaced by a direct AC/AC converter. Finally, an improved topology is presented in Figure 3.1(c). The induction machine is replaced by a permanent magnet synchronous generator. Besides of the superior efficiency of this type of machine compared with asynchronous generator, the last stage of conversion is simplified. In contradistinction to asynchronous generators which require the AC/DC converter to be designed using controlled devices (IGBTs), a simple full bridge diode rectifier can be used for PMSG. This is because an asynchronous generator requires to be magnetized at the starting point. There is not lost controllability in the machine, since the wind velocity is controlled by the AC/AC converter.

The AC/AC converter to be used is a reduced matrix converter. In general, it has been demonstrated in several articles the advantages of the matrix converter in terms of efficiency, reliability and power density [90, 91, 92, 16, 93]. These three aspects are the main objectives for offshore technologies. Unlike conventional AC/AC converters which require an intermediate stage of DC conversion, a matrix converter can achieve direct AC/AC conversion. An indirect AC/DC-DC/AC conversion implies the use of electrolytic capacitors to maintain a constant DC voltage (see Figure 3.1(a)). In addition to the cost, electrolytic capacitors present some disadvantages such as decreasing the converter's lifetime, and increasing its weight and volume. The matrix converter is therefore more efficient and reliable than other types of AC/AC converters.

Topologies based on the matrix converter (see Figure 3.2) have been used in specific applications where size and reliability are a key issues. Examples of such applications are motor drives [94], aircraft [95], marine electric propulsion [96] and offshore wind farms. The matrix converter can also be used in distribution systems as electronic transformer [49]. The matrix converter presents some advantages over conventional topologies namely:
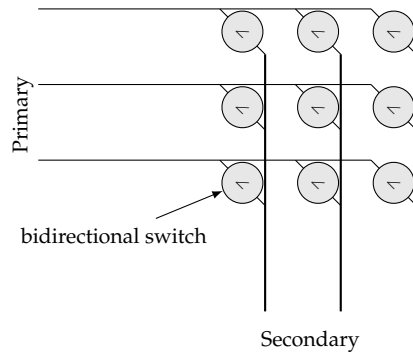
Figure 3.2: Schematic representation of a three-phase matrix converter

- reduction in size and weight

- increase in reliability

- elimination of the electrolytic capacitor

- high controllability

- sinusoidal input and output currents

- bidirectional power flow

Despite being used for relatively low power applications, the matrix converter has shown its potential for high power applications such as UPFCs [97] wind energy [15, 98] and reactive power compensation [99].

The basic configuration of a three-phase matrix converter is shown in Figure 3.2. It consists on nine bidirectional switches connected in a matrix array. A matrix converter works as a current source converter in the input and as voltage source converter in the output. Therefore, modulation must be designed so that it avoids open circuits in the output and short circuits in the input. Other topologies of the matrix converter are also possible. For example, in [20] and [21] modular approaches of matrix converters are presented. Multilevel topologies have been also suggested [28, 29, 25]. So far, after the classic matrix converter, the most studied topology is the indirect matrix converter [100, 101].

Unlike conventional matrix converters, a reduced matrix converter converts three-phase AC voltages/currents into a single phase system [102]. The conversion is achieved by eliminating one leg in the conventional three-phase topology. Modulation is completely different since the output is not three-phase as will be explained later in this chapter.

43

3.1   Bidirectional switches

A reduced matrix converter requires bidirectional switches to allow AC-AC conversion. A bidirectional switch can be constructed using two IGBTs+Diodes as shown in Figure 3.3(a) and (b). The first configuration is called a common emitter connection while the second is called a common collector. Here, (b) presents some advantages over (a) since only one gate drive can be used for both switches. Nevertheless, some modulation techniques require independent control of the switches. Two anti-parallel diodes are placed in each IGBT since conventional IGBTs lacks reverse blocking capability for nominal voltages. A third option is to build a bidirectional switch with two reverse blocking IGBTs without additional diodes (Figure 3.3(c)).
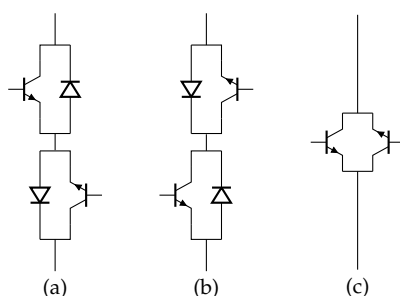
Figure 3.3: Possible topologies to build a bidirectional switch: (a) Common emitter, (b) Common collector, (c) Reverse blocking-IGBTs

A RB-IGBT has the same functionality as a conventional IGBT but with additional reverse blocking capability. In principle a bidirectional switch with RB-IGBT has less conduction losses since the current flows for just one element. In bidirectional switches (a) and (b) the current flows always by one diode and one IGBT. However, early bidirectional switches built with reverse blocking IGBTs presented presented higher switching losses compared with conventional semiconductors [92]. Nevertheless, modern technology of RB-IGBT could be competitive respect to an implementation with discrete IGBTs+Diodes [103] for some particular applications. The matrix converter has been studied for low power applications because of the lack of high power bidirectional devices. High power bidirectional switches can be built by using a set of series-connected IGBTs with series diodes as was proposed by Bucknall in [96]. Similar ideas could be used for RB-IGBTs.

Other alternative for building bidirectional switches is the Integrated Gate Commutated Thyristors (IGCT). In particular the type with reverse blocking capability. IGCTs for 10 kV and 6.5 kA have been reported in [104] and [105]. The semiconductor structure of an IGCT has low intrinsic inductance so that the current can be shut off almost instantaneously. This new type of semiconductors is typically operated at 500 Hz [106]. However, the switching frequency can be increased up to 40 kHz being limited only by the thermal losses and the design of the cooling system.

3.2 Operation of the converter

A detailed power circuit for the proposed high frequency link is shown in Figure 3.4. Two main operation principles are possible according to the controlled variable in the three-phase side: current or voltage control. These two operation principles can be implemented with carrier-based modulation or space vector modulation. Therefore, four modulation cases will be studied in this chapter:

- Carrier-based modulation and voltage operation mode

- Carrier-based modulation and current operation mode

- Space vector modulation and voltage operation mode

- Space vector modulation and current operation mode
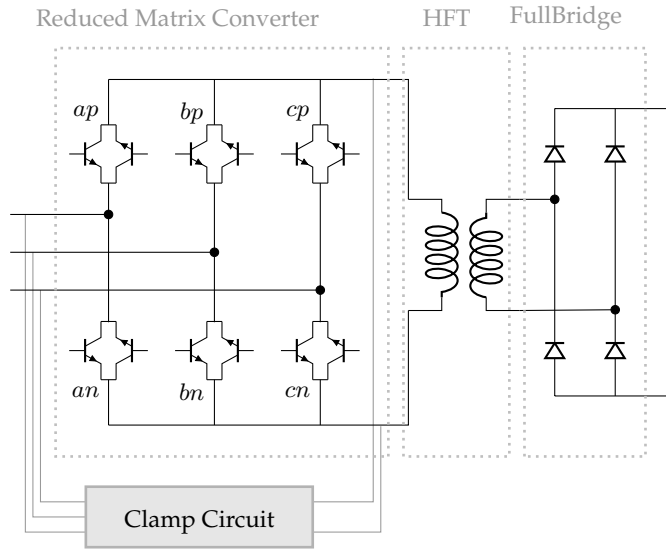
Figure 3.4: Detailed circuit of the proposed high frequency link

Passive filters placed in the input and output of the converter are different according to each operation type as shown Figure 3.5. The design of passive filters is an important task for matrix converter[107]. In this case a simple capacitive filter is used. The value of this capacitor is designed according to the switching frequency. The cut off frequency of the filter is selected as 10 % of the switching frequency. Therefore, the capacitive filter C_s can be calculated as shown in Equation 3.1 where L_s is the series inductance and f_s the switching frequency.

$$C_s = \frac{1}{L_s \cdot (2\pi f_s/10)^2} \tag{3.1}$$
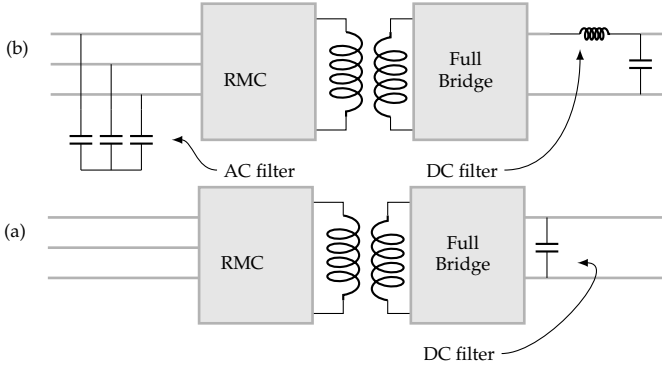
Figure 3.5: Passive filters for different operation modes. (a) Voltage source operation. (b) Current source operation

For voltage source operation, a capacitive filter must be placed in the output of the full bridge converter to reduce the DC current ripple. The inductance of the machine acts as a filter to reduce the harmonics in the input current. For current source operation, a three-phase capacitive filter must be placed in the input to reduce the harmonic content of the three-phase current, unless the machine is designed to support distorted currents. In order to compare these two operating modes, it is assumed that the machine is the same, therefore capacitive filters are required for current source operation. The filters do not necessarily represents a disadvantage because of their small size inherent in high frequency switching. A filter in the output is also required to reduce the voltage DC ripple.

While conventional matrix converters have reduced voltage utilization, the proposed converter presents 100% for voltage source operation, due to the fact that its operation is similar to a three-phase inverter which constantly changes the polarity of the DC side. The RMC should not be confused with a single phase matrix converter, since the output wave form is not a sinosoidal, but a square wave. Therefore the power is not in an oscilatory form as in a single phase system, but is constant on both the single and three-phase sides.

If the converter is operated as a voltage source, the input and output voltages are related as shown in Equation 3.2.

$$V_{AC} = \sqrt{\frac{3}{2}} \cdot m_s \cdot \frac{V_{DC}}{2 \cdot N} \tag{3.2}$$

where N is the ratio of the transformer and m_s is the modulation index. Even for a 1:1 transformer, the DC voltage is therefore higher than the AC voltage. In addition, the transformer can be used to raise the voltage in order to reduce the transmission losses.
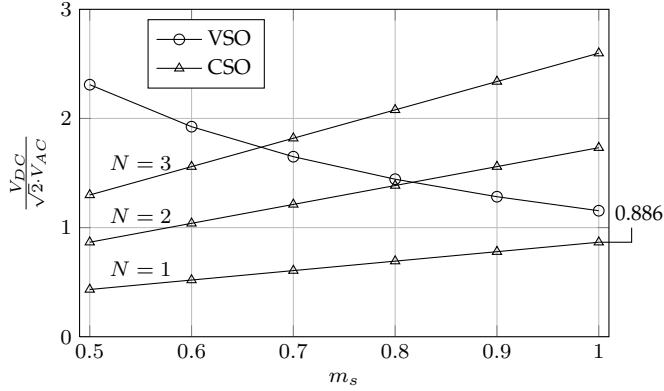
Figure 3.6: Voltage ratio for voltage source operation (VSO) with 1:1 transformer and current source operation (CSO) for different transformer ratios (1:N)

On the other hand, if the converter is operated as a current source, the current in the generator is related to the output DC current (I_{DC}) through the following equation:

$$I_{AC} = I_{DC} \cdot m_s \cdot \frac{N}{\sqrt{2}} \tag{3.3}$$

and the voltage as:

$$V_{AC} = \sqrt{\frac{2}{3}} \cdot \frac{1}{m_s \cdot cos(\theta) \cdot N} \cdot V_{DC} \tag{3.4}$$

where $cos(\theta)$ is the power factor. For a unity power factor, the maximum output DC voltage is 86.6 % of the peak line to line AC voltage.

The voltage ratio for current and voltage source operation are shown in Figure 3.6. In this research a 1:2 ratio is used for current source operation while a 1:1 ratio is used for voltage source operation. In that case, the output voltage and currents are within the same range and the comparison of losses will be fair.

3.3 Protection

Because of the absence a of free wheeling path in the RMC, a clamp circuit must be used for protection as shown in Figure 3.7. This protection scheme is similar to the one used in a conventional three-phase matrix converter. Other protection schemes use varistors and/or zener diodes [86] to avoid over-voltages [85], but clamp circuit

is one of the most secure and effective solutions for high power applications due to the additional losses introduces by those components. A reduction in the clamp circuit resistance and capacitance can be achieved by using a strategy based on the use of an IGBT as proposed in [87].
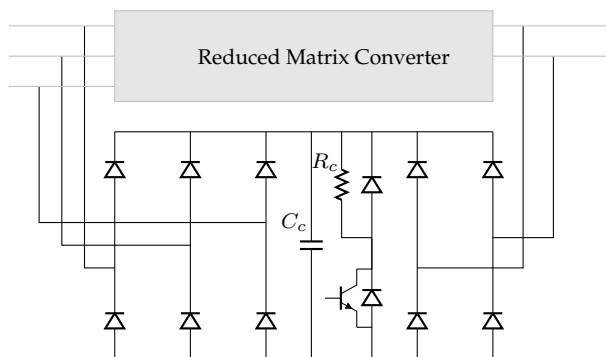
Figure 3.7: Clamp circuit for protection of the reduced matrix converter

The over-voltage elimination capacity of the clamp circuit is given by the voltage in its capacitance C_c which can be controlled by the discharge chopper circuit. In this situation, the IGBT in the clamp circuit must operate to reduce the voltage in the clamp, and therefore the over-voltage limit. The resistor R_c connected in series with the IGBT allows energy dissipation. This resistance must be low enough to discharge the capacitor when the voltage is too high. A design criteria to achieve reasonable losses is 0.5 % of the nominal power of the converter. Gating control in the IGBT can be achieved using a zener diode or a simple analog circuit with a voltage sensor. The IGBT in the clamp circuit reduces the required value of the capacitor. The size on the whole converter is not increased as diodes in the clamp circuit require only 10 % of the current capability of the main circuit. This is because the maximum surge current in a power diode is much higher than the maximum average current. On the other hand, voltage in the clamp circuit can also be used to supply power to control circuits and anciliary services inside the nancelle, increasing the reliability of the whole system.

Over-current protection consists of a control circuit which inhibits the bidirectional switches during a fault. The clamp circuit creates the path for the current in the machine and the transformer. A DC chopper must be placed in the capacitive filter in order to avoid over-voltages and undesired oscillations during transients. This DC chopper does not add losses to the system in the stationary state since it operates only during transients. It also increases the controllability of the entire system since the AC/DC converter is only a full bridge diode rectifier.

3.4 Possible types of modulation

3.4.1 Carrier based modulation for voltage source operation

Carrier-based modulation is one of the most popular switching techniques for three-phase converters due to its easy implementation. In the proposed high frequency link, the modulation must be modified to take into account the polarity change at the input of the high frequency transformer. This modulation is schematically explained in Figure 3.8. Likewise a conventional converter, an, bn and cn is modulated using the inverse signal for ap, bp and cp respectively.
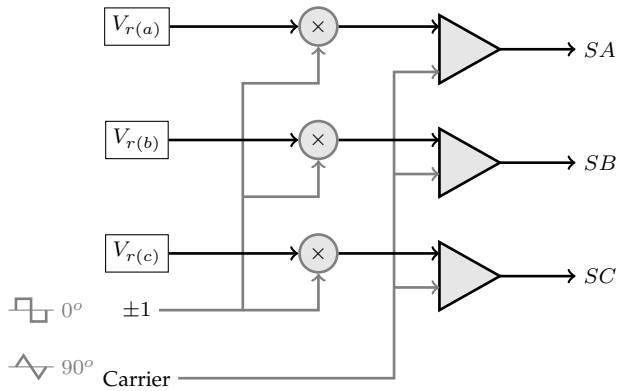
Figure 3.8: Modified carrier-based modulation for the RMC and VSO

$V_{r(a)}$, $V_{r(b)}$ and $V_{r(c)}$ are the per unit voltage reference signals generated to control the speed of the machine in order to achieve a maximum tracking point in the turbine. In stationary state, these reference signals are three-phase sinusoidal waveforms at low frequency (around the nominal frequency, in this case 50 Hz). Due to the large difference between the frequency of these reference signals and the triangular carrier, it appears as a constant as shown Figure 3.9.
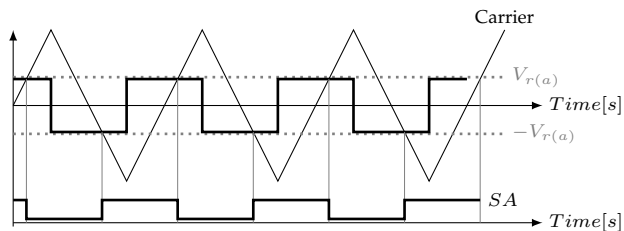
Figure 3.9: Timing diagram for carrier based modulation VSO

A center-aligned triangular signal is used as carrier, which produces less harmonic contents in comparison with other triangular carriers. The modulation of

the RMC is responsible for the change in the polarity in the high frequency transformer and the control of the voltage applied to the generator. Consequently, two
independent and orthogonal carriers are required to avoid unnecessary additional
switching actions as shown in Figure 3.8. Notice that only two switching actions are
executed each period and the time between switching actions is longer for the same
carrier frequency in comparison with the modulation for a conventional inverter.
Therefore, the RMC can achieve higher frequency operation. It is possible also to
use different frequencies between the carrier for the three-phase and single-phase
sides. Nevertheless, different angles and carrier based-modulation schemes where
studied for the proposed converter, and the optimal operation was achieved when
both carriers have the same frequency and $\pi/2$ shift angle (orthogonal carriers).

Instead of dead time as in a conventional voltage source converter, the proposed
converter requires overlapping to guarantee a path for the current. Therefore, when
one change occurs in one leg, both bidirectionals are turned on (for example AP and
AN) creating a continuous path for the current and a short circuit in the transformer.
This action reduces also the turn on and reverse recovery losses, but increases the
turn off losses. The total effect is a small decrease in losses.

3.4.2   Carrier based modulation and current source operation

Carrier-based PWM techniques are very simple for the voltage source converter
compared to the current source converter. In a conventional VSC the switching
state of two semiconductors in the same leg are opposite to avoid a short circuit in
the DC side. Therefore, it is necessary to only have one modulation signal per leg
since the output for the other can be achieved with a logic NOT gate. On the other
hand, in current source mode, it is necessary to guarantee a path for the currents at
all instants. As a result of that, two switches must be on conduction all the time and
a more complex logic circuit is required as shown in Figure 3.10.

The input signals (m_a,m_b,m_c) are calculated by comparison between the reference currents $I_{abc(reff)}$ with a centre aligned triangular signal used as carrier. In the
proposed converter, the DC side is replaced by a single phase, high frequency square
wave output. To achieve this current waveform, the logic circuit must be modified
according to a second carrier by building an additional logic circuit in each output
as is shown in Figure 3.11. This type of modification is easily achieved for FPGA
implementation, where the output is exactly the same as conventional modulation
when the desired polarity in the transformer is positive and the opposite when it is
negative. The frequency of the output is fixed by the frequency in the second carrier
(Sign(σ)) and must be greater than the frequency of the first carrier.

However it must be a multiple of 2 in order to avoid undesired harmonics on the
three-phase side. Other important difference between the proposed converter and
the conventional converters is the use of overlapping. In a conventional voltage
source converter the presence of an electrolytic capacitor on the DC side constrains
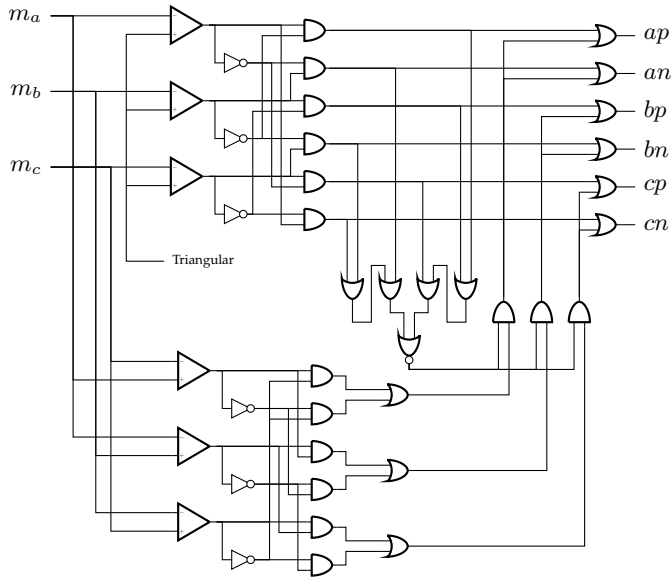
Figure 3.10: Logic circuit for carrier based modulation in a conventional current source converter

the switching actions. A short circuit in the DC side must be avoided even if it is for a very short time. The solution to this problem is the use of dead time. On the other hand, in a conventional current source converter, an open circuit must be avoided due to the high inductance on the DC side. Therefore, overlapping is required in the modulation. Both, dead time or overlapping can be easily implemented by analog circuits or digitally in an FPGA. In the proposed converter, the high inductance is after the full bridge diode rectifier and not in the transformer itself. Therefore, overlapping or dead time can be or not implemented. This depends on the magnitude of the leakage inductance and the parasitic capacitances of the transformer.

3.4.3 Space vector modulation and voltage source operation

For space vector modulation and voltage source operation, the reference voltage is represented in α, β coordinates as given in Equation 3.5

$$\vec{V}_r \angle \phi = \frac{2}{3} \left(V_{r(a)} + V_{r(b)} \cdot e^{j2\pi/3} + V_{r(c)} \cdot e^{-j2\pi/3} \right) \tag{3.5}$$

All possible stages are classified into two sets: Active states are A_s and zeros states are Z_s. These states are defined by the bidirectional switches conducting in each leg:
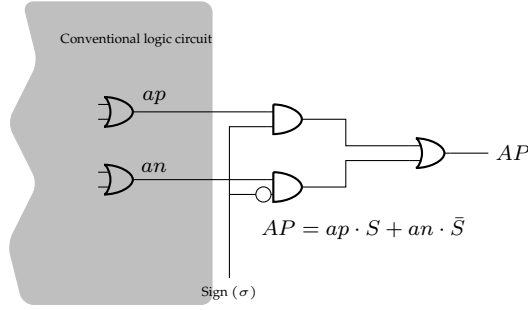
Figure 3.11: Modification in the logic circuit to achieve a square wave in the RMC for current source operation

$$A_s = \{(ap, an, cn), (ap, bp, cn), (an, bp, cn),$$
$$(an, bp, cp), (an, bn, cp), (ap, bn, cp)\} \tag{3.6}$$

$$Z_s = \{(ap, bp, cp), (an, bn, cn), (ap, an, bp, bn),$$
$$(ap, an, bn, cn), (ap, bp, bn, cp), (an, bp, bn, cp),$$
$$(ap, bp, cp, cn), (an, bn, cp, cn)\} \tag{3.7}$$

Notice that there are more zero states than in a conventional voltage source converter. This is because no capacitor is required and the system can be short circuited on both sides. This gives an additional degree of freedom to minimize the losses when a zero space vector is required. However, since both sides are mainly inductive, some-over voltages are going to be induced in the transformer. Therefore this voltage operation mode is only feasible if the leakage inductance is low enough to guarantee reasonable losses and low over-voltages. This over-voltages can be eliminated by the clamp circuit but its impact on the losses must be evaluated as will be presented after.

All feasible states of voltage space vector drawn as an hexagon like the one shown in Figure 3.12.

A symmetrical and periodic voltage square wave form is required in the high frequency transformer V_T. Therefore, the desired reference voltage is represented as a linear combination of the possible states and the voltage in the transformer:

$$\vec{V}_r = m_s \cdot \frac{V_T}{2} \cdot e^{j\phi} = \sum_{k \in A_s} d_k \cdot \vec{V}_k + \sum_{i \in Z_s} d_i \cdot \vec{V}_i \tag{3.8}$$

where m_s is the modulation index and ϕ is the angle of the space vector reference voltage. The scalars d_k and d_i are duty cycles for each feasible space vector. The
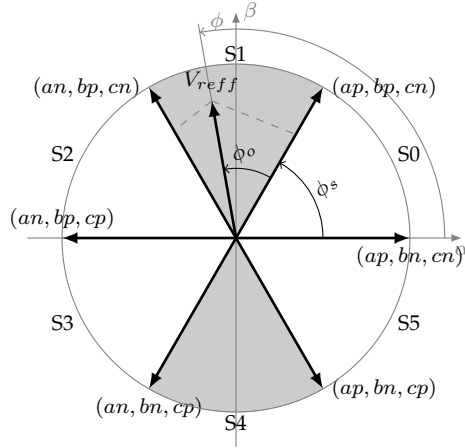
Figure 3.12: All possible voltage space vectors states for voltage operation mode

angles of the active sectors in Figure 3.12 divide the space in six sectors; each sector determines the set of vectors which are used to compound the vector $\vec{V}_r$. An integer variable S (sector index) is associated with each sector and defined according to the angle ϕ as:

$$S = \left\lfloor \frac{\phi}{\pi/3} \right\rfloor, \quad 0 \leq \phi \leq 2\pi \tag{3.9}$$

where $\lfloor,\rfloor$ represents the floor function defined by Equation 3.10.

$$\lfloor x \rfloor = max\left\{ n \in \mathbb{Z} \,|\, n \leq x \right\} \tag{3.10}$$

In a conventional converter, the two adjacent active vectors and one zero vector are enough to generate the desired output. In an RMC, it is necessary to generate not only the desired three-phase input reference but also the desired output square wave in the transformer. Consequently, more space vectors are required: two adjacent vectors to generate the positive part of $\vec{V}_r$; two vectors opposite to the adjacent to generate the negative part of $\vec{V}_r$ and finally some zero vectors to complete the set. For example in the sector $S1$, the vectors (ap, bp, cn), (an, bp, cn), (an, bn, cp), (ap, bn, cp) and the zero vectors can be used to generate the desired input and output voltage. Other combinations are possible but they will produce more switching losses, therefore they are discarded.

A relative angle ϕ_o is defined as:

$$\phi_o = \phi - \phi_s \tag{3.11}$$

Let us define A_{right} and A_{left} as the right and left active vectors adjacent to the expected reference, while ϕ_s is the angle of the right vector A_{right} and can be calculated using the sector index S. For example $A_{right} = (ap, bp, cn)$ and $A_{left} = (an, bp, cn)$ for the positive part in sector $S = 1$ (See Figure 3.12):

$$\phi_s = S \cdot \frac{\pi}{3} \tag{3.12}$$

In each switching period, the voltage must achieve the desired references for the input and the output. In the first half of the period, the mean input voltage is given by:

$$\vec{V_r} = \frac{2}{T_p} \int\limits_0^{T_p/2} \vec{V}_{(t)} dt = \frac{\tau_x}{T_p/2} \cdot \vec{V_x} + \frac{\tau_y}{T_p/2} \cdot \vec{V_y} + \frac{\tau_z}{T_p/2} \cdot \vec{V_z} \tag{3.13}$$

where $\vec{V_x}$ is the voltage corresponding to the state A_{left}, $\vec{V_y}$ is the voltage corresponding to the state A_{right} and $\vec{V_z}$ corresponds to the zero states Z_s. These voltages can be easily defined as:

$$\vec{V_x} = \frac{1}{2} \cdot V_T \cdot e^{j\phi_s} \tag{3.14}$$

$$\vec{V_y} = \frac{1}{2} \cdot V_T \cdot e^{j(\phi_s + \frac{\pi}{3})} \tag{3.15}$$

$$\vec{V_z} = \vec{0} \tag{3.16}$$

τ_x, τ_y and τ_z are the pulse duration in each state. By replacing Equation 3.8 in 3.13, the duty cycles for each state are calculated as:

$$d_y = \frac{\tau_y}{T_p/2} = \frac{2 \cdot m_s}{\sqrt{3}} \cdot sin(\phi_o) \tag{3.17}$$

$$d_x = \frac{\tau_x}{T_p/2} = \frac{2 \cdot m_s}{\sqrt{3}} \cdot sin(\pi/3 - \phi_o) \tag{3.18}$$

$$d_z = 1 - d_x - d_y \tag{3.19}$$

Notice that the duty cycles depend on the relative angle ϕ_o and not on the reference angle ϕ. Therefore, these equations are general for any sector S. Since a square
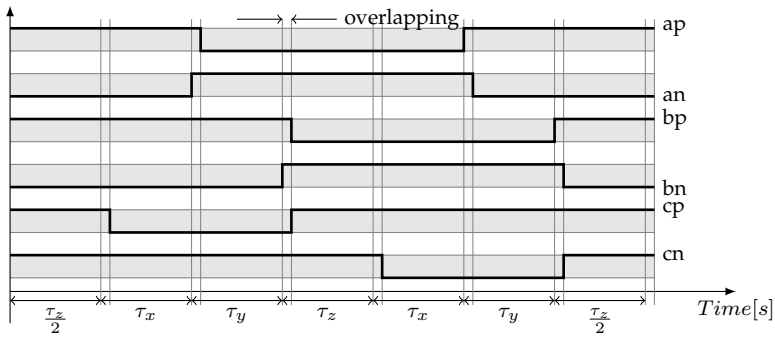
Figure 3.13: Switching action for space vector modulation and voltage source operation for a reference voltage in sector $S = 1$

waveform is required in the transformer, the calculated duty cycles must be applied twice, for the positive and negative periods of the transformers voltage.

The zero vectors can be any in the set Z_s; they are selected to minimize the number of switching actions. An overlapping can be used. Figure 3.13 illustrates the modulation for a voltage in sector $S1$. Notice that the overlapping generates a short circuit in both sides of the converter. Moreover, the used zero vectors avoid an open circuit in the transformer.

3.4.4   Space vector modulation and current control

The space vector principle is similar for the current source converter. In this case, the feasible set of active and zero vectors are given by:

$$A_s = \{(ap, bn), (ap, cn), (bp, cn),$$
$$(bp, an), (cp, an), (cp, bn)\} \tag{3.20}$$

$$Z_s = \{(ap, an), (bp, bn), (cp, cn)\} \tag{3.21}$$

All feasible active states of current vectors are drawn in a hexagon like the one shown in Figure 3.14. Three additional zero current state completes the array. These zero states are placed in the origin of the axes and despite presenting a current equal to zero on the three-phase side, it is different from zero on the single phase side.

The objective is to find a symmetrical and periodic square wave form in the output which can be defined in one period T_p as:
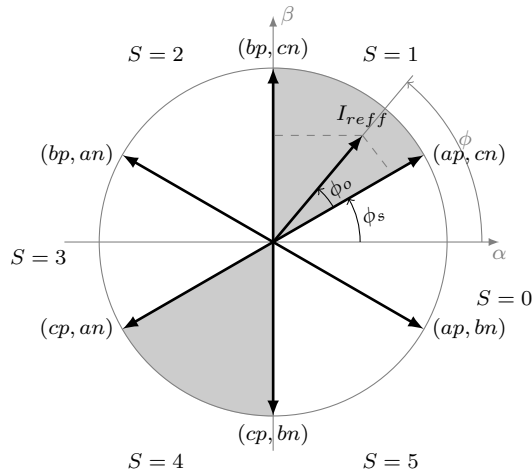
Figure 3.14: All possible active current vector states when implementing space vector modulation

$$I_{out} = \left\{ \begin{array}{lll} I_{DC}, & if & 0 \leq t \leq T_p/2 \\ -I_{DC}, & if & T_p/2 < t \leq T_p \end{array} \right\} \tag{3.22}$$

Sector index is rotated $\pi/6$ in comparison with case III.

$$S = \left\lfloor \frac{\phi}{\pi/3} + \frac{1}{2} \right\rfloor, \quad 0 \leq \phi \leq 2\pi \tag{3.23}$$

Polarity of the adjacent vectors are changed to achieve a square wave form. The alternated effect of this switching signal is compensated by the full bridge. As a result of that, the output is a DC current I_{DC}, just like a current source rectifier. In order to reduce the harmonic distortion, space vectors must change in order from one high frequency period to the next. Hence a complete sequence for a reference current in the sector $S = 1$ is given in Figure 3.15.

In a conventional current source converter, a reference current I_{ref} in the sector $S = 1$ can be achieved by placing the vectors $(ap, cn) - (bp, cn) - (cp, cn)$. In this case it is also necessary to use the vectors $(cp, an) - (cp, bn)$. This is represented by the blue-filled section in Figure 3.14. Notice that applying the space vectors below will produce the same output in the three-phase side since the polarity of the current has changed. In order to reduce the harmonic distortion, space vectors must change in order from one high frequency period to the next. Hence a complete sequence for a reference current in the sector $S = 1$ is given in Figure 3.15. Transitions between steps can be made using overlapping or dead time. The capacitances and inductances in the transformer are small enough to permit both possibilities. However, as
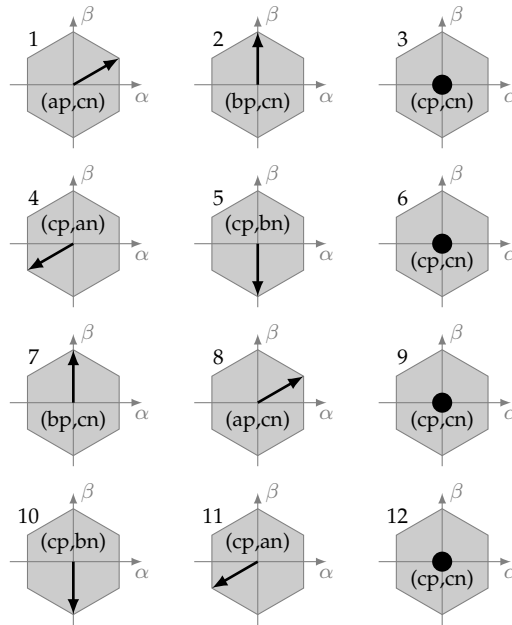
Figure 3.15: Sequence of switching actions for a reference current in the sector $S = 1$

will be demonstrated in the results, the use of overlapping is more suitable.

Figure 3.16 shows the modulation for one reference vector in the second sector ($S = 1$). Initially, the vector $\vec{I}_x$ is used. For $S = 1$, the vector $I_x = I_{ac}$ is applied during the first τ_x seconds. Then the vector must be changed to $\vec{I}_y$ which in this case is I_{bc}. Notice that only two switches change state: bp turns ON while ap turns OFF. Next, a zero vector $\vec{I}_z$ is used which can be any of the three zeros vectors in Z_s. Nevertheless, the vector which produces less switching changes is used, in this case $\vec{I}_{cc}$. This could constitute a complete switching cycle from the point of view of the three-phase side, however, the current in the single-phase side is just the positive part. To complete the square wave on the high frequency transformer, the same duty cycles (d_x, d_y and d_z) are used but with the opposite active vector; in this case, $\vec{I}_{ca}$ instead of $\vec{I}_{ac}$ and $\vec{I}_{cb}$ instead of $\vec{I}_{bc}$. The zero vector remains the same in order to minimize losses. Since the current in the transformer is now negative, the current in the AC side will be again the desired values. The frequency of the single phase side is therefore half the PWM frequency on the three-phase side. Other multiple integer values of the square wave frequency are possible, but the higher the frequency the lower the size of the transformer. Consequently, two times is the most suitable value.
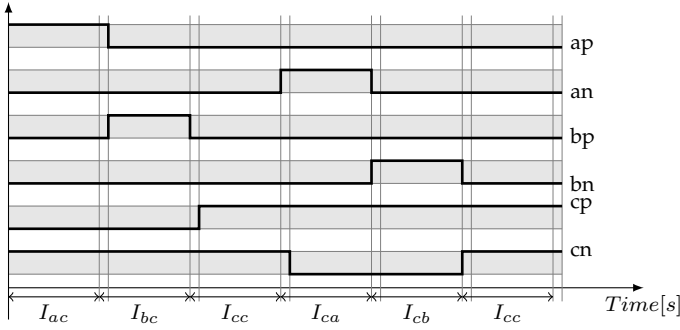
Figure 3.16: Switching action for space vector modulation and current control for a reference current in sector $S = 1$

3.5 Methodology for losses calculation

Comparison between different operation strategies is made to investigate the losses. A detailed behavioural model based on the methodology presented by Itoh in [108] was used. This model was implemented in an external dynamic link library (dll) programmed in visual c++ and connected to PSIM as simulation software.

Semiconductor devices, generate conduction and switching losses. Conduction losses in an IGBT as well as an RB-IGBT are function of collector current (I_C) and voltage collector emitter V_{CE}. Voltage V_{CE} can be approximated as quadratic function of the current as shown in Equation 3.24:

$$V_{CE} = \alpha_1 + \alpha_2 \cdot I_C + \alpha_3 \cdot I_C^2 \qquad (3.24)$$

The average dissipated power due to the conduction in each IGBT in one period T is calculated as in Equation 3.25.

$$P_{cond} = \frac{1}{T} \int_{t_o}^{t_o+T} V_{CE} \cdot I_C \, dt \qquad (3.25)$$

On the other hand, switching losses are a function of the blocking voltage and the current in each semiconductor. The energy dissipated in each switching action can be described by Equation 3.26

$$E_{sw} = g_{sw}(I_C, V_{CE}) \qquad (3.26)$$

where g_{sw} are a non-linear functions of the blocking voltage and current. There

are a different functions for each type of switching action (turn on, turn off or reverse recovery). The model of this function depends on the information available of the semiconductor. For example in [109] there is a complete model of g_{sw} for a particular class of RB-IGBT. However, this type of model is not always available in data sheets. Therefore, g_{sw} can be approximated to a proportional function as the one presented in Equation 3.27 when the only available information is the dissipated energy (E_{nom}) at nominal conditions.

$$g_{(aprox)}(I_C, V_{CE}) = E_{nom} \cdot \left(\frac{V_{CE}}{V_{nom}} \right) \cdot \left(\frac{I_C}{V_{nom}} \right) \tag{3.27}$$

The two models are presented in Figure 3.17 for the turn on losses of an RB-IGBT. Notice both models are very similar. Equation 3.28 shows a measurement of the error between this two models.

$$E_R^2 = \frac{1}{I_{nom}} \cdot \frac{1}{V_{nom}} \int\limits_0^{I_{nom}} \int\limits_0^{V_{nom}} (g_{sw} - g_{aprox})^2 \cdot dV_c \cdot dI_c \tag{3.28}$$

For this particular case $E_{nom} = 18[mJ]$. The parameters of the exact model are referenced in [109]. The value of E_R is $1.8263[mJ]$ which is around 10% of E_{nom}. This error is even lower at nominal conditions. Consequently, the function g_{aprox} is a good approximation in most of the cases. In addition, for this particular study, the waveform of the voltages and currents are square. Therefore, the values of I_C and V_{CE} for each switching action is close to the nominal.
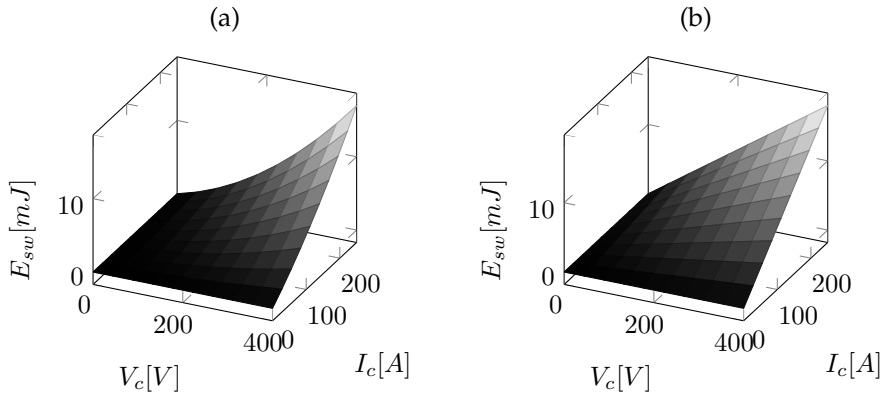
Figure 3.17: Turn on losses for an RB-IGBT. (a) Exact model. (b) Approximated model

Generator and passive elements must be taken into account in this study. The model of the generator can be simplified in stationary state as a Thevening equivalent if $L_d \approx L_q$. The losses in the machine are therefore just a function of the line

current and the stator resistance R_s. The Thevening voltage is dependent on the wind velocity. Harmonic distortion in the current will affect the losses in the machine and create additional stress in the shaft.

In the transformer, two types of losses were considered: core and winding losses. The first are function of voltage magnitude, frequency and the core material. These three variables are not affected by the modulation at a fixed frequency and therefore core losses are not necessary to be considered in this analysis, despite having a high importance in the design of the transformer. Winding losses depend mainly on the current, therefore they are considered as a series resistance. Parasitic capacitances are also considered in the transformer. These capacitances are not important in a conventional low frequency transformer but they become more important as the frequency is increased. As the leakage inductance modifies the ideal square wave, it must be considered in the study. It modifies the current/voltage applied to the semiconductors and could create over voltages which must be faced by the clamp circuit. Indeed, the losses in the clamp circuit must be calculated due to the effect of this leakage inductance, otherwise they would be negligible.

3.5.1 Analytical model of the losses

Using the approximated model of the losses it is possible to determine an analytical model for losses calculation at nominal conditions. This is a general method for the four considered cases are considered. As shown in Equation 3.24 the conduction losses depend on the collector current. For voltage source operation the current in each phase is given by Equation 3.29.

$$I_c = \sqrt{2} \cdot I_{rms} \cdot Cos(\omega t) \tag{3.29}$$

The total conduction losses can be easily calculated replacing expressions 3.29 and 3.24 into Equation 3.25 and taking into account that in VSO three semiconductors are conducting each instant of time. The result of this calculation is shown in Equation 3.31.

$$P_{cond} = \frac{6 \cdot \sqrt{2} \cdot \alpha_1}{\pi} I_{rms} + 3\alpha_2 \cdot I_{rms}^2 + \frac{8 \cdot \sqrt{2} \cdot \alpha_3}{\pi} I_{rms}^3 \tag{3.30}$$

For current source operation, the magnitude of the collector current is constant changing only in polarity. Two semiconductors are conducting all the time. Therefore the conduction losses in one period are given by Equation 3.31.

$$P_{cond} = (2\alpha_1) \cdot I_{cso} + (2\alpha_2) \cdot I_{cso}^2 + (2\alpha_3) \cdot I_{cso}^3 \tag{3.31}$$

Both are cubic equation with almost same coefficients since at nominal operation $I_{cso} = \sqrt{3/2}I_{rms}$. Therefore conduction losses are almost the same in both cases. This result does not depend on the type of modulation.

Conversely, the switching losses depend on the type of modulation and operation principle. The total power dissipated in one period is given by Equation 3.32.

$$P_{sw} = \frac{1}{T}k_f \sum_0^T E_{sw}(I_C, V_C) \qquad (3.32)$$

where E_{sw} is given by Equation 3.26 and k_f is a factor which takes into account the number of switching actions according to the modulation strategy. At high frequency operation the approximation given in Equation 3.33 is possible.

$$\sum_0^T E_{sw} \approx f \int_0^T E_{sw}dt \qquad (3.33)$$

Notice the integral term does not depends on the switching frequency. Therefore, the switching losses are linearly dependent on the frequency.

3.6 Simulation results

A simulation study for a 2 MW wind turbine was carried out. The values of two ABB StackPak 5SNR20H2500 module were used in the calculation. Parameters of the simulation are given in Appendix B. Results for the studied modulations at switching frequency of 10[kHz] are shown in Figure 3.18.
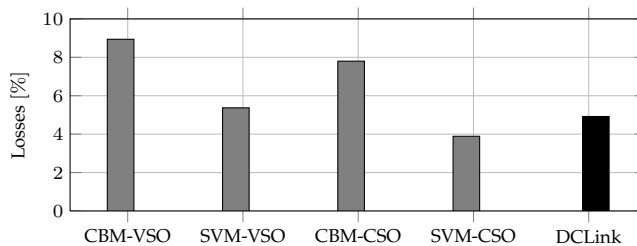
Figure 3.18: Comparison of losses for different modulation schemes and 10 [kHz]

The bar in black represents losses in the back-to-back configuration presented in Figure 3.1(a) used as reference and operated at 10 kHz. Space vector modulation

presents a more efficient behaviour in both type of operations as a result of a suitable use of the zero state vectors and a correct order of the active vectors to achieve less switching actions. Voltage source operation is more efficient from the RMC point of view, due to the fact that for the same output rating in the high frequency link, the semiconductors in the RMC receive higher current. However, from the point of view of the entire conversion system, current source operation is more efficient. In current source operation, the current magnitude in the conduction of IGBTs is the same as the one in the transformer while in a voltage source operation, it is the same as the generator. Therefore, for voltage source operation, it is a sinusoidal waveform while for current source operation it is square wave form.

Figure 3.19 presents the losses for current source operation space vector modulation (lowest losses), and the losses for the back to back configuration at different frequencies. The reduced matrix converter is more efficient than back-to-back topology when the frequency increases with a crossing point around 6 kHz.
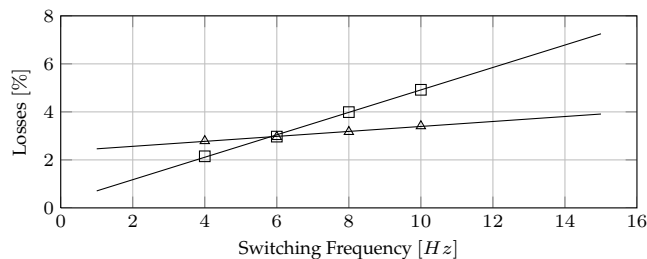
Figure 3.19: Comparison between the matrix converter SVM-CSO (△) and a DC link conversion system (□)

Figure 3.20 shows the losses for the four considered cases. The spikes in the voltage for voltage source operation, create over voltages in the clamp circuit which have to be eliminated by the DC chopper generating additional losses. In current source operation, the clamp circuit is not used in the stationary state, therefore, total losses are low.

Losses in the full-bridge are constant in the frequency and operational modes. In all cases, space vector modulation presents less losses in comparison with carrier-based modulation. The losses in the machine and the transformer represent less than 1% of the losses in the system. Current source operation is more suitable for series connection since the converter offshore can maintain constant the current. Moreover, both the voltage and the current in the generator are sinusoidal wave forms. For parallel connection, voltage source operation is more suitable since the DC/DC converters offshore can maintain the voltage constant. In both cases the generator can be controlled by the reduced matrix converter.

Medium frequency could also be used (for example 1[kHz]) with a greater reduction in the switching losses, however, the present work uses higher frequencies due to its potential reduction of size and weight. In addition, lower frequencies deal
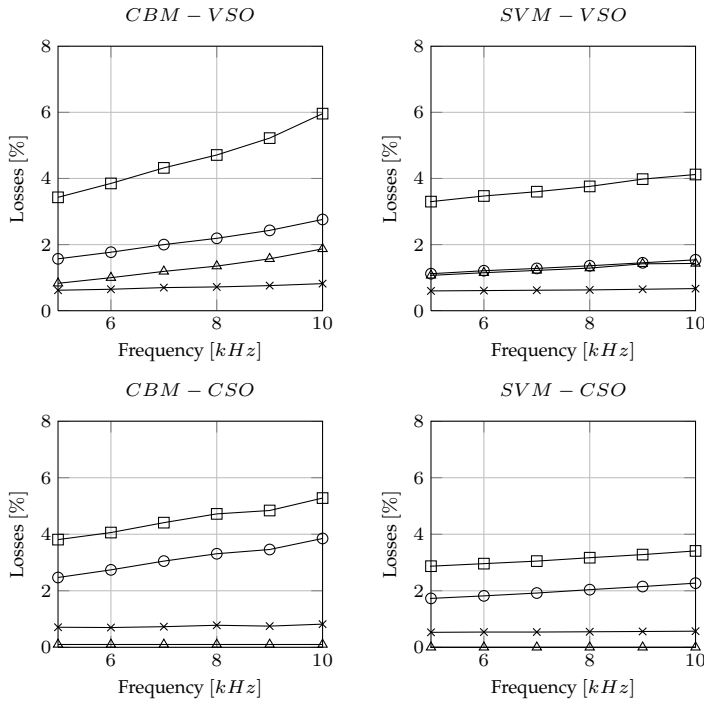
Figure 3.20: Losses for different types of modulation and operation principles: Reduced matrix converter(—○—), full bridge diode rectifier (—×—), clamp circuit(—△—), total losses (—□—)

with higher harmonic distortion on the three-phase side. This harmonic distortion has influence on machine losses and the torque. Oscillating torque reduces lifetime of the shaft.

The wind velocity has an influence on the operation of the converter as shown in Figure 3.21. For conventional maximum tracking point control, the rotational and electric speed in the permanent magnet machine is proportional to the wind velocity for values below the nominal (which is $10[m/s]$ in this case). For values higher than the nominal velocity, the rotational speed is fixed to the nominal value. The currents in the machine are controlled by the RMC in such a way that I_d is maintained in zero and I_q is calculated according to the power generated by the turbine. In all the cases, space vector modulation presents better results. Current source operation is efficient for wind velocities higher than $7[m/s]$. High wind velocities are expected in offshore wind farms. Therefore, current source operation is the most suitable solution. However, with wind velocities between $4[m/s]$ and $7[m/s]$ voltage source operation is more efficient. Notice that the simulation was carried out for nominal DC voltage in VSO and nominal DC current in CSO; for series connection the current is controlled by the converter on-land and depends on the dispatch strategy of the
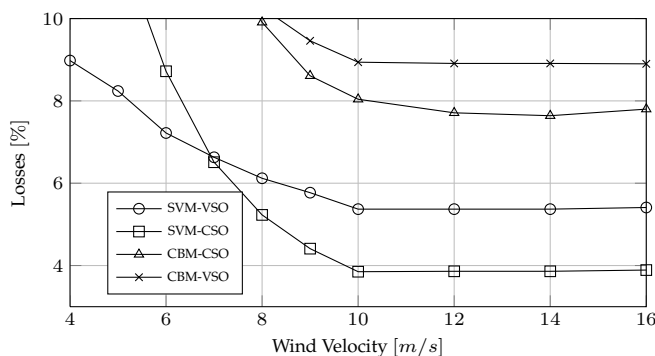
Figure 3.21: Comparison of losses at different wind velocities

entire park as will be discussed in Chapter 5. An optimal power flow must be used for low wind velocities to reduce the losses of the entire system. For example, if the DC current was reduced to $800[A]$ for a wind velocity of $6[m/s]$ the total losses would be reduced from 8.72% to 7.27%.

3.7   Proof of concept

In order to prove the modulation, an experimental set-up was built as shown in Figure 3.22. Only space vector modulation for current source operation was tested since the simulation and analysis demonstrated the advantages of this type of operation. The parameters of this set-up are shown in Appendix B. The modulation was programmed using Verilog as programming language and an APA300 field programmable array (FPGA) board. The FPGA board receives the pulse duration τ_{xyz} from a digital signal processing board (DSP). In this case, a TSM320C6713 floating point Texas Instrument DSP was used.

Figure 3.23 shows the waveform of the current in the high frequency transformer. Notice some spikes when the polarity of the current changes. This is because of the parasitic capacitances in the transformer. This effect is negligible at low-frequency but becomes important at high frequency operation. In order to reduce this parasitic capacitances the design of the transformer must be to faced. A very compact transformer could have a high capacitance. Therefore, designing the transformer is a compromise between losses, size and parasitic capacitances. The design of the transformer was not part of the objectives of the thesis. The simulation results considering this parasitic capacitance effects are shown in Figure 3.24.

Voltage and current in the high frequency transformer are shown in Figure 3.25. The voltage is symmetrical without any spikes. As aforementioned, the current presents some spikes that can be visualized in this figure. Overlapping can be used
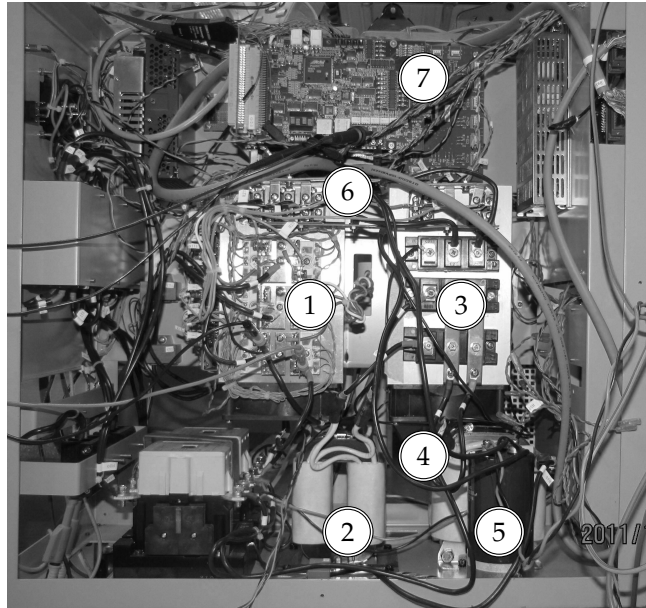
Figure 3.22: Experimental set-up. (1) Reduced matrix converter. (2) High frequency transformer. (3) Full bridge diode rectifier. (4) DC filter. (5) Capacitance clamp circuit. (6) Clamp circuit. (7) Control board

in this type of modulation since it is a current source converter. However, when overlapping is used, the spikes are not eliminated but moved ahead as shown in Figure 3.26. This test was made at low voltage and current. Notice the spikes are proportionally larger at low voltage than at high voltage. Moreover, the current waveform is less flat and noisy.

A second option is to use dead time instead of overlapping as shown in Figure 3.27. In this case there are spikes in both voltage and current. This is an expected result since the operation of the converter is current source. As a consequence of that, a small overlapping is beneficial for the operation of the converter in order to avoid spikes on the voltages. However, spikes in the current cannot be eliminated by the modulation itself.

The AC current in the three-phase side is shown in Figure 3.28. Low harmonic distortion is obtained. This is a good feature of the converter since the harmonic distortion in the current is directly related with oscillations in the torque which reduce the lifetime of the shaft.

In all cases described above, the converter was operated at constant modulation index. The angle required for space vector modulation was calculated using the voltage in terminals of the converter and phase locked loop algorithm. Unity power factor is achieved. The phase locked loop will be presented in the next chapter

where the control of the converter are going to be studied.
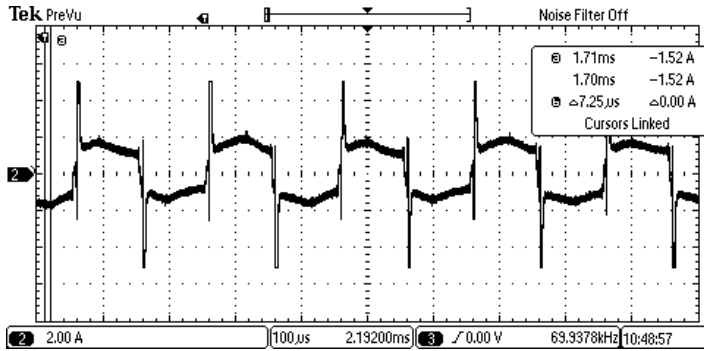
Figure 3.23: Experimental result of the current at the high frequency transformer for operation at 120 V and 4 A
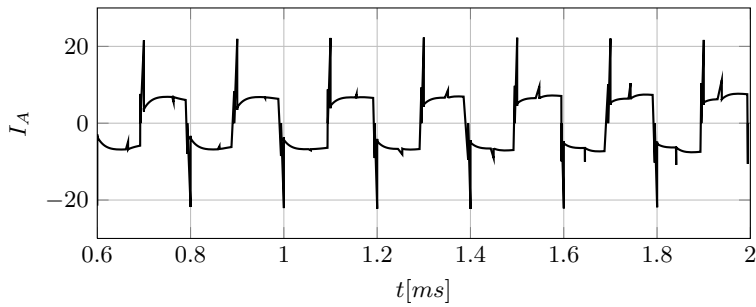
Figure 3.24: Simulation result of the current at the high frequency transformer for operation at 120 V and 4 A
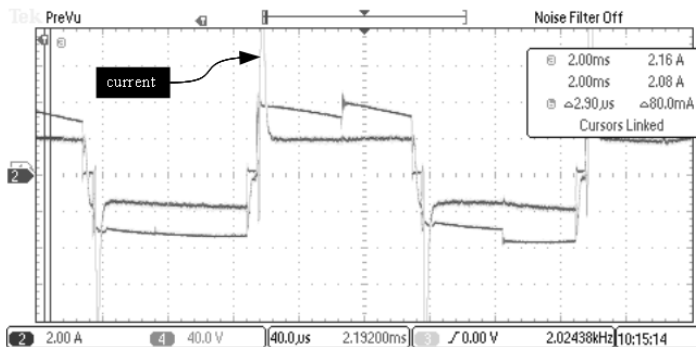
Figure 3.25: Current and Voltage in the high frequency transformer for operation at 80V
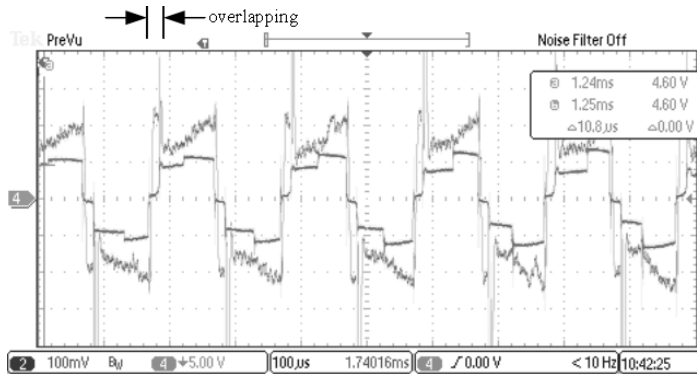
Figure 3.26: Current and Voltage in the high frequency transformer with overlapping
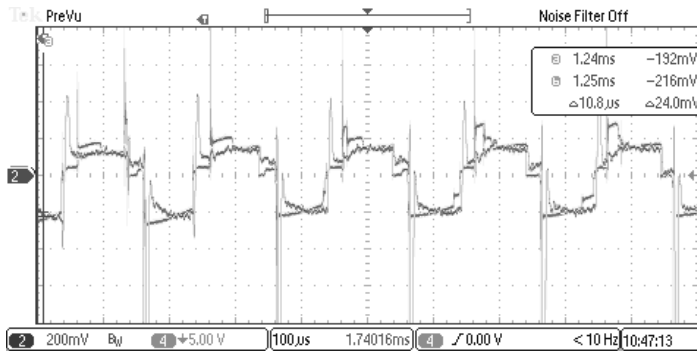
Figure 3.27: Current and voltage in the high frequency transformer with dead time
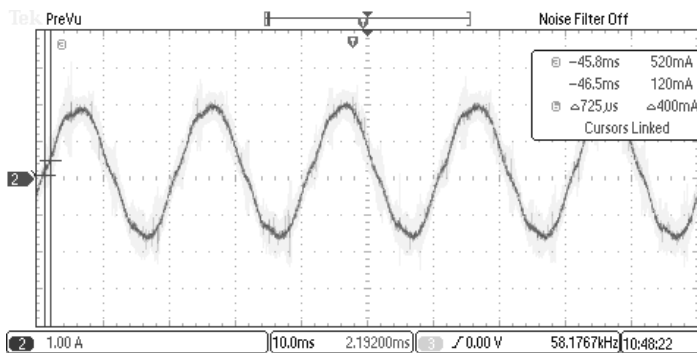
Figure 3.28: AC current in the reduced matrix converter (Experimental)

3.8 Final considerations about the modulation

In all the cases studied a modified space vector modulation presents lower losses than carrier-based modulations. Conduction losses are the same no mater the type of modulation or operation principle. In general current source operation is more convenient for series connection since the current can be controlled on-land. Total losses were lowest in current source operation since the DC chopper in the clamp circuit is not operated in stationary state. This operation is most suitable for series connection because the DC current can be controlled by the converter on-land. Therefore, series connection is the most efficient alternative not only according to the grid losses but also to the converter losses themselves. However, current source operation poses considerable challenge from the control point of view. This issue will be discussed in the next chapter.

Comparatively, losses in the machine and the transformer are lower than the losses in the reduced matrix converter. On the other hand, the wind velocity as well as the DC current affects the losses from the converter. Due to the small value of the modulation index at low wind velocities, the losses in percentage are higher if the DC current is maintained at the nominal value. Therefore, an optimal power flow must be developed to reduce the losses at such operative conditions.

4

Control of the Converters

This chapter studies the optimal control for the high frequency link and the pulse width modulated current source converter placed on-land. A linear quadratic regulator is used in the inner loop. The operation features of this control are tested in stationary state and transients.

THE proposed conversion system as well as the series connection require operation as a current source converter. As was demonstrated in the last chapter, the proposed a high frequency link operates at maximum efficiency when it is modulated in current mode. On the other hand, the shared current in the grid must be controlled by the on-shore converter. As was presented, in Chapter 2, this converter is a pulse width modulated current source converter (PWM-CSC) which must be controlled to achieve two objectives: to maintain a constant DC current and compensate the power factor in the AC side. Both, the RMC and the PWM-CSC are then controlled by the same principle.

Figure 4.1 depicts the control of the on-land converter and the reduced matrix converter. An inner loop controls the current in the three phase side. Then, an outer loop controls the speed and the power in the converters placed offshore and the DC current and power factor in the PWM-CSC placed on-land. These controls are local and designed using optimal control theory. A secondary control is proposed for stationary state in order to coordinate the generation resources. This chapter will study the control of the converters while the stationary state control will be investigated in the next chapter.
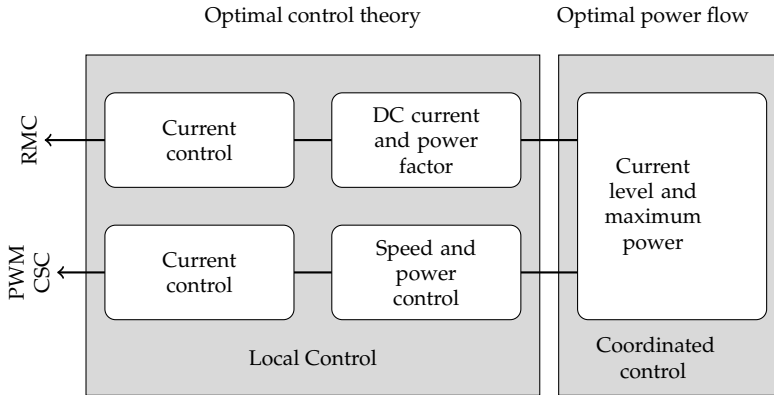
Figure 4.1: Schematic representation of the control

4.1 Optimal control

Proportional-Integral (PI) controls have for years been the standard in power electronic applications. PI controls have some advantages compared with other techniques. For example, a PI control can deal with linear as well as non-linear systems. In addition, they are simple and robust for practical implementation. However, most of the time, PI controls are tuned by trial and error approaches. Multiple input - multiple output (MIMO) systems are not directly considered and anti-windup strategies are required to avoid saturation in the integral gain when the control objective changes or the converter operates in over-modulation. More sophisticated techniques can deal with MIMO systems with changes in the control objective. However, they are usually more complex in implementation and require high computation effort.

Another approach is optimal control which is based on an optimization algorithm. Optimal control can achieve a simple implementation with low computational effort and at the same time a rigorous mathematical formulation. Moreover, it can deal naturally with a multiple input - multiple output system. The general optimal control formulation for a linear system is as follows:

$$Min \int_0^t X^T Q X + U^T R U \, dt \tag{4.1}$$

subject to:

$$\dot{X} = A \cdot X + B \cdot U \tag{4.2}$$

where X are the state variables and U are the control variables. The objective function 4.1 is a measure of performance of the control.
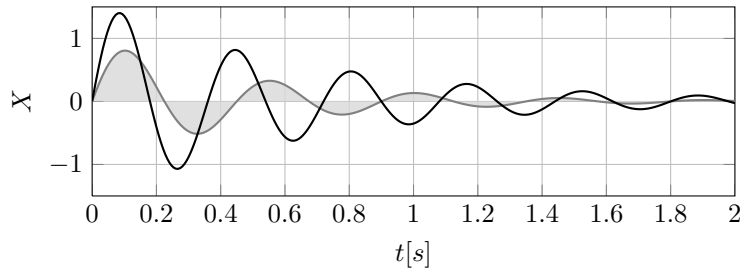
Figure 4.2: Two different trajectories

The solution of this type of optimization problems deals with calculus of variations. In this case, the problem is named optimal linear-quadratic regulator (LQR) since the system is linear and the objective function is quadratic. LQR has some well known advantages for power system applications [110], namely:

- Good gain margin

- High phase margin

- Tolerance to non-linearities

- It can manage directly MIMO systems

- The control is optimal according to a desired performance index

- Over-voltages and over-currents are directly considered in the performance index

- Implementation is as simple as proportional controls and therefore antiwindup strategies are not required when the control objective changes

Designing an LQR control requires to define correctly the objective function. To understand the idea behind this objective function consider Figure 4.2 where two different trajectories are depicted. Both trajectories are stable and achieve the desired zero reference. However, their performance is different, for example maximum overshoot, oscillations and setting time are lower in the trajectory represented by the fill area than in the trajectory represented by the thick line. Notice that that the filled area is a good measurement of the performance of the control, since the lower this area is the better the performance is. In conclusion, by minimizing this filled area in the trajectories of the state variables and the control variables, the over-voltages and over-current are minimized as well as the settle time. The problem is now how to define the performance measurement (Q and R) in a MIMO system where each variable could have a different measurement unit (Volts,Amperes,etc). However, as will be discussed in the following sections, in electrical systems it is straightforward to define the objective function due to the per unit representation.

71

In order to solve the optimization problem, let us define the Hamiltonian function $\mathcal{H}$. This function is analogous to the Lagrangian in conventional optimization problems, and permits introducing the constrains (which in this case is the dynamic system itself) inside a single objective function as given in Equation 4.3.

$$\mathcal{H} = X^T Q X + U^T R U + \lambda \cdot (A X + B U) \tag{4.3}$$

The optimality conditions are given by the following equations.

$$\frac{\partial \mathcal{H}}{\partial U} = 0 \tag{4.4}$$

$$\frac{\partial \mathcal{H}}{\partial \lambda} = \frac{dX}{dt} \tag{4.5}$$

$$\frac{\partial \mathcal{H}}{\partial X} = -\frac{d\lambda}{dt} \tag{4.6}$$

Interested reader are referred to [111] and [112] for more details about optimal control. For the proposed linear problem with R and Q constant, semidefinite positive and an infinite horizon, the feedback control defined by Equation 4.7 fulfills the optimal conditions.

$$X = K_p \cdot U \tag{4.7}$$

where the proportional gain matrix K_p is defined as Equation 4.8.

$$K_p = R^{-1} \cdot B \cdot S \tag{4.8}$$

with S calculated from the Riccati's algebraic equation:

$$A^T \cdot S + S^T \cdot A + Q - S \cdot B \cdot R^{-1} \cdot B^T \cdot S = 0 \tag{4.9}$$

In some cases, it is possible to obtain an analytical solution of S from Equation 4.9. However, most of the cases it is required a numerical approximation. This numerical algorithm is well known and is available in all mathematical softwares such as Matlab, Mathematica or Octave.

4.2 Optimal control of the generator

Although optimal control can deal directly with multiple input multiple output systems, it is more convenient to separate the control in different hierarchical stages. This is because the dynamic response of the electric part is faster than the mechanical response. This division is classical in motor drives and wind energy applications.
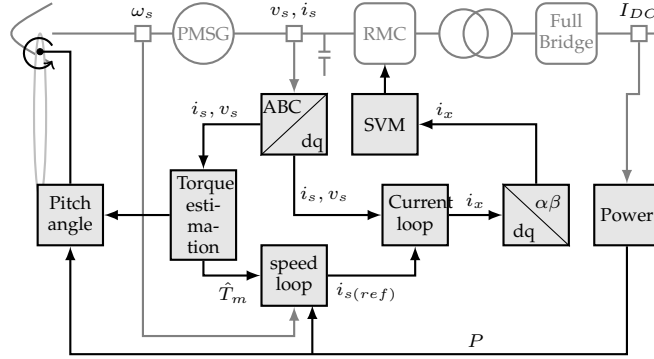
Figure 4.3: Schematic representation of the proposed optimal control

The complete control is depicted in Fig 4.3. It is separated in two hierarchical stages, namely: speed-loop and current-loop. The speed-loop controls the speed and the power according to the maximum-power-extraction strategy. Torque estimation and pitch angle control are required in this stage. The current-loop controls the currents i_s in the PMSG while the modulation directly controls the currents in the converter. Next sub-section describes the dynamic model of the electrical subsystem and the conventional approach using PI controls. After that the proposed current and speed loops using LQR are presented.

4.2.1 Dynamic model of the machine and the converter

Input and output currents in the HFL are related as given in Equation 4.10 using an average model.

$$i_{x(\alpha\beta)} = m \cdot e^{j\theta} \cdot N \cdot I_{DC} \tag{4.10}$$

where $i_{x(\alpha\beta)}$ are the input currents in $\alpha\beta$ reference frame, N is the transformation ratio of the high frequency transformer, I_{DC} is the DC current and m and θ are the modulation index and its angle respectively. i_x is directly controlled by the modulation of the converter. Figure 4.4 shows the schematic representation of the variables in the converter in dq reference frame.
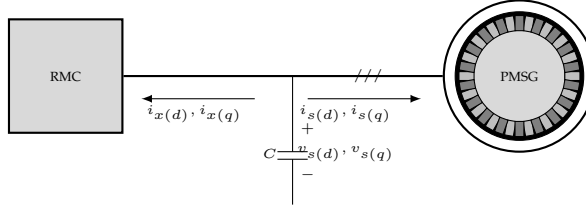
Figure 4.4: Schematic representation of the converter

The PMSG is modeled in the rotor reference frame (dq) as follows:

$$v_{s(d)} = R_s \cdot i_{s(d)} + L_d \cdot \frac{d}{dt} i_{s(d)} - L_q \cdot \omega_s \cdot i_{s(q)} \tag{4.11}$$

$$v_{s(q)} = R_s \cdot i_{s(q)} + L_q \cdot \frac{d}{dt} i_{s(q)} + L_d \cdot \omega_s \cdot i_{s(d)} + \psi_m \cdot \omega_s \tag{4.12}$$

where ω_s is the electric rotational speed, R_s is the stator resistance, L_d and L_q are the inductances of direct and quadrature axes, $i_{s(d)}$ and $i_{s(q)}$ are the stator currents, $v_{s(d)}$ and $v_{s(q)}$ are the stator voltages and ψ_m is the flux of the permanent magnets.

On the other hand, the dynamics of the capacitive filter in dq reference frame is given by Equation 4.13

$$C_s \cdot \frac{dv_{s(dq)}}{dt} + i_{x(dq)} + i_{s(dq)} + j\omega_s C_s \cdot v_{s(dq)} = 0 \tag{4.13}$$

where C_s is the capacitance, i_s is the current of the PMSG and v_s its voltage (which is the same as the capacitive filter). The capacitive filter is selected using a cut-off frequency w_c lower than the switching frequency:

$$C_s = \frac{1}{L_q \cdot w_c^2} \tag{4.14}$$

The electromagnetic torque is defined by Equation 4.15:

$$T_E = \frac{3}{2} \cdot \left(\frac{np}{2}\right) \cdot i_{s(q)} \cdot \psi_T \tag{4.15}$$

with ψ_T the total flux defined as in Equation 4.16.

$$\psi_T = \psi_m + (L_d - L_q) \cdot i_{s(d)} \tag{4.16}$$

74
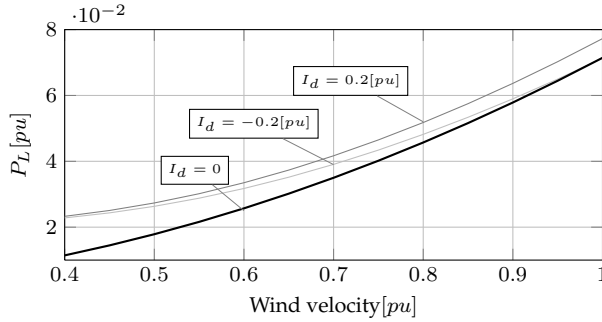
Figure 4.5: Losses in the PMSG for different V_ω and I_d

If the current $i_{s(d)}$ is kept constant, the flux ψ_T is also maintained constant. The value of $i_{s(d)}$ deals with the efficiency of the machine, and must be determined according to the electric parameters. Losses in the permanent magnet synchronous generator with different wind velocities are presented in Figure 4.5. The parameters of the machine are described in Appendix B, Table B.1. For most cases $L_d \approx L_q$ and therefore $i_{s(d)} = 0$ produces the lowest losses. In that case the torque becomes proportional to $i_{s(q)}$. In the case of a wind turbine a one-mass model describes the dynamics of the mechanical speed as given in Equation 4.17.

$$\frac{d\omega_m}{dt} = \frac{1}{J_m}\left(T_m + T_E\right)$$
(4.17)

where ω_m is the mechanical rotational speed, T_m is the mechanical torque, T_E is the electrical torque and J_m is the inertia machine-turbine. The mechanical torque T_m is related to the mechanical power P_m and the rotational speed ω as given in Equation 4.18.

$$T_m = \frac{P_m}{\omega}$$
(4.18)

Notice the mechanical power is directly related to the wind velocity as was demonstrated in Chapter 2 and Equation 2.5.

4.2.2 Conventional approaches

In some applications the line current i_s is indirectly controlled by the modulation of the converter without any additional control, by imposing the references values $i_{x(d)} = 0$ and $i_{x(q)} = I_{q(ref)}$. However, the dynamic behaviour of this approach is not suitable for wind energy applications. For the sake of simplicity, let us consider
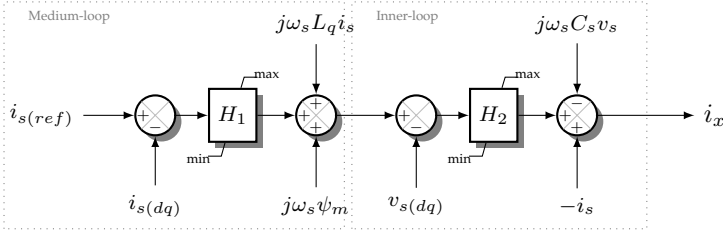
Figure 4.6: Current control using an inner and medium loop in dq reference frame

$L_d = L_q$ and define a new term $\sigma = R_s/L_s$. In that case, the current in the machine is given by Equation 4.19.

$$i_{q(s)} = \frac{w_c^2 \left(S^2 + \sigma S + w_c^2 - w_s^2\right) I_{q(ref)} - S \cdot \left(S^2 + \sigma S + w_c^2 + w_s^2\right) w_s \psi_m + \sigma w_s^3 \psi_m}{S^4 + 2\sigma S^3 + (\sigma^2 S^2 + 2(w_s^2 + w_c^2))S^2 + 2\sigma(w_c^2 + w_s^2)S + w_s^2 \sigma^2 + (w_c^2 - w_s^2)^2}$$
(4.19)

By using this open-loop control the stationary state, although is small, is not zero. In addition, the poles of the system are highly dependent of the operative frequency w_s which changes according to the wind velocity.

Another approach is to use proportional-integral controls. In that case, the control requires three stages [51]: an inner-loop which controls v_s using i_x, a medium-loop which controls i_s using v_s, and an outer-loop which controls ω_s using i_s. The inner and medium loop in dq reference frame are shown in Figure 4.6 where H_1 and H_2 are proportional-integral controls as given in Equation 4.20 and 4.21 using Laplace representation.

$$H_1 = k_{p1} \left(1 + \frac{1}{\tau_1 S}\right)$$
(4.20)

$$H_2 = k_{p2} \left(1 + \frac{1}{\tau_2 S}\right)$$
(4.21)

The desired current $i_{s(ref)} = 0 + jI_{q(ref)}$ in the PMSG is given by the speed/power loop. Let us replace the control in Equations 4.13, 4.11 and 4.12 (in Laplace representation):

$$C_s S \left((R_s + L_d S)i_{s(d)} - \omega_s L_q i_{s(q)}\right) - H_2 \left(H_1 + R_s + L_d S\right) i_{s(d)} = 0$$
(4.22)

$$
\begin{aligned}
&C_s S\left((R_s + L_q S)i_{s(q)} + \omega_s L_d i_{s(d)} + \psi_m \omega_s\right) - \\
&H_2\left(R_s + L_q S\right)i_{s(q)} + H_2 H_1(I_{q(ref)} - i_{s(q)}) = 0
\end{aligned}
\tag{4.23}
$$

Notice that, as desired, $i_{s(d)} \to 0$ and $i_{s(q)} \to I_{q(ref)}$ when $S \to 0$. However, the resulting transfer function is a 12-order function. It is true that by proper design of the proportional and integral gains is possible to improve the transient behaviour of this control, but is equally true that the overshooting and oscillatory behavior cannot be completely eliminated. Optimal control reduces the inner and medium loops to only one inner current control as will be demonstrated in the next section with a better transient behaviour.

4.2.3 Inner loop using optimal control

A linearized model of the machine is defined in Equation 4.2 where X are the state variables as follows:

$$
X = \left(\begin{array}{cccc} i_{s(d)}, & i_{s(q)}, & v_{s(d)}, & v_{s(q)} - \psi_m \omega_s \end{array}\right)^T
\tag{4.24}
$$

U are the currents that are directly controlled by the modulation of the converter:

$$
U = \left(\begin{array}{cc} i_{x(d)}, & i_{x(q)} \end{array}\right)^T
\tag{4.25}
$$

The state matrix A depends on the speed as given in Equation 4.26. However, it can be assumed as a constant matrix since the speed has a slow dynamic response in comparison to the electrical variables.

$$
A(\omega_s) = \begin{pmatrix}
-\frac{R_s}{L_d} & \frac{L_q}{L_d}\omega_s & \frac{1}{L_d} & 0 \\
-\frac{L_d}{L_q}\omega_s & -\frac{R_s}{L_q} & 0 & \frac{1}{L_q} \\
-\frac{1}{C} & 0 & 0 & \omega_s \\
0 & -\frac{1}{C} & -\omega_s & 0
\end{pmatrix}
\tag{4.26}
$$

The input matrix B is given by 4.27.

$$
B = \frac{1}{C_s}\begin{pmatrix} 0 & 0 & -1 & 0 \\ 0 & 0 & 0 & -1 \end{pmatrix}^T
\tag{4.27}
$$

Conventional optimal control is designed for a zero-equilibrium point. In this case, $i_{s(d)} \to 0$ but the current $i_{s(q)}$ must be a value defined by the speed/power

controller (outer loop). Therefore, the feedback control has to be modified as given in Equation 4.28.

$$U = K_p \cdot (X_r - X) + U_r \tag{4.28}$$

The reference vectors $X_r = \left(x_{r(1)}, x_{r(2)}, x_{r(3)}, x_{r(4)} \right)^T$ and $U_r = \left(u_{r(1)}, u_{r(2)} \right)^T$ are defined as follows:

$$X_r = \begin{pmatrix} 1 & 0 & R_s & L_d \omega_s \\ 0 & 1 & -L_q \omega_s & R_s \end{pmatrix}^T \cdot \begin{pmatrix} i_{sd(ref)} \\ i_{sq(ref)} \end{pmatrix} \tag{4.29}$$

$$U_r = \begin{pmatrix} x_{r(1)} \\ x_{r(2)} \end{pmatrix} + \omega_s C \begin{pmatrix} -x_{r(4)} \\ x_{r(3)} \end{pmatrix} \tag{4.30}$$

The weight factors Q and R are defined according to the nominal voltages and currents in order to achieve per unit representation as shown in Equations 4.31 and 4.32

$$Q = Diag \left(\frac{1}{I_{nom}^2}, \quad \frac{1}{I_{nom}^2}, \quad \frac{1}{V_{nom}^2}, \quad \frac{1}{V_{nom}^2} \right) \tag{4.31}$$

and

$$R = Diag \left(\frac{1}{I_{nom}^2}, \quad \frac{1}{I_{nom}^2} \right) \tag{4.32}$$

The entire control is represented in Figure 4.7. Notice the feedback control represented by Equation 4.28 is as simple as a proportional control from the implementation point of view. Nevertheless, the proportional gain is a matrix and not a simple constant. Therefore, interactions between variables are considered. This interaction between variables is taken into account in conventional PI controls by subtracting the coupling terms $j\omega_s C v_s$. In this case, it is considered by the terms $K_{p(13)} \cdot v_{s(d)}$ and $K_{p(24)} \cdot v_{s(q)}$.
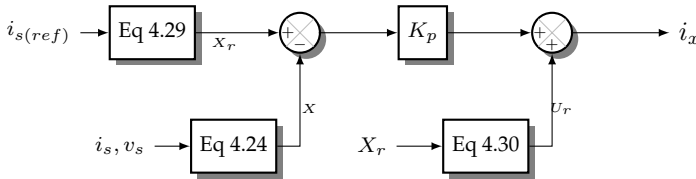
Figure 4.7: Inner current control in the matrix converter

Conventionally, current source converters have undesired resonances due to the capacitive filter. To avoid these negative effects, an active damping strategy must

be used [113]. Optimal control however, can solve the problem in just one stage of control without active damping control. This is due to the capability to deal with multiple input - multiple output systems.

4.2.4 Outer loop

According to the maximum usable energy, the proposed control considers two main operative points: maximum tracking point and constant power. For wind velocities below the nominal, the rotor speed must be controlled to extract the maximum power available from the wind. When the wind velocity increases, the available power becomes superior to $1[pu]$. However, due to physical constrains in the turbine ($T_{E(max)}$) and the electric conversion system ($I_{dq(max)}$), the generated power must be reduced until $1[pu]$. Thus, the available power considering these constrains is given by Equation 4.33

$$P_{pu} = \left\{ \begin{array}{cc} V_{w(pu)}^3 & V_{w(pu)} < 1 \\ 1 & V_{w(pu)} \geq 1 \end{array} \right. \tag{4.33}$$

At high wind velocities, the reduced matrix converter must be controlled to maintain a constant active power. The pitch angle is used to reduce the required torque and to maintain the speed. The maximum available power is below $1[pu]$ for low wind velocity conditions. In this operative point, the reference for the speed is equal to the wind velocity per unit in order to extract the available energy from the wind and maintain optimal tip speed ratio (see Equation 2.6). From the point of view of the converter, the torque equation is linear and the mechanical torque is considered as a disturbance. Therefore, an estimator of the mechanical torque is required.

The rotational speed ω_s is used as a variable to estimate the mechanical torque. The value of ω_s is known by measurement or by the PLL. If the mechanical torque is estimated, then it is possible to have an estimation of the rotational speed. Therefore, the estimated speed $\hat{\omega}_s$ is given by:

$$\hat{\omega}_s = \frac{1}{J_m} \int_0^t \left(T_E(\tau) + \hat{T}_m(\tau) \right) d\tau \tag{4.34}$$

where $\hat{T}_m$ is the estimated mechanical torque. Suppose there is a proportional estimation as shown in Equation 4.35.

$$\hat{T}_m = K_E \cdot (\omega_s - \hat{\omega}_s) \tag{4.35}$$

By replacing Equation 4.35 into Equation 4.34 it is straightforward to demonstrate this proportional gain can estimate T_m and when $\hat{\omega}_s \rightarrow \omega_s$ then $\hat{T}_m \rightarrow T_m$. The estimator is depicted in Figure 4.8.
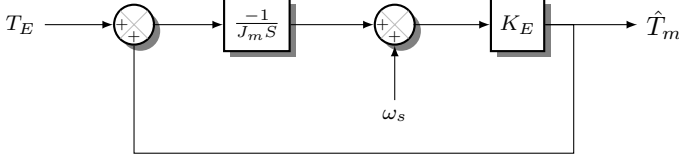
Figure 4.8: Estimation of the mechanical torque

Once the mechanical torque is known, Equation 4.17 becomes linear and can be solved using linear optimal control with the control variable U defined as:

$$U = T_E + \hat{T}_m \tag{4.36}$$

and only one state variable X:

$$X = \omega_s - \omega_{s(ref)} \tag{4.37}$$

The parameters of the resulting linear model are $A = 0$ and $B = \frac{1}{J_m}$. The optimal control is again a simple proportional control as follows:

$$U = K_m \cdot X \tag{4.38}$$

with the weight factors defined as:

$$Q = \frac{1}{w_{nom}^2} \tag{4.39}$$

$$R = \frac{1}{T_{nom}^2} \tag{4.40}$$

Returning to the original variables the control is given by Equation 4.41.

$$I_{q(ref)} = \frac{3/2}{np \cdot \psi_m} \left(K_m \cdot (\omega_s - \omega_{s(ref)}) - \hat{T}_m \right) \tag{4.41}$$

Notice that the final control is similar to a PI control where the optimal feedback K_m is the proportional part and the estimation of the torque is the integral part. Optimal control can also be used to design PI controls. However, the advantage of

this approach is the behaviour when the control objective changes. In a PI control, if the control objective changes, the integral part saturates and special anti-windup techniques are required. When the objective control returns to velocity control, the integral part is saturated or restarted from zero. In this case, the integral part is replaced by an estimator. The estimator continues to estimate the mechanical torque even during power control. After return to speed control the value of $\hat{T}_m$ is not saturated and even more accurate. The pitch angle is maintained in zero during speed control in order to achieve maximum transfer of power.

When the wind velocity is higher than $1[pu]$ the control objective changes. I_q must be controlled in order to obtain nominal power while the pitch angle maintains the velocity. For power control the model becomes in a static plant where a proportional control is enough. The power equation is linearized as follows:

$$\Delta P = \omega_s \Delta T_E + T_E \Delta \omega_s \tag{4.42}$$

A proportional control over the linearized model gives:

$$\Delta T_E = -K_g \cdot \frac{1}{\omega_s} \left(P_{(ref)} - P \right) \tag{4.43}$$

Replacing the control on the model, the expected mismatch in the power can be calculated:

$$\Delta P = \frac{T_E \Delta \omega_s}{1 + K_g} \tag{4.44}$$

Notice that if $\Delta \omega_s \to 0$ then $\Delta P \to 0$. In addition, if $K_g \geq 0$ then the error in P is even lower. Therefore, a proportional control is suitable to control the power, the tracking error is not completely zero but it is small enough. A wind farm is never in a real stationary state and hence a precise power control is not really required.

The speed is controlled by the pitch angle. In this case the same optimal strategy can be used, so that T_m is used as control variable. The value of T_E can be calculated directly using the measured current I_q. The control for the mechanical torque becomes:

$$T_m = K_m \cdot (\omega_s - \omega_{s(ref)}) - T_E \tag{4.45}$$

once the desired T_m is calculated the mechanical power is $P_m = T_m \cdot \omega_m$ and the required pitch angle is given as following:

$$\beta = -27.54 - 68.33 \cdot P_m + 81.35 \cdot V_\omega + 58.91 \cdot V_\omega \cdot P_m - (39.06 - 13.3 \cdot P_m) \cdot V_\omega^2 + 6.871 \cdot V_\omega^3$$
$$(4.46)$$

The above expression was found fitting the data obtained by mapping the Equation 2.5 over a grid of 50 different pitch angles in the domain $[0^o - 40^o]$ and same amount wind velocities in the domain $[4m/s, 20m/s]$. This non-linear function could be also approximated by a look-up table or by a neural network. The control of the pitch angle must consider the maximum available change $\approx 8^o/s$. When the wind velocity is below to the nominal value, the pitch angle must decrease to zero considering this maximum change constrain. Wind velocity V_ω is required in order to determine the set-point of the proposed control. In this case $\hat{T}_m$ is used to estimate the wind velocity by inversion of the Equation 2.5 using numerical approximation [114].

4.2.5 Control during abnormal operation and stationary state

During abnormal operation, for example short circuit, the generated power must be reduced in order to guarantee safe operation. For voltages or currents higher than maximum feasible, the power must be reduced. The reference for the power control is given by Equation 4.47.

$$P_{ref(r)} = P_{ref} - K_{s1} \cdot H \left(V - V_{max} \right) - K_{s2} \cdot H \left(I - I_{max} \right) \qquad (4.47)$$

where H is the Heaviside step function. Using this function, the reference of the power (P_{ref}) corresponds to the maximum power tracking strategy unless an abnormal operation is detected. In that case, the electric power must be decreased according to the values of K_{s1} and K_{s2}. An over-voltage occurs when one turbine has high wind conditions and other very low wind conditions. This condition must be avoided in stationary state by means of the tertiary control, but during transients it must be faced by the control. By reducing the power in this case, the voltage will be also reduced. On the other hand, over-current conditions must be avoided by the same strategy when reducing the generated power. The most feasible case for over-current is a short circuit in the DC line. In this case, the short circuit current is supplied by the turbines. Therefore, the turbines must reduce their power until the fault is cleared.

In stationary state, the reference of the power and the DC current must be calculated according to an optimal power flow for series connection which will be presented in Chapter 5. It consist in a non-linear programming model which minimizes the transmission losses taking into account the electric constrains. The result of the optimization algorithm is the set point for the maximum power at each turbine and the DC current. Is specially important the set point of the current, since low currents

mean low losses, but the capability to control the output power is reduced. Therefore, at high wind velocities, the set point of the current must be increased in order to extract the maximum amount of power. The complete process could be done by defining a relation between the average wind velocity and the current but an optimization approach is better since the electric constrains are taken into account in the model.

4.3 On shore converter

The on-land converter is a PWM-CSC operated at medium frequency ($2[kHz]$). This converter has the capability of controlling the DC current and the output power factor. The PWM-CSC converter was presented in Figure 2.9. The currents i_x are directly controlled by the modulation while the output currents i_r are used to control the reactive power and the DC current. Therefore, an strategy of inner and outer loop is required. The state matrix is modified as follows:

$$A = \begin{pmatrix} -\frac{R_r}{L_r} & -\omega & \frac{1}{L_r} & 0 \\ \omega & -\frac{R_r}{L_r} & 0 & \frac{1}{L_r} \\ -\frac{1}{C_r} & 0 & 0 & -\omega \\ 0 & -\frac{1}{C_r} & \omega & 0 \end{pmatrix} \tag{4.48}$$

and the state variables are:

$$X = \begin{pmatrix} i_{r(d)}, & i_{r(q)}, & v_{r(d)} - v_{grid(d)}, & v_{r(q)} \end{pmatrix}^T \tag{4.49}$$

where v_{grid} is the voltage in the point of common coupling. The model is exactly the same as the model for the permanent magnet synchronous generator, just now the parameters are different. Therefore the same strategy for the inner loop is used. For the outer loop, the DC current must be controlled. For unity power factor $i_{sq(ref)} = 0$ and the DC current is controlled using i_{rd}. Let us consider the DC power given by Equation 4.50

$$P = \left(\frac{L_{dc}}{2}\right) \frac{d}{dt}(I_{dc}^2 - I_{ref}^2) + R_{dc} \cdot I_{dc}^2 + P_o \tag{4.50}$$

where P is the active power delivered to the grid which is proportional to the current I_d in the AC side if losses in the converter are neglected. P_o is the power generated offshore and I_{dc} is the DC current. The system is linear with $X = I_{dc}^2 - I_{ref}^2$. The disturbance P_o must be estimated. The problem is very similar to the pitch angle control. However, in this case, a different approach will be used. Since it is not required to change between control objectives, a PI control is more suitable than

an estimation. Fortunately, optimal regulator theory also permits the design of PI controls [112].

The system has the same structure as Equation 4.2 with $A = 2R_{dc}/L_{dc}$ and $B = 2/L_{dc}$. Although the disturbance P_o can be estimated or even measured, it will be assumed unknown. (This is a practical advantage since no fast communication will be required). Lets us define an augmented system:

$$\frac{d}{dt}\begin{pmatrix} X \\ U_x \end{pmatrix} = \begin{pmatrix} A & B \\ 0 & 0 \end{pmatrix} \cdot \begin{pmatrix} X \\ U_x \end{pmatrix} + \begin{pmatrix} 0 \\ 1 \end{pmatrix} \cdot U_N \tag{4.51}$$

with $U_x = U + F \cdot B^{-1}$ (notice in this particular case B is a constant and therefore it has simple inverse). This system is exactly the same as the original one, but one additional estate variable is considered. The optimal control of the augmented system results in:

$$U_N = K_{y(1)} \cdot X + K_{y(2)} \cdot U_x \tag{4.52}$$

returning to the original variables:

$$U = \left(\frac{K_{y(2)}}{B}\right) \cdot X + \left(K_{y(1)} - \frac{K_{y(2)} \cdot A}{B}\right) \int X dt \tag{4.53}$$

which is a PI control where the control variable U gives the reference for the current $I_d = U/V_{nom}$. On the other hand I_q is maintained in zero in order to obtain unity power factor. The complete control is presented in Figure 4.9. Notice the voltage is measure in the common connection point as well as in the capacitive filters. The voltage in the common connection point is required for the phase locked loop (PLL) while the voltage in the capacitive filters is required for the inner loop control.
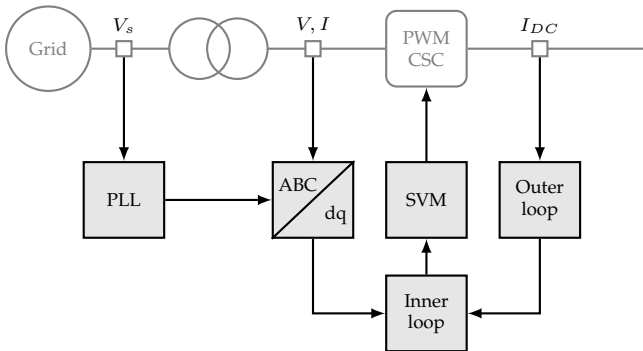
Figure 4.9: Schematic representation of the control of the pulse width modulated current source converter placed on-shore

4.4 Phase locked loop

A simple phase-locked-loop (PLL) is used to synchronize the control to the voltage of the system. This element can be used in the permanent magnet machine in order to avoid the speed sensor. It is also important in the PWM-CSC placed on-land. The structure of the control is presented in Figure 4.10. Three phase voltages are measured and transformed to the α/β reference frame. Then using a PLL and the value of the angle θ the operative frequency is calculated. Despite having an integral gain, an offset of $2\pi50$ is used in order to increase the velocity and stability of the algorithm. Finally, the angle is calculated integrating the frequency. All these calculations are made using the DSP (TMS320C6713 DSK) which allows floating point calculations.
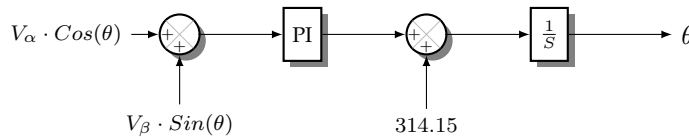
Figure 4.10: Phase locked loop for sincronization

Figure 4.11 depicts the experimental results of the implemented PLL. The black signal is the voltage after the $\alpha - \beta$ transformation while the grey signal is the angle calculated by the PLL. The algorithm was implemented as a backward Euler method. Notice the PLL can work even with a distorted sinusoidal waveform. This distortion is because of the accumulated noise due to the multiple stage of amplification in the acquisition board.
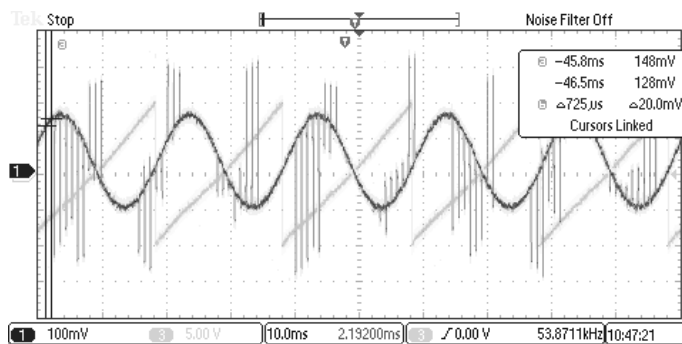
Figure 4.11: Experimental results of the implemented PLL

To visualize this result of the PLL the digital-to-analog converter in the control board was used. Therefore, the scale of the voltage doe not correspond directly to the real voltage in the converter.

4.5 Results

A simulation study was carried out to demonstrate the concept of optimal operation of series connected wind turbines. Parameters of the on-shore PWM-CSC are presented in Table B.4. Parameters of the high frequency link and the permanent magnet machine are presented in Table B.1. The optimal gain matrix K_p is given by Equation 4.54. Notice the sparsity characteristic of this matrix. Sparsity simplify the implementation of the control in a real application.

$$K_p = \begin{pmatrix} 0.399 & 0.000 & 0.166 & 0.000 \\ 0.000 & 0.399 & 0.000 & 0.166 \end{pmatrix} \tag{4.54}$$

The proposed LQR requires the parameters of the model in order to determine the feedback control. However, some parameters changes during normal operation and hence, sensitivity analysis is required. Let us define a vector χ_α as the variation of the state variables respect to each parameter in the dynamic model as follows:

$$\chi_\alpha = \frac{\partial X}{\partial \alpha} \text{ with } \alpha = \{R_s, L_q, C_s, \omega_s, \psi_m\} \tag{4.55}$$

The sensitivity function is obtained by derivation of Eq 4.2 as given in 4.56 for each parameter α.

$$\dot{\chi}_\alpha = (A - B \cdot K_p) \cdot \chi_\alpha + \left(\frac{\partial A}{\partial \alpha}\right) \cdot X + \left(\frac{\partial B}{\partial \alpha}\right) \cdot U \tag{4.56}$$

where α is the parameter to consider. Simulation results are shown in Fig 4.12. The dynamic response of the current-loop is more sensitive to the capacitance and inductance than the resistance.
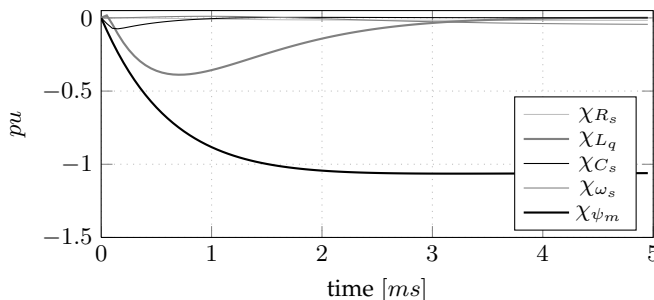
Figure 4.12: Sensitivity analysis of i_{sq} respect to the parameters of the system

The stationary state error is almost zero for different variation on these parameters. The speed and the flux are involved in the state equation but the speed is a

feedback value while the flux is a constant. Consequently, the control is almost no sensitive to variations on the speed but is very sensitive to variations on the flux. There is almost not influence in the setting time. To demonstrate that, the closed-loop eigenvalues for different rotational speed were calculated. The real part of these eigenvalues remains constant in all cases.

On the other hand, optimal gains are very robust to small variations of the parameters of the system. For example in Figure 4.13 the optimal gain $K_{p(1,1)}$ is plotted for values between 50 % to 150 % of the resistance R_s, inductance L_s, capacitance C_s and electrical speed ω_s.
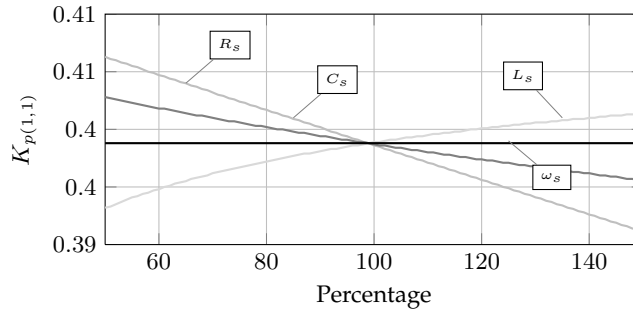
Figure 4.13: Optimal values for small variations in the parameters of the converter

Notice that the optimal value is almost invariant with respect to the velocity while variations with respect to the other parameters are very small. Robustness in the optimal tuning is important from a practical point of view since the resistance as well as the electric speed can change during normal operation.

Figure 4.14 shows the operation of the entire system. The offshore grid is represented by a Thevenin equivalent. The Thevenin voltage was determined according to the available power from the wind.
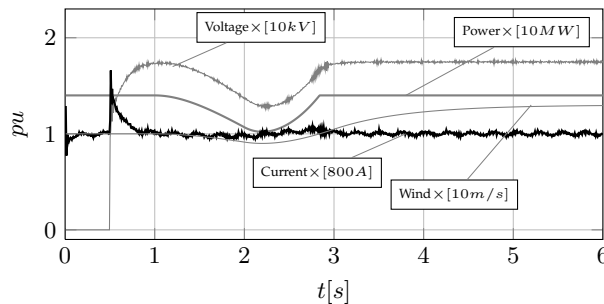
Figure 4.14: Start-up and normal operation of the PWM-CSC converter.

A single pole controller was used to model the inertia of the machines. The desired DC current is $800[A]$ and the available power is given according to the average

wind velocity. From $t = 0$ to $t = 0.5$ the offshore system is disconnected. A path for the current is given by the full bridge diode rectifier placed at the output of each turbine. The on-shore converter maintains the current at $800[A]$. At $t = 0.5$ the turbines start to generate power, a transient is created but the optimal control can lead the current to the desired value. Variations in the wind velocity after $t = 1.5[s]$ produce variations on the power and therefore in the output voltage. Nevertheless, the current remains constant in all cases.

Performance of series connection for a three phase short circuit in the network is presented in Figure 4.15. The voltage in the point of common coupling decreases creating an over current in the DC line.
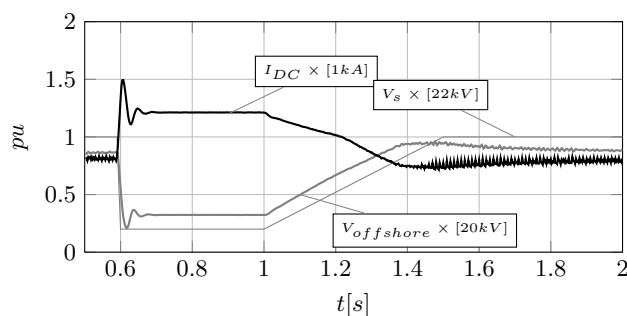
Figure 4.15: Performance of the PWM-CSC for a short circuit in the AC grid

Once the turbines detects this over-current, the output power is decreased. Due to this, the offshore voltage is also decreased. Once the grid voltage returns to its nominal value, the DC current as well as the power return to nominal operation.

For a DC fault two new mesh are created. One between the PWM-CSC and point of fault and other between the point in fault and the offshore grid. The DC current in the first mesh decreases while the DC current in the second mesh increases.
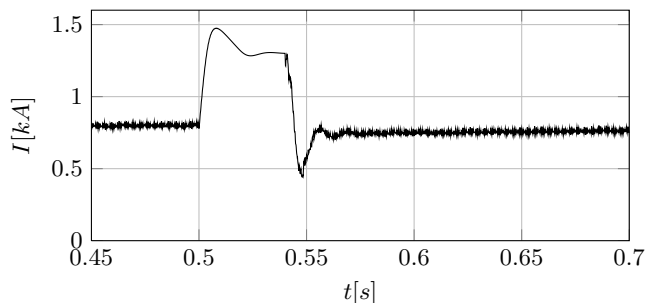
Figure 4.16: Performance of the PWM-CSC for a short circuit in the DC grid

Figure 4.16 shows the current in the second mesh. This situation is detected by the offshore grid and the output power is reduced by using the secondary control

given in Equation 4.47. The action of the control of the converters offshore is not fast enough and the current continues raising to 1.47 kA. After the fault is eliminated the complete system is restarted.

Faults in the transformer and the generator do not represent a big challenge since are AC circuits. In case of fault in a particular wind turbine the DC chopper and the full bridge diode rectifier act as a bypass (see Figure 2.11). The possible over voltage in the other turbines is faced by the DC chopper and the secondary control. The current in the DC grid for this case is depicted in Figure 4.17. The current decreases as consequence of the reduction of the power but returns to its reference value.
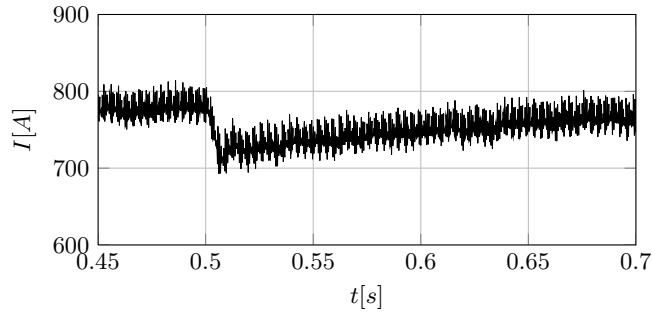
Figure 4.17: Performance of the DC current for a fault in one turbine

Three-phase voltages in the PWM-CSC are presented in Figure 4.18 for nominal operation. The harmonic contents are very low considering it is a current source converter operated at a relatively low frequency 2[kHz]. In the offshore converters, the voltage waveform is almost sinusoidal due to the high frequency operation.
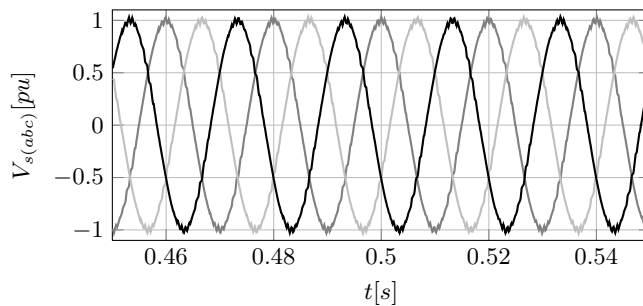
Figure 4.18: Voltages at the capacitive filter of the PWM-CSC on-land ($V_{base} = 22kV$)

Figure 4.19 illustrates the start-up of a wind generator with the high frequency link based on reduced matrix converter and optimal control. The modulation index m as well as the rotational velocity and generated power are plotted in the same figure. Behaviour is very smooth and the tracking error is zero. However, a wind park rarely has smooth and constant wind velocity - although is more probable to have

this condition in offshore parks than on land. Therefore, a simulation study with a more accurate model of the wind is presented. To avoid the undesirable effects of the ripple in the state variables, a simple low pass digital filter was implemented in order to obtain a smooth state variables.
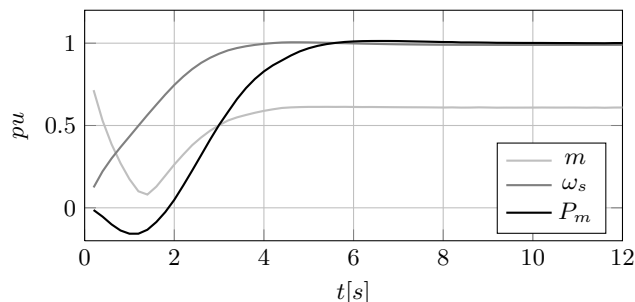
Figure 4.19: Starting up of the wind-generator with a constant wind velocity

The applied wind profile is shown in Figure 4.20. This was generated using the methodology described in Appendix C. In the simulation, the wind turbine receives the wind velocity (depicted in grey) while the controls received the average wind (in black). This average was calculated using a second order low pass filter.
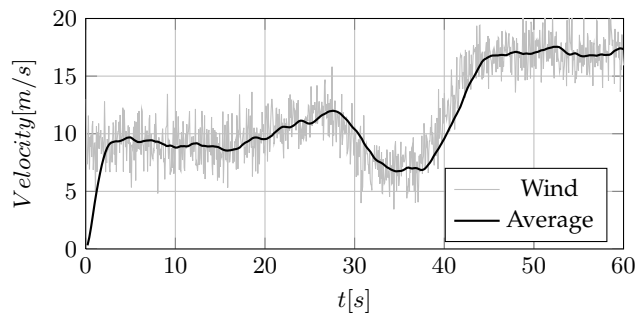
Figure 4.20: Wind Profile

Figure 4.21 presents the generated power and wind velocity for this wind profile condition. The low value of the modulation index is due to the high DC current which is controlled by the on-shore converter.

Notice the set point of the current is important from the point of view of the losses. A high DC current leads to high transmission losses. Moreover, as will be demonstrated in Chapter 5, high current also deals with a low modulation index which in turns produce low efficiency in the RMC. Nevertheless, a low DC current could lead to over-modulation in the offshore converters. The set point of the DC current is therefore an important task from the operation point of view.
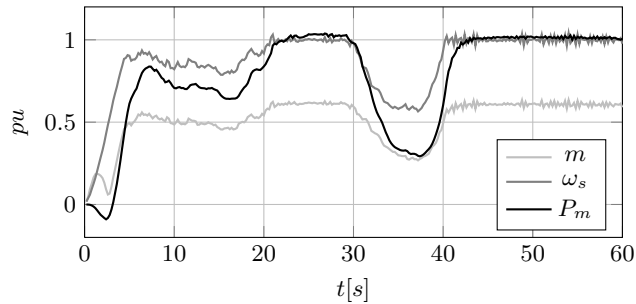
Figure 4.21: Generated power, wind velocity and modulation index for different wind conditions

4.6 Final considerations about the control

Controlling the current in a PWM-CSC is a complex task. Therefore, in this chapter, an optimal control methodology was proposed. This control is applicable to the on-shore as well as the offshore converters. A proportional plus estimation strategy was used for controlling the wind turbines. Optimal control is an efficient solution for controlling a PWM-CSC since only one stage of control is required without active damping. Output voltages and currents have a very low harmonic distortion. The proposed system can face short circuits for both the AC and DC sides.

5

Operative Considerations

This chapter presents some details about the operation of the entire park. An optimal power flow based on a non-linear programming method is presented. Long term studies based on Montecarlo simulation show some limitations of series connection when the number of series connected turbines is big and the wind velocities are not homogeneous between turbines.

SERIES connection could reduce the grid losses and investment cost since high voltage is achieved without any additional conversion/transformation stage. However, due to the aleatory nature of the wind and its turbulence, a coordinated control is necessary to avoid unequal distribution of voltages resulting in over-voltages in some turbines and under-voltages in the others. Wind velocity can be different in each turbine, meaning that the available power is also different. The DC current must be the same for all the turbines in the same cluster. Therefore, differences in the output power will create differences in the output voltage, the turbines with reduced wind velocity will present low voltages which can lead the converters into unstable operation. Meanwhile, turbines with high wind velocity will present high voltages which must be faced by the clamp circuit generating additional losses and stress.

On the other hand, the set point of the DC current must be calculated according to the wind conditions. At high wind conditions, the wind turbines are controlled in order to maintain their nominal power. Therefore, the voltages and currents are nominal. However, at low wind conditions it is desirable to decrease the set point of

the current in order to reduce transmission losses. The set point of this current is an optimization problem. Very low values of current lead to low transmission losses but could produce over-modulation in the RMCs loosing controllability. Nominal current will guarantee controllability sacrificing efficiency. At wind velocities below the nominal, the rotational speed must be equal to the wind velocity (in per unit) in order to achieve maximum tracking point. The maximum power that can be extracted from the wind is given by Equation 5.1:

$$P_{pu} = V_{w(pu)}^3 \qquad (5.1)$$

where P_{pu} and $V_{w(pu)}$ are the active power and the wind velocity both in per unit. The emf voltage in the permanent magnet machine is proportional to rotational speed. Therefore the AC current is proportional to the square of the wind velocity giving as result the minimal DC current $I_{(min)}$ required to avoid over-modulation in the reduced matrix converter. This relation is given by Equation 5.2.

$$I_{(min)} = Min \left\{ V_{w(pu)}^2 \, , \, 1 \right\} \qquad (5.2)$$

If all the wind turbines received the same wind velocity, the set point of the current is simply determined by Equation 5.2. In that case fast communication would not be required and only the value of the average wind velocity is necessary. However, for large series connected wind farms, this minimal current as well as the generated power must be determined by a coordinated control.

The objective of the coordinated control is to transfer the maximum power to the grid taking into account transmission losses and the operative limits of the system. It works as a secondary-tertiary frequency control in a conventional power system. The interconnection between on shore and offshore is calculated considering the model of the cable (T model in this case). In stationary state, only resistances have a real effect. Fast communication is not requires since this control is operated in stationary state.

A simple way to control the entire system, is to guarantee equal power generated by each turbine. This solution is possible for small and medium sized wind parks where wind velocity differences between generators are small. However, this type of strategy would be inefficient in large wind farms because the generated power would be limited by the turbine with lower wind velocity. It should be noted that in large wind farms the difference between wind velocities in the turbines could be high. Another alternative is to use conventional maximum tracking point strategy in each wind turbine. In this case, the voltage capability of each converter must be increased. Wind turbines with high wind velocities would have high voltage since the current in the entire system is constant. On the other hand, wind turbines with low wind velocities would have very low voltage. In addition, DC current must be high enough to avoid over-modulation in the wind turbines with high wind velocities. Meanwhile, the modulation index in the wind turbine with low wind velocity

is very small because the high DC current and low generated power. Efficiency in the converter is very low in this operative conditions.

On the other hand, By imposing proper constrains, it is also possible to use an optimal load flow algorithm to maximize the power on shore and minimize the losses. This optimal power flow can be solved during the operation of the system and acts as a tertiary control. Another alternative is to solve the optimization problem off-line for different scenarios. These results can be latter synthetised in a neural network or a simple lock-up table which is used for the operation of the system. The non-linear programming optimization model is presented in Equations 5.3 to 5.8:

$$max \ P_T = \sum_k P_k - R_L \cdot I_{(DC)}^2 \tag{5.3}$$

subject to

$$P_k = U_k \cdot I_{(DC)} \tag{5.4}$$

$$U_{k(min)} \le U_k \le U_{k(max)} \tag{5.5}$$

$$I_{(min)} \le I_{(DC)} \le I_{(max)} \tag{5.6}$$

$$P_{k(min)} \le P_k \le P_{k(max)} \tag{5.7}$$

$$P_{k(max)} = \left\{ \begin{array}{ll} P_{nom} \cdot \left(\frac{V_w}{V_{w(nom)}} \right)^3 & V_w \le V_{w(nom)} \\ P_{nom} & V_w > V_{w(nom)} \end{array} \right\} \tag{5.8}$$

Equation 5.3 represents the objective function which is to maximize the power transfered to shore. Equations 5.4 to 5.8 represent technical constrains. Equation 5.4 represents the active power generated by the turbine k. Equations 5.5, 5.6 and 5.7 are the operative limits in each turbine. Finally, Equation 5.8 is the available power in each turbine according to the wind velocity. Notice this value changes according to the wind fluctuations. For operation below the nominal value, the available power is proportional to the cube of the wind velocity in per unit. For wind velocities above the nominal values, the pitch angle operates in order to reduce the mechanical torque and avoid high rotational speeds and torques.

It is possible to achieve maximum-tracking point in each turbine if the electric variables in the entire cluster are within the constraints, otherwise, the electric constrains impose limits to the generated power. The optimization algorithm can

be modified to maintain more constant output power instead of maximum output power. In this case, the objective function is replaced by the one shown in Equation 5.9

$$min \ \Delta P = \frac{1}{2} \cdot (P_{expected} - P_T)^2 \tag{5.9}$$

This optimization model could be solved using any non-linear programming technique (for example the interior point method), and represents a control in stationary state. The optimization algorithm itself is so simple in this case that is not required a detailed analysis. The control is coordinated between offshore and onshore, but since it is a stationary state, no fast communication system is required. $P_{k(max)}$ is calculated according to the measured mean wind velocity. The desired output power in each turbine (P_k) as well as the set point of the DC current are the result of the optimization process. This power is used to find the reference values of pitch angle and speed. Notice the losses in the converters are not taken into account in this model. This type of losses will be considered in the next section.

The layout of the system used for the simulations is depicted in Figure 5.1. It consist on 10 series connected wind turbines of 2 MW each one. The nominal DC current is 800 A. Distance between turbines is 560 m and transmission distance is 40 km. These values were selected according to real data from [115] and [116].
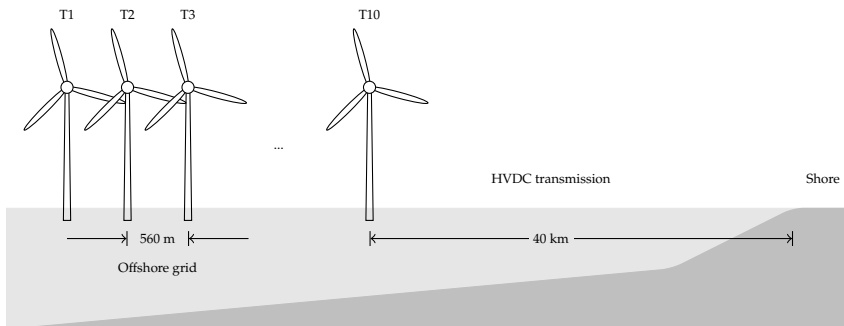
Figure 5.1: Layout of the series connected wind farm

Simulation results are depicted in Figure 5.2. Turbine T1 receives variable wind velocities while the other nine turbines receive constant wind velocities. The power in T1 varies according to the wind velocity while the power in T2-10 remains constant. The current in the DC grid is maintained on its minimal value until the wind velocity in turbine T1 achieves its nominal value. In that case the DC current must be increased in order to avoid over modulation in the converter.

Specially important is the dual variable λ_{im} related with the Constrain 5.6. It represents the variation of the objective function if the constraint is relaxed as shown in Equation 5.10:
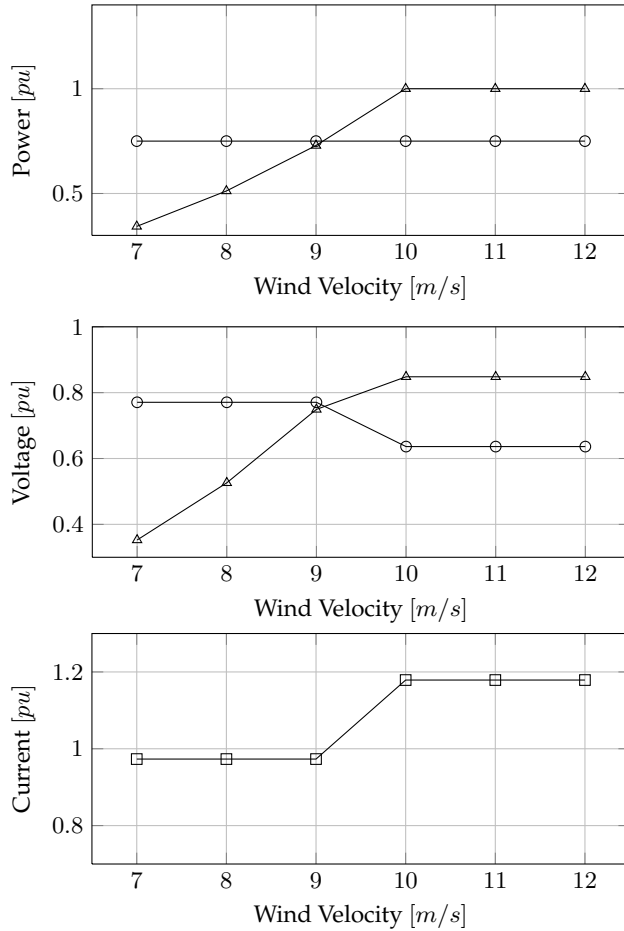
Figure 5.2: Results for the optimal operation of 10 series connected wind turbines. T1 (—△—) and T2-10 (—⊙—)

$$\lambda_{im} = \frac{\partial P_L}{\partial I_{kmin}} \tag{5.10}$$

This dual variable is off course zero for high values of wind velocity. It represents the reduction of losses if I_{min} is decreased. It means to increase the voltage ratio of the transformer. A voltage ratio grater than $1 : \frac{2}{\sqrt{3}}$ leads to lower current when the wind velocity is low. However, it decreases the efficiency of the converter since the modulation index will be lower than 1 even for nominal conditions.

5.1 Long term operation of the park

Long-term operation of the wind farm must be studied taking into account the stochastic behavior of the wind. The wind velocity is modelled as a Weibull distribution as is presented in Appendix C. A Montecarlo simulation is used to evaluate the energy production of the entire wind park. This type of stochastic simulation gives the probability distribution of the generated power and the losses. As the wind is a stochastic variable, the output power could not be guarantee in long term. What is possible to determine is the generated power and losses with a certain probability.

The pseudo-code for Montecarlo simulation is presented in Algorithm 1. In each scenario, the mean wind velocity is calculated by a random number using the Weibull cumulative distribution. Then, the wind velocity in each turbine is calculated using a normal distribution with mean equal to the mean velocity calculated previously. Variance is defined a priori. Then the optimization algorithm is called.

Algorithm 1 Montecarlo Simulation

1: **while** Convergence **do**
2: $\quad V_{w(mean)} \leftarrow WeibullDistribution(Rand)$
3: $\quad [V_w(k)] \leftarrow NormalDistribution(V_{w(mean)}, Rand)$
4: $\quad [I_{DC}, U_k, P_k] \leftarrow Optimization \qquad \triangleright$ Call non-linear programming function
5: $\quad P_L \leftarrow R_L \cdot I_{DC}^2$
6: $\quad P_G \leftarrow Sum(P_k)$
7: $\quad P_M \leftarrow LossesHFL(P_k, I_{DC}) \qquad\qquad\qquad \triangleright$ Call lookup table
8: $\quad P_D \leftarrow P_G - P_L - P_M$
9: **end while**

The non-linear optimization problem is very simple and can be solved by using recursive linearizations. The result of the optimization algorithm determines the DC current and the optimal power in each turbine for each scenario. Therefore, transmission losses P_L and total generated power P_G can be calculated. The losses in the energy conversion system (machine, RMC, transformer, clamp, diode-rectifier, filters) are calculated using a lookup table with linear interpolation. Finally, the total delivery power P_D is calculated.

The lookup table is created before using PSIM. A set of 500 simulations for different operative conditions was carried out. The losses were calculated taking into account the on-state losses of the semiconductors and passive elements as well as the turn on, turn off and reverse recovery losses at the IGBT and diodes. This is a dynamic simulation but only the stationary state values are required. Since the machine and the turbine have very low constant time, they were replaced by a Thevenin equivalent. The Thevenin's impedance is equal to the impedance of the machine. The Thevenin's voltage is calculated using the value of the power obtained in the optimization algorithm. If the power obtained in the simulation process is lower than the available power, then the voltage in per-unit is 1 otherwise it

is equal to wind velocity. The losses (P_L) of the converter in per unit over the basis of the generated power and for 10 KHz are presented in Figure 5.3.
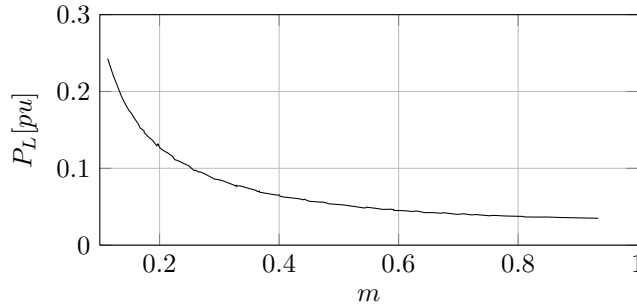
Figure 5.3: Efficiency of the high frequency link for different modulation indexes at 10 kHz operation

On the other hand, Figure 5.4 depicts the result of the Montecarlo simulation for 20000 different wind scenarios with a covariance of $\sigma^2 = 25m^2/s^2$. Each point represents a particular scenario. Notice that a conventional maximum tracking point algorithm would produce a quadratic curve in interval $[5-10]m/s$. In this case, particular scenarios require a power set-pint different from the ideal maximum tracking point curve. Therefore, the generated power is sometimes lower than ideal. For high wind conditions the dispersion of the data decrease due to the smooth action of the pitch control.

Figure 5.5 shows a histogram of the energy production of the entire park for two different covariances $\sigma^2 = 0$ and $\sigma^2 = 25m^2/s^2$. For $\sigma = 0$ all the series connected turbines receive the same wind velocity, therefore, the voltage limits are fulfilled and the energy production is maximum. For other value of covariance the energy production decreases.

Series connection is a very efficient alternative when the wind velocities are close to the turbines, otherwise it could present some negative consequences at high vari-
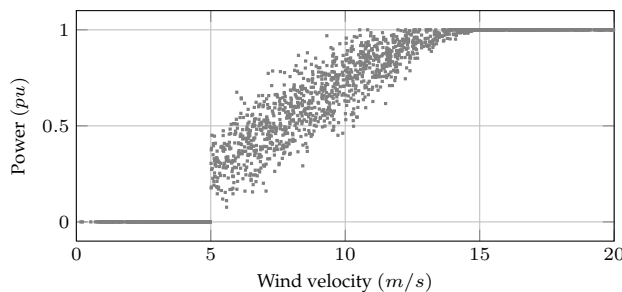
Figure 5.4: Total Generated Power for 2000 different scenarios
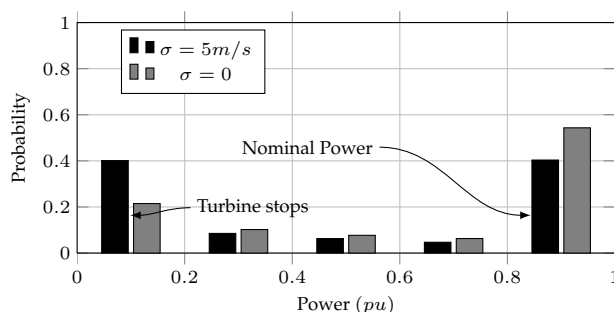
Figure 5.5: Total generated power for two different values of covariance of the wind velocity between the turbines
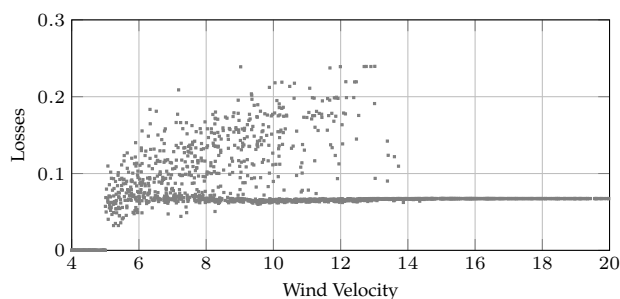
Figure 5.6: Total losses for different conditions

ation of the wind velocity; for example, the frequency of the scenario is increased when the wind park stops due to low wind conditions. In addition, the frequency of nominal power generation is decreased. However, the improvement in the efficiency and reduction on investment cost could compensate these drawbacks.

The total losses of the wind park for different wind velocities and high covariance are presented in Figure 5.6. Parameters for a cable of 2500 mm^2 cross area and 40 km length were used for calculating the grid losses. At nominal power the total losses are 0.0674 pu where 0.035 pu are due to the conversion system and 0.0324 are transmission losses.

Notice the total losses decrease as the wind velocity is increased. The DC current must be adjusted according to the wind conditions. However, only a short margin remains between high wind velocities and what from a practical point of view could be maintained constant. On the other hand, the voltage in each turbine is much more variable than in a conventional parallel system. Figure 5.7 shows the DC current versus the mean wind velocity. At high wind velocities the current is the nominal value which is 800 A in this case. At low wind velocities, the set point of the DC current is highly variable. Compare this behaviour with the theoretical minimum current shown in Equation 5.2. This minimum value is the desired set
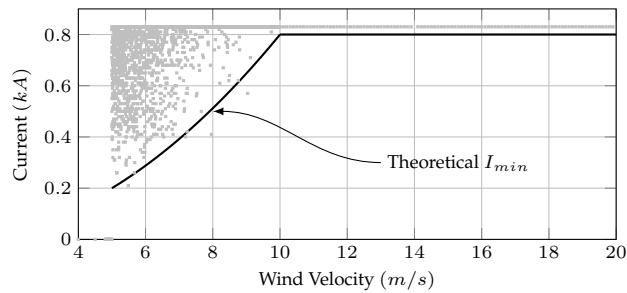
Figure 5.7: Transmission current versus mean wind velocity

point of the DC current if and only if all turbines receive the same wind velocity. In the real case, the optimization algorithm determines a higher set point. This behavior could seem contradictory since the minimal losses occur at minimal current. However, minimal current could lead over-modulation in some turbines. This over-modulation must be counteracted by the pitch angle which reduces the generated power.

Figure 5.8 shows the results of voltage and generated power for one single turbine. The results show a linear tendency of the voltage and the power due to the relatively constant value of the current. The maximum voltage is set as 1.2 pu. Therefore it is not necessary to get any information from the other turbines to define the power reference. This is a simplification in the control strategy
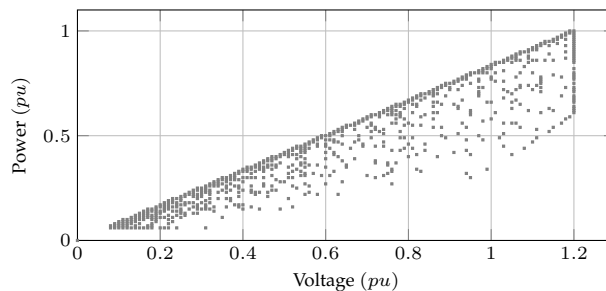
Figure 5.8: Generated voltage versus generated power for a single turbine

Figure 5.9 shows the operation of the system with a simplified strategy and is compared with the optimization approach. The same covariance is used for both simulations ($\sigma = 5m/s$). In this case the set point of the current is calculated according to the Equation 5.2 without any optimization process. The wind park operates less time on its nominal capacity because of the low current. Transmission losses are decreased in magnitude but increased in percentage since the generated power is lower. Nevertheless, a simplified strategy is a feasible solution from the point of view of the physical implementation since no communication at all is required. The only required variable is the mean wind velocity.
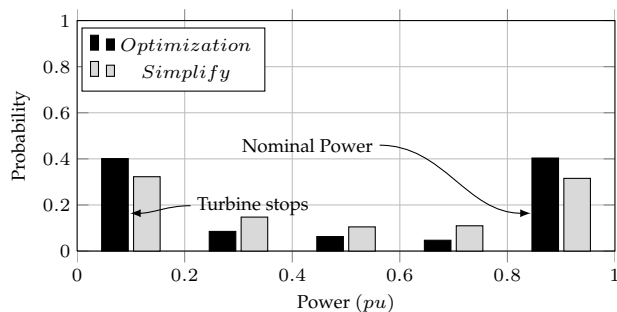
Figure 5.9: Total generated power with and without optimization and $\sigma = 5m/s$

5.2   Final considerations about the operation of the system

Series connection is an efficient alternative for grid integration of offshore wind turbines. However, high variations in the wind velocity between turbines deteriorates the performance of the park. In order to face this problem an optimization algorithm based on non-linear programming was proposed. The algorithm acts as a secondary-tertiary control in stationary state. A simplified algorithm based exclusively on the mean wind velocity is also feasible. The final strategy to be used depends on the stochastic characteristics of the place. The physical placement of the turbines can significantly affect the results. In addition, a very high number of wind turbines could be self-defeating because of the difference in the wind velocity between turbines. This refines the results presented in Chapter 2 where it was demonstrated that the higher the number of turbines is the lower the value of the transmission losses. The number of turbines to be installed is therefore a planning problem that involves stochastic optimization.

6

Conclusions

This chapter recapitulates the main results of this this thesis and presents some recommendations for further investigations.

HVDC systems based on a series connection of an offshore wind farm is an open research problem. This thesis has demonstrated the advantages of this type of topology but also new challenges which were not studied before.

Series connection leads to fewer transmission losses which is one of the main desirable features in an offshore wind park. In addition, series connection reduces investment because support platforms are not required to centralize the power to be transmitted to on-shore. A new converter topology was developed. This converter was designed based on matrix converter topology at high frequency operation.

The matrix converter was selected because it reduces the stages of conversion. On the other hand, high frequency operation reduces the size and weight of the passive elements. Simulation and experimental results demonstrates the efficiency and feasibility of this converter. Four main types of modulation were studied in this converter. Current source operation with space vector modulation is demonstrated to be the most efficient of these modulations. A modulation based on voltage source operation is also possible despite both sides being mainly inductive. However, voltage source operation is feasible if and only if the inductance at the high frequency transformer is very small. Nevertheless, simulation results demonstrated an over use of the clamp to reduce the spikes in the voltage. The clamp circuit is used to face faults in the converter but should not operate in stationary state since this type

of operation increases the losses. As a consequence of the clamp circuit operation, the modulation as current source converter is more efficient than the operation as voltage source converter. This result fulfills the requirements of series connection where DC current is the same in the entire grid.

Experimental studies proved the concept of reduced matrix converter. High frequency operation was achieved with a 10 kW converter. As expected in the simulation study, the voltage in the high frequency transformer is spikes-free and the three-phase voltage and current present low harmonic distortion. Nevertheless, some spikes were found in the current due to the parasitic capacitances in the high frequency transformer. These spikes correspond with simulations although very small integration step was required.

The next challenge that was faced in the thesis was the control of the converter. This control was exclusively studied by simulations. Controlling current source converters is a complex task. The main problem is the resonances of the capacitive filters with the grid. Such resonances have been faced using active damping controls. In this work an optimal control approach was used. Results demonstrated the advantages of the control since only one stage of control is required for controlling the currents. A proportional plus estimation strategy was used for controlling the wind turbines. Output voltages and currents have a very low harmonic distortion. The proposed control can deal with short circuit and transients.

Finally, a stationary state control was developed in order to optimize the operation of the entire wind farm. A non-linear programming methodology was used which fixes the set point of the DC current and the generated power. A Montecarlo simulation was carried out in order to determine the long-term behavior of the proposal. Results demonstrate that differences in the wind speed between turbines leads to low levels of efficiency in the park.

6.1 Future work

6.1.1 Micro-grids

Series connection can be applied to micro-grids as depicted in Figure 6.1. A matrix converter is not used in this configuration but is a possibility if the micro-grid requires fast control. Connection of the turbines in series is potentially more efficient and has lower investment cost due to the use of only one control device and less stages of conversion. Insulation is not a big problem in this type of configuration since the voltage level is the same as the solar panels which are usually connected in series until 500 or 600 V.
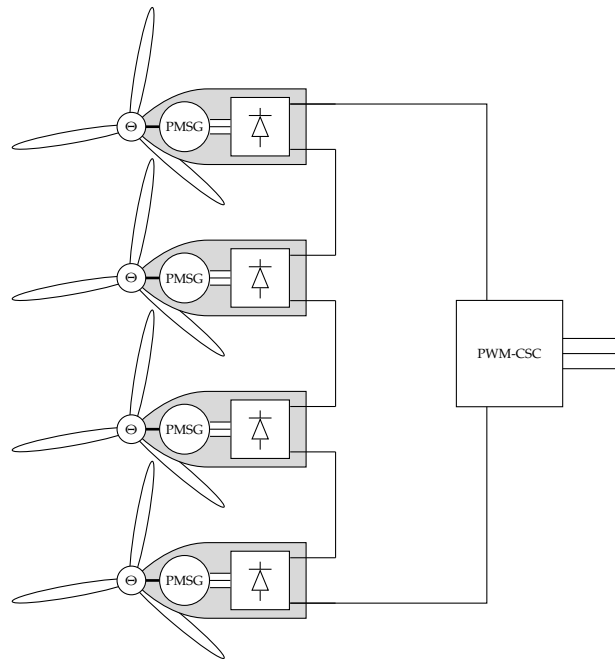
Figure 6.1: Series connection of small-scale wind turbines for micro-grids applications.

6.1.2 New technology of semiconductors

In the current state-of-the-art of high power semiconductor devices, it is clear that integrated-gate-commutated thyristors (IGCTs) have potential advantages. The proposed matrix converter as well as the PWM-CSC can be investigated using these new type of semiconductors. The available technology of IGCTs permit operation at high power and high frequencies that are suitable for wind turbines applications. Frequencies up to 40 kHz can be achieved with this technology. The limitation is only the switching losses but there are not any intrinsic physical limitation of the semiconductor itself. An study of the optimal operative frequency is also required. Low frequencies have less switching losses in the semiconductors but higher losses in the passive elements due to the harmonic distortion and the required size of inductive elements.

6.1.3 New topologies

Other topologies of matrix converter can be studied not only for series connection of wind farms but also for parallel connections. The three-phase matrix converter is a promising alternative together with a three phase high frequency transformer. The efficiency between a three phase and a single phase high frequency transformer

must be compared. It is well known that three-phase transformers are more efficient than single phase transformers for 50 or 60 Hz systems. However this condition has not been proved in high frequency transformer with square wave forms. Even if the three phase transformer is more efficient than single phase, it is required to evaluate the total losses of the system, considering also the losses in the matrix converter.

6.1.4   Six phase generators

Six phase generators as well as six phase matrix converter could be studied for this type of applications. The potential advantage of a six phase system is the increase on the reliability. Modular approaches of matrix converter can be also used to improve the reliability of the system. For example, tandem wind rotors with planetary gear box. In this case, two high frequency links can be used to control the two machines coordinated.

Appendices

A

Active Filtering Using Mathematical Optimization

This appendix summarize and independent investigation about non-active power compensation. However an active filter can be placed in any part of the park to reduce the harmonic distortion, this research is more general and can be applied to any grid. Since this work was not directly connected with the main objectives of the thesis, it is presented as an appendix.

H̲ARMONIC content in the grid is a problem that must be faced. The PWM-CSC can generate power with low harmonic distortion if the commutation frequency is high enough. However, the proposed concept of series connection can be also applied using line commutated converters. In that case, the DC current can be controlled by the converter on-land. The harmonic distortion in that case is high. Therefore, either a passive or an active filter should be used. Usually, a passive filter is enough for this type of applications. However, active an active filter has many advantages. In this appendix a compensation theory based on mathematical optimization is presented. This technique can be used in the proposed concept but is general and can be applied to any active filter application.

Compensation strategies for active filters can be classified in many different ways. In this thesis, a classification according to the reference frame is proposed namely:

- *pq-dq* based strategies

- *ABC* based strategies

The *pq* strategy uses the Clark transformation to define reactive power and all variables in α, β stationary frame [117]. A more specialized compensation strategy is the *dq* which is based on the same principles as the *pq* but in a rotational reference frame [118]. Many other modifications have been proposed for *pq* theory, for example in [119] a *pqr* power theory applicable to four wired systems was presented where the main basis remains the same.

On the other hand, the *ABC* theory, also known as vectorial theory due to the formulation presented by Peng [120], is defined in the three phase reference frame, simplifying the analysis and the implementation. Despite of the advantages of the *ABC* frame, theories based on the Clark or Park transformations are the most widely implemented in reactive power compensation due to their robust functionality. However, these theories do not foresee a framework that allows integration of network loss models and at the same time system intrinsic constraints.

The main contribution of this appendix is a generalized compensation strategy based on mathematical optimization on the *ABC* reference frame that deals with several conflictive objectives and includes among them the minimization of the network losses. Four different compensation cases are investigated for which a simple generalized formulation is derived. The simplicity of implementation and the flexibility for different compensation cases are retained as the most important contribution in this approach.

A.1 Classic ABC theory

The classic ABC theory has been investigated by Peng using a vectorial approach [121]. However, the problem can be also presented, as an optimization algorithm aimed at the minimization of the line currents, as follows:

$$min \sum_{k\in\{a,b,c\}} (I_k - I_{qk})^2 \tag{A.1}$$

subject to

$$\sum_{k\in\{a,b,c\}} V_k \cdot I_{qk} = 0 \tag{A.2}$$

Throughout this appendix the voltage and current variables involved in the mathematical models will refer to the terms schematically represented in Figure A.1. The objective function (Eq. A.1) is proportional to the line losses while the constraint (Eq. A.2) requires that the instantaneous power delivered by the shunt

compensator is zero. Therefore the optimization model minimizes the line currents, (and therefore line losses) subject to zero active power delivered by the filter. This non-linear optimization model is resolved using the first order conditions, giving the compensation currents in Equation A.3.
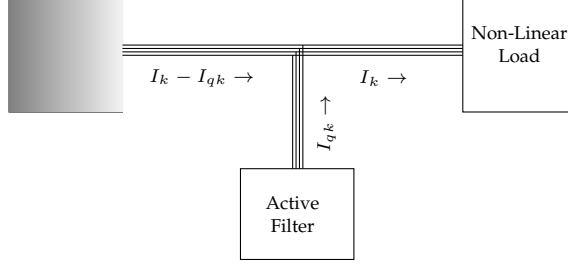
Figure A.1: Schematic representation of the voltages and currents involved in the model for active filter compensation

$$I_{qk} = I_k - \frac{P}{\sum V_k^2} \cdot V_k \tag{A.3}$$

where

$$P = \sum_{k \in \{a,b,c\}} V_k \cdot I_k \tag{A.4}$$

The voltages are measured with respect to the neutral point. A vectorial representation of Equation (A.3) was proposed by Peng [120]. In that case, reactive power was defined as a cross product between instantaneous three-phase vectors of voltage and current while active power was defined in the conventional way as in Eq. (A.4).

A.2 Effect of the Neutral Current

The neutral current I_N in the transmission line can be eliminated by a shunt compensator controlled by an algorithm based on the ABC theory, if and only if the supply voltage does not contain a zero sequence. This undesirable feature is caused by an incomplete understanding of the optimization problem. To demonstrate this point, lets us modify the optimization model considering the neutral current:

$$min \ \alpha \cdot I_N^2 + \sum_{k \in \{a,b,c\}} (I_k - I_{qk})^2 \tag{A.5}$$

subject to

$$\sum_{k \in \{a,b,c\}} V_k \cdot I_{qk} = 0 \tag{A.6}$$

with I_N the neutral current in the transmission line.

$$I_N = \sum_{k \in \{a,b,c\}} I_k - \sum_{k \in \{a,b,c\}} I_{qk} \tag{A.7}$$

and with

$$\alpha = \frac{R_N}{R_L} \tag{A.8}$$

Thus, α is the relation between the line resistance and the neutral resistance. For the classic ABC theory the neutral resistance is considered to be zero. Clearly, the classic ABC theory is a particular case of this model.

Let the Lagrangian function associated with the optimization problem be:

$$\mathcal{L}(I_{qk}, \lambda_E) = \alpha \cdot I_N^2 + \sum_{k \in \{a,b,c\}} (I_k - I_{qk})^2 + \lambda_E \cdot \sum_{k \in \{a,b,c\}} V_k \cdot I_{qk} \tag{A.9}$$

The optimality conditions are found deriving $\mathcal{L}$ as function of I_{qk} and λ_E:

$$\frac{\partial \mathcal{L}}{\partial I_{qk}} = -2 \cdot (I_k - I_{qk}) - 2 \cdot \alpha \cdot I_N + \lambda_E \cdot V_k = 0 \forall k \in \{a, b, c\} \tag{A.10}$$

The derivative of $\mathcal{L}$ with respect to λ_E results in Equation (A.6) and represents power delivered by the shunt compensator. Multiplying the set of Equations (A.10) by V_k and adding the three phases results:

$$P + \alpha \cdot I_N \cdot (3 \cdot V_o) = \frac{\lambda_E}{2} \cdot \sum V_k^2 \tag{A.11}$$

therefore, the dual variable, or Lagrange multiplier, corresponding to Constraint (A.6) for a four wire system is:

$$\lambda_E = \frac{2}{\sum V_k^2} (P + 3 \cdot \alpha \cdot I_N \cdot V_o) \tag{A.12}$$

with:

$$V_o = \frac{1}{3} \sum_{k \in \{a,b,c\}} V_k \tag{A.13}$$

and the set of equations (A.10) becomes:

$$I_k - I_{qk} + \alpha \cdot I_N = \frac{V_k}{\sum V_k^2} \left(P + 3\alpha \cdot I_N \cdot V_o \right) \tag{A.14}$$

In this equation, I_N is still an unknown variable since is the neutral current in the four wire system, and not the load. To obtain this value, the set of Equations (A.14) is added in the three phases:

$$(1 + 3\alpha) \cdot I_N = \frac{3V_o}{\left(\sum V_k^2\right)} \left(P + 3 \cdot \alpha \cdot I_N \cdot V_o \right) \tag{A.15}$$

Therefore, the optimal neutral current for ensuring minimal losses is:

$$I_N = \frac{V_o \cdot P}{\left(\sum V_k^2\right)} \cdot \left(\frac{3}{1 + 3\alpha - 9\alpha \left(V_o^2 / \sum V_k^2 \right)} \right) \tag{A.16}$$

The expression obtained in (A.16) requires a thorough analysis as follows:

- The optimal value from the point of view of the losses in a four wire system, is not necessarily the one with zero neutral current. However, it is not the one generated by the classic ABC theory.

- The value of the optimal neutral current should decrease being zero in the limit, for two different situations: when the neutral resistance increases or when zero sequence voltage increases.

- It is desirable to reduce the neutral current especially when the zero sequence voltage increases.

- These two cases are not considered by the classic ABC theory [122].

- If the zero sequence voltage V_o is zero, then the optimal neutral current is also equal to zero. This is even in the case when the load presents zero sequence current.

- If the neutral resistance was zero ($\alpha = 0$) then the optimal neutral current would be:

$$I_N = \frac{3V_o}{\left(\sum V_k^2\right)} P \tag{A.17}$$

Notice this is the current that appears in the classic ABC theory. As a consequence, the classic ABC theory results in optimal losses if and only if the neutral resistance is zero, which is never the case in a four wire system.

- A compensation strategy that minimizes the total losses must take into account the neutral resistance, being particular to each system. However, from the practical point of view the optimal solution must eliminate the neutral current.

Equation (A.16) could be separated into two terms as a function of Equation (A.17) defining a dimensionless value Ψ (let us call it optimal neutral factor):

$$I_N = \frac{3V_o \cdot P}{\left(\sum V_k^2\right)} \cdot \Psi \tag{A.18}$$

with

$$\Psi = \frac{1}{1 + 3\alpha - 9\alpha \left(V_o^2 / \sum V_k^2\right)} \tag{A.19}$$

This factor Ψ, is a function of α and $\left(V_o^2 / \sum V_k^2\right)$ which can be considered as a measure of the voltage unbalance. Figure A.2 shows the optimal neutral factor Ψ as function of α for different degrees of unbalance. Notice that Ψ is very robust to the voltage unbalance, for example it is less than 30% for values of α above 1, which is the most common case in real four wire systems. In other words, a shunt compensator operated with the classic ABC theory permits currents which are more than 70 % higher than the optimal value. Therefore, to eliminate the neutral current is more convenient than mantaining in the value generated by the classic ABC theory.
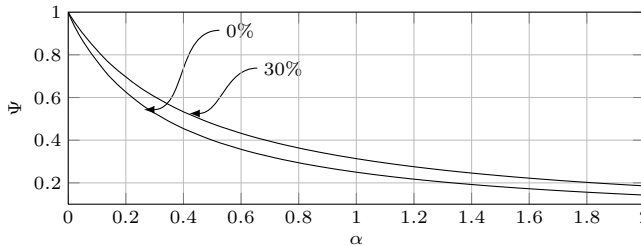
Figure A.2: Optimal neutral factor as function of the neutral resistance α for voltage unbalance of 0 % and 30 %

As α is a weight factor in the objective function, then, increasing this term is equivalent to decreasing the desired neutral current. Therefore, if the compensation objective includes elimination of the neutral current, then the following condition must be satisfied:

$$\lim_{\alpha \to +\infty} \alpha \cdot I_N = \frac{V_o \cdot P}{\left(\sum V_k^2\right) - 3 \cdot V_o^2} \tag{A.20}$$

replacing Equation (A.20) in the expression (A.14), the new compensation current is calculated:

$$I_{qk} = I_k - \frac{P \cdot (V_k - V_o)}{\left(\sum V_k^2\right) - 3 \cdot V_o^2} \tag{A.21}$$

This extended compensation strategy expressed in Equation (A.21) can deal with the most general case, unbalance and distortion in both voltages and currents. From the optimization point of view, the best solution corresponds to expression (A.10) where the power is transfered not only by the phases but also by the neutral wire. As a consequence of this, neither the optimal neutral current is zero nor the one generated by the classic compensation theories. However, as shown in Figure A.2, the optimal neutral current is less than 30 % of the one calculated with the classic ABC theory. Therefore, a compensation strategy which entirely eliminates the neutral current is closer to the real optimal strategy. Moreover, from a practical point of view, it is always preferable to have zero neutral current. This can be added as an additional constraint in the optimization model, to avoid the calculation of the limit, as will be presented in the next sections.

A.3 A flexible ABC theory with zero neutral current

An extended ABC theory is presented in this appendix with a clear mathematical interpretation by means of a simple optimization approach. Four main cases are studied to show its flexibility:

- Case I: Invariant instantaneous power (not energy storage required).

- Case II: Constant power (not oscillating power).

- Case III: Unity power factor (proportionality between voltages and currents).

- Case IV: Pure sinusoidal currents (zero line current harmonics).

The first case is the same as considered in classic ABC power theory except that a more general model is presented; this case avoids energy storage requirement in the shunt compensator and reduces but does not eliminate harmonic distortion. The second case is a natural extension of Case I which allows reducing or eliminating oscillating power and hence the harmonic distortion. The third case was considered by Fryze [123]. In that case, the system was balanced and without neutral current

elimination; thus proportionality between voltages and currents makes non-linear loads appear as if they were resistive from the network point of view. Finally case IV eliminates harmonic distortion in the line current acting as an active filter. The proposed compensation strategy can be as flexible as pq theories, but with a simpler implementation (no need for reference frame transformation) and optimal line losses.

All cases mentioned above were simulated in $PSIM$ under the same conditions in order to compare the performance of each compensation objective. Three-phase voltage sources contain distortion and unbalance as shows in Figure A.4 and Table A.1. The loads consist of a full-bridge diode rectifier with a high inductance and a pure reactive single phase load connected to phase $k = (c)$. Parameters of the load and the distribution line for simulation results are shown in Figure A.3.
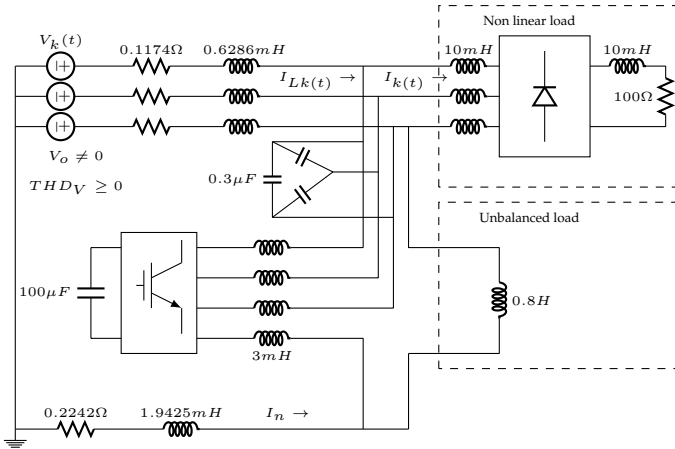
Figure A.3: Circuit for simulations of the proposed reactive power compensation

Table A.1: Voltages in the source

Magnitude [V]	Angle [deg]	Frequency [Hz]
13200	0	60
800	0	60 (zero sequence)
400	10	7×60
200	0	11×60

The impedance of the distribution line was selected using the values of the 4 node IEEE test system [124]. Simulations are based on an ideal compensator. More accurate simulations considering the control of the DC link and the distortion owing to the modulation are presented in next section.
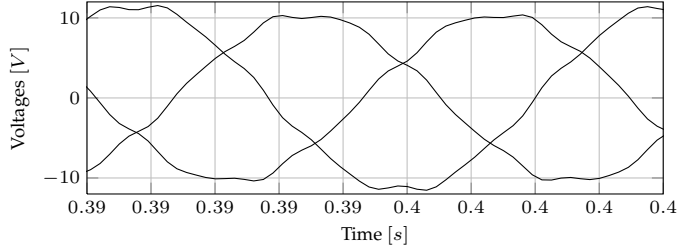
Figure A.4: Waveforms of the three phase unbalanced and distorted voltage source

A.3.1 Case I: invariant instantaneous power

The optimization model is modified to consider the zero sequence:

$$min \sum_{k \in \{a,b,c\}} (I_k - I_{qk})^2 \tag{A.22}$$

subject to:

$$\sum_{k \in \{a,b,c\}} V_k \cdot I_{qk} = 0 \tag{A.23}$$

$$\sum_{k \in \{a,b,c\}} I_{qk} = 3 \cdot I_o \tag{A.24}$$

The objective function as well as energy storage constraints are the same as classic ABC theory, but a second constraint related with neutral current ($3 \cdot I_o$) is added to ensure that the line neutral current be eliminated. Lagrangean function is calculated as:

$$\mathcal{L}(I_{qk}, \lambda_E, \lambda_o) = \left(\sum_{k \in \{a,b,c\}} (I_k - I_{qk})^2 \right) + \lambda_E \cdot \left(\sum_{k \in \{a,b,c\}} V_k \cdot I_{qk} \right)$$
$$+ \lambda_o \left(\sum_{k \in \{a,b,c\}} I_{qk} - 3 \cdot I_o \right) \tag{A.25}$$

The optimization model is solved deriving $\mathcal{L}$ with respect to I_{qk}, λ_E and λ_o. The resulting non-linear equation system generates two Lagrange multipliers to be

considered according to each constraint. From Equation (A.23):

$$\lambda_E = \frac{2 \cdot P}{(\sum V_k^2) - 3V_o^2} \tag{A.26}$$

and from Equation (A.24):

$$\lambda_o = -\lambda_E \cdot V_o \tag{A.27}$$

The compensation equation is given by Equation (A.28):

$$I_{qk} = I_k - \left(\frac{P}{(\sum V_k^2) - 3V_o^2} \right) \cdot (V_k - V_o) \tag{A.28}$$

Notice that Equation (A.3) from classic ABC theory is a particular case of Equation (A.28) when voltage is balanced $V_o = 0$. The zero sequence current is considered in equation (A.24) although the term I_o is eliminated in the calculation process. This explains why classic ABC theory can deal with zero sequence current under balanced voltage conditions, in spite of the fact that it is not considered in the model. The present model can deal with zero sequence current under-balanced and unbalanced voltages.

One interesting aspect of the mathematical optimization approach is the use of the Lagrange multipliers as sensitivity factor which brings important information in order to select the compensation objective. For example, the energy storage capability of the compensation device is directly related to the cost of the converter. Different energy storage capability are required according to the compensation objective. In Case I, the energy storage is zero. However, it is not in a more general situation. The energy storage requirement E_q and the instantaneous power delivered by the shunt compensator are related by the following equation:

$$\frac{d}{dt} E_q = P_q \tag{A.29}$$

with

$$P_q = \sum_{k \in \{a,b,c\}} V_k \cdot I_{qk} \tag{A.30}$$

The objective function can be changed to minimize the losses in the transmission line obtaining the same compensation equation:

$$P_L = R_L \cdot \sum_{k \in \{a,b,c\}} (I_k - I_{qk})^2 \tag{A.31}$$

At the optimal solution, both the Lagrangian and the objective functions are the same. In addition, all the constraints must be satisfied. Therefore, the derivative of the Lagrangian $\mathcal{L}$ with respect to P_q is the same in the stationary point (optimal solution):

$$R_L \cdot \frac{d\mathcal{L}_{(optimum)}}{dP_q} = \frac{dP_{L(optimum)}}{dP_q} \tag{A.32}$$

Notice that P_q is the second addend in Equation (A.25). In general, Lagrange multipliers represent the variation of the objective as function of the constraint. In this case, λ_E represents the value of decreasing in line losses when energy storage is increased. The sign changes according to the definition of the Lagrangian:

$$\frac{\partial P_L}{\partial P_q} = -R_L \cdot \lambda_E \tag{A.33}$$

In the same way, λ_o represents the increasing in line losses if the zero sequence current was not eliminated:

$$\frac{\partial P_L}{\partial I_o} = -R_L \cdot \lambda_o \tag{A.34}$$

λ_E can be used in the decision of the compensation objective since it represents the improvement in the transmission losses if the energy storage capability is increased. Moreover, λ_o can be used in the decision about the converter topology (three of four legs).

A simulation result for line and neutral current in this compensation case is shown in Figure A.5; compensation starts after $0.4[s]$. In spite of the zero sequence in the voltage source, neutral current is eliminated completely. The currents become smoother although they are non-sinusoidal and the main objective is achieved.
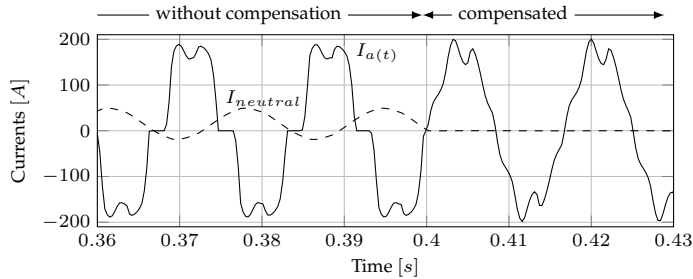
Figure A.5: Waveform of currents for invariant instantaneous power (case I)

A.3.2 Case II: constant power

In this case, shunt compensation requires suppling the oscillating power to maintain the line power constant. Energy storage is required depending on the magnitude of the oscillating power and its frequency. The optimization model is as follows:

$$min \quad \sum_{k \in \{a,b,c\}} (I_k - I_{qk})^2 \tag{A.35}$$

subject to

$$\sum_{k \in \{a,b,c\}} V_k \cdot I_{qk} = \tilde{P} \tag{A.36}$$

$$\sum_{k \in \{a,b,c\}} I_{qk} = 3 \cdot I_o \tag{A.37}$$

After the optimization problem is solved, the compensating currents are:

$$I_{qk} = I_k - \left(\frac{\bar{P}_m}{(\sum V_k^2) - 3V_o^2} \right) \cdot (V_k - V_o) \tag{A.38}$$

with

$$\bar{P}_m = P - \tilde{P} \tag{A.39}$$

$\bar{P}_m$ can be calculated easily with a digital low pass filter applied to the signal of P or by an arithmetic moving average filter.

Results for this case are shown in Figure A.6. As in case I, compensation starts at $0.4\ [s]$ and the zero sequence current is completely eliminated even though the voltage source is unbalanced. New line currents are smoother than in case I but not completely sinusoidal; the power becomes constant after $0.4\ [s]$ which is the objective of this case of compensation.

Power before and after compensation for this case is shown in Figure A.7. Oscillating power is completely eliminated.

A.3.3 Case III: unity power factor

This is an extension of the theory proposed by Fryze [125] but in this case the derivation of the algorithm results from the same optimization principle as in cases I and II. In those cases, the objective function was instantaneous while in this case the

120
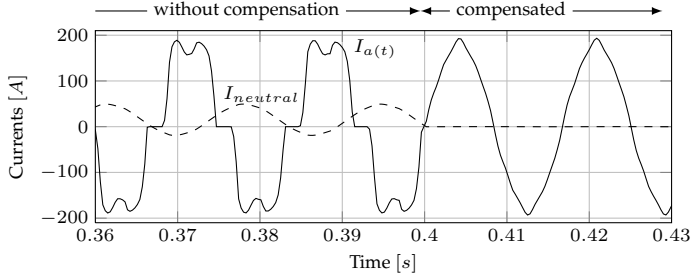
Figure A.6: Waveform of currents for constant power compensation (case II)
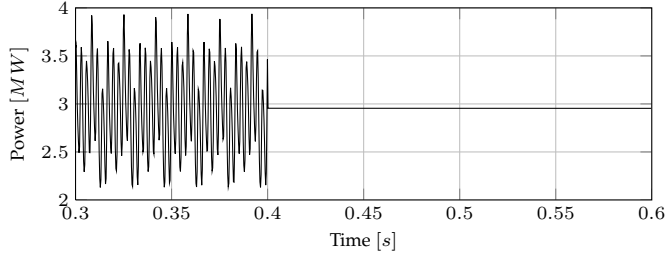
Figure A.7: Instantaneous power before and after compensation for case II

model is modified to consider a complete period. Consequently, rms line currents are minimized instead of the instantaneous currents as follows:

$$min \; \frac{1}{T} \int_{t_o}^{t_o+T} \left(\sum_{k \in \{a,b,c\}} (I_k - I_{qk})^2 \right) dt \qquad (A.40)$$

Subject to

$$\frac{1}{T} \int_{t_o}^{t_o+T} \left(\sum_{k \in \{a,b,c\}} V_k \cdot I_{qk} \right) dt = 0 \qquad (A.41)$$

$$\sum_{k \in \{a,b,c\}} I_{qk} = 3 \cdot I_o \qquad (A.42)$$

The objective is to achieve unity power factor constrained to the elimination of the neutral current. The objective function and constraint are not compatible in all the cases. However the optimization approach finds the solution nearest to the unit power factor that at the same time eliminates the neutral current.

Notice that constraint (A.41) is not dependent on the time while constraint (A.42)

121

is time dependent. As in all power theories, V_k and I_k are considered as independent. Lagrangean function is calculated:

$$
\mathcal{L}(I_{qk}, \lambda_E, \lambda_o) = \frac{1}{T} \int\limits_{t_o}^{t_o+T} \left(\sum_{k \in \{a,b,c\}} (I_k - I_{qk})^2 \right) dt +
$$
$$
\frac{\lambda_E}{T} \cdot \int\limits_{t_o}^{t_o+T} \left(\sum_{k \in \{a,b,c\}} V_k \cdot I_{qk} \right) dt + \lambda_o \cdot \left(\sum_{k \in \{a,b,c\}} I_{qk} - I_o \right)
$$

(A.43)

The instantaneous derivative of $\mathcal{L}$ with respect to three-phase currents is equal to zero (first optimality condition):

$$
\frac{-2}{T} \cdot (I_k - I_{qk}) + \frac{\lambda_E}{T} V_k + \lambda_o = 0
$$

(A.44)

Multiplying by V_k, adding in the three-phases and integrating in one period, Equation (A.44) becomes:

$$
- 2 \cdot \bar{P}_m + \lambda_E \cdot \sum_{k \in \{a,b,c\}} V_{k(rms)}^2 + \int\limits_{t_o}^{t_o+T} 3 \cdot \lambda_o \cdot V_o \, dt = 0
$$

(A.45)

adding Equation (A.44) in the three phases, and taking into account $\frac{\partial \mathcal{L}}{\partial \lambda_o}$ which is nothing but Equation (A.42), this results in:

$$
0 = \frac{\lambda_E}{T} \cdot V_o + \lambda_o
$$

(A.46)

Combining these two equations, the Lagrange multipliers are found:

$$
\lambda_E = \frac{2 \cdot \bar{P}_m}{\left(\sum V_{k(rms)}^2 \right) - 3V_{o(rms)}^2}
$$

(A.47)

Finally, compensation currents are given by:

$$
I_{qk} = I_k - \left(\frac{\bar{P}_m}{\left(\sum V_{k(rms)}^2 \right) - 3V_{o(rms)}^2} \right) \cdot (V_k - V_o)
$$

(A.48)

Figure A.8 shows the current wave forms for this case. In the other cases, compensation starts at $0.4[s]$ in order to show the currents before and after the compensation. Neutral current is eliminated. The objective is achieved since line currents present almost the same waveform than voltage sources. Some energy storage capacity is required but the power is not constant as shown Figure A.9. Nevertheless, oscillating power decreases considerably.
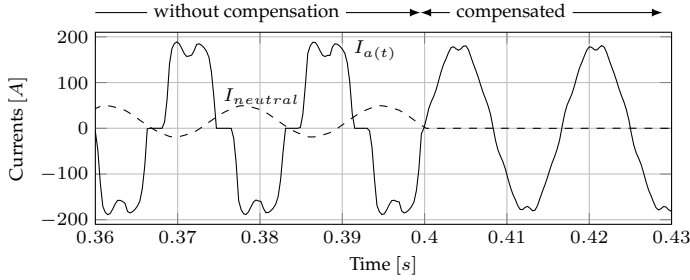
Figure A.8: Waveform of currents for unity power factor compensation (case III)
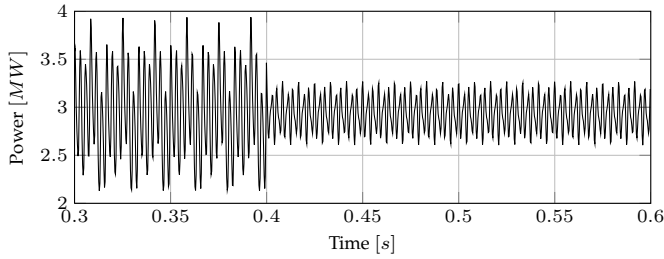
Figure A.9: Instantaneous power before and after compensation for case III

Compared to cases I and II, computational effort increases due to the rms calculation. However, the algorithm is still very simple for real implementation.

Figure A.10 shows the voltage and current in phase A for case III before and after compensation. Notice that the relation between voltage and current is almost but not completely linear. Small gaps in the compensated waveform are the result of the elimination of the neutral current. This result is expected since the compensation objective is to achieve a proportionality but the constraint of the neutral current elimination limits this ideal objective. The results are however, the best possible compensation according to the objective of proportionality that at the same time eliminates the neutral current.

A.3.4   Case IV: sinusoidal current

In this case a sinusoidal waveform in line currents is desired, therefore:
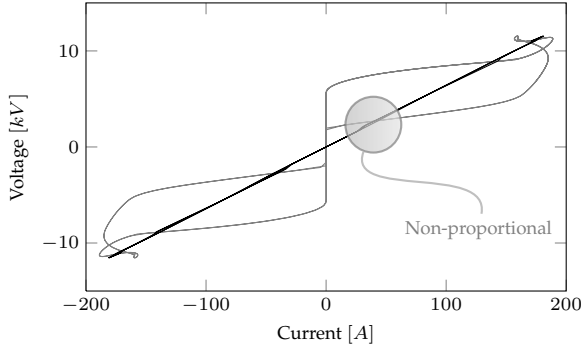
Figure A.10: Voltage vs Current for the case III. Before compensation (grey). After compensation (black)

$$I_{Lk} = I_{mk} \cdot sin(\omega_s \cdot t + \phi_k) \tag{A.49}$$

where I_{mk} are constant which will be set by the optimization process while ϕ_k is set as the phase of the fundamental voltages. The objective function is represented by Equation (A.40) but Equation (A.41) becomes time invariant in one period:

$$\frac{\sqrt{2}}{2} \cdot V_{1k(rms)} \cdot I_{mk} = \bar{P}_m \tag{A.50}$$

Finally, the compensation current is given by:

$$I_{qk} = I_k - \left(\frac{\bar{P}_m}{(\sum V_{1k(rms)}^2) - 3V_{o(rms)}^2} \right) \cdot (V_{1k} - V_o) \tag{A.51}$$

The compensation algorithm is similar to case III except that here fundamental voltage is used instead of V_k; This voltage V_{1k} can be obtained through a low pass filter, by integration methods or by a fast Fourier transformation. In this case, the voltage waveform is sinusoidal (see fig. A.11). However, in some other cases, the optimization approach cannot obtain pure sinusoidal waveform and at the same time zero neutral current. Instead of that it will obtain the solution closest to this ideal objective.
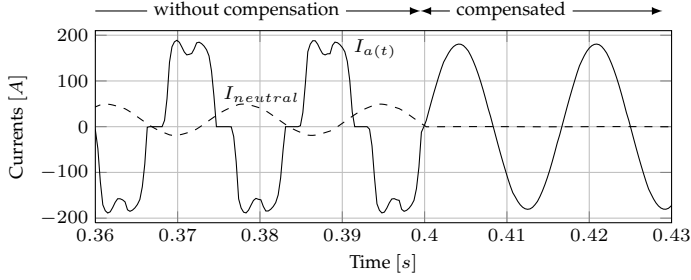
Figure A.11: Waveform of currents for sinusoidal current compensation (case IV)

A.4   Other compensation objectives

A.4.1   Negative sequence currents

A negative sequence in currents can be caused by single phase loads connected to two phases. Case I cannot compensate for these currents, since they create oscillating power. However, they can be compensated for the other three cases.

A.4.2   Reduced power oscillations

For economical reasons, it could be desirable only partial elimination of power oscillations. In order to reduce the power oscillations by a constant value $\xi \in [0, \dots, 1]$ Equation (A.36) becomes:

$$\sum_{k \in \{a,b,c\}} V_k \cdot I_{qk} = \xi \cdot \tilde{P} \tag{A.52}$$

and the compensation currents are given by:

$$I_{qk} = I_k - \left(\frac{(1 - \xi) \cdot P + \xi \cdot \bar{P}_m}{(\sum V_k^2) - 3V_o^2} \right) \cdot (V_k - V_o) \tag{A.53}$$

The required energy storage capacity is proportional to ξ and therefore a compromise relation between oscillating power and cost can be achieved. This equation is a generalization of cases I and II since for $\xi = 0$ the instantaneous power is as oscillating as the load and for $\xi = 1$ the power is constant. Figures A.12 and A.13 show the currents and power for this case with $\xi = 0.5$.
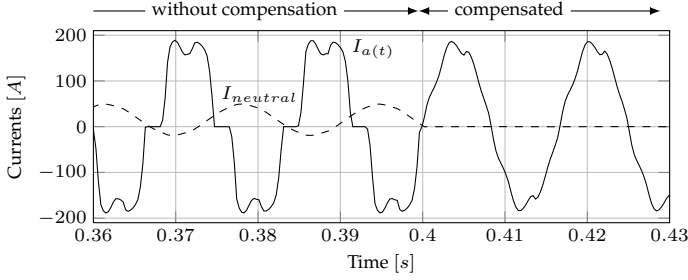
Figure A.12: Waveform of currents for reduction of oscillating power with $\xi = 0.5$
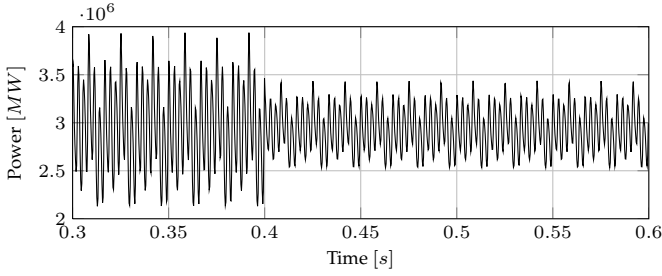
Figure A.13: Line power for reduction of oscillating power with $\xi = 0.5$

A.5 A single generalized formulation and some remarks about the implementation

The four studied cases have different objectives but similar structure. Therefore, it is possible to generalize the compensation expression as follows:

$$I_{qk} = I_k - \left(\frac{P_s}{\left(\sum V_s^2 - 3V_{s(o)}^2 \right)} \right) \cdot \left(V_r - V_{r(o)} \right) \tag{A.54}$$

where $V_{s(o)}$ and $V_{r(o)}$ are the zero sequence voltage associated with V_s and V_r. The values of P_s, V_s and V_r are shown in table A.2 for each case.

Table A.2: Values of power and voltage for a generalized compensation expression

Case	P_s	V_s	V_r
I Invariant power	P	V_k	V_k
II Constant power	$\bar{P}_m$	V_k	V_k
III Unity power factor	$\bar{P}_m$	$V_{k(rms)}$	$V_{k(rms)}$
IV Sinusoidal current	$\bar{P}_m$	$V_{1k(rms)}$	V_{1k}

126

It is important to note that the compensation objective cannot be perfectly achieved as an ideal case due to the imposed constraint of neutral current elimination. What can be guaranteed is the best possible solution according to each objective, that at the same time eliminates the neutral current. By the general formulation presented in Equation (A.54) it is clear that the optimization approach is more flexible from the point of view of losses and its ability to deal with conflictive objectives.

Real implementation of the proposed power strategy requires taking into account the control of the DC link and the modulation of the converter. An example of this control is shown in Figure A.14 where a PI regulator is used to maintain the DC link constant; this signal is added to the power reference (P) according to the compensation objective. For the simulation, voltage reference $V_{DC(reff)}$ was selected as $30[kV]$ and the same parameters presented in Figure A.3. Modulation is based on hysteresis control, although other types of modulation can be used. The simplicity of the control scheme is maintained since only one PI regulator requires to be tuned. Other types of control, modulation or converter topology can be used in combination with the presented power compensation theory without significant changes.
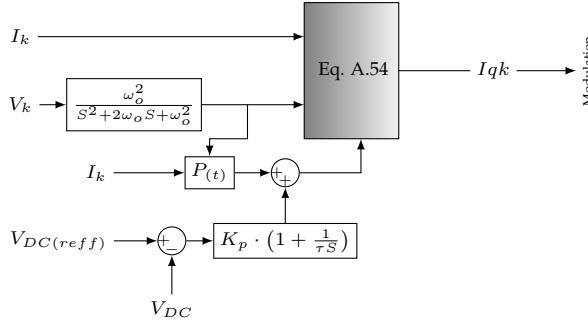
Figure A.14: Control scheme to implement the proposed theory

A low pass filter must be placed in the voltage inputs (V_k) to avoid undesired oscillations; the value of the cut-off frequency for the case implemented here was $\omega_o = 1[kHz]$.

The frequency spectrum for the same harmonics present in the voltage in the four considered cases and the base current are shown in Figure A.15. In all cases harmonic currents decrease, especially in cases II and IV. Case III follows the waveform of the voltage and consequently, its spectrum depends on the spectrum of the voltage. Objectives with less energy storage requirement will result in more harmonic distortion. Nevertheless in all cases, the harmonic content is greatly decreased.

Decreasing the losses in the system is one of the most important objectives of power compensation from the point of view of the system operator. These losses for different cases are presented in Table A.3. The results demonstrate that Case III
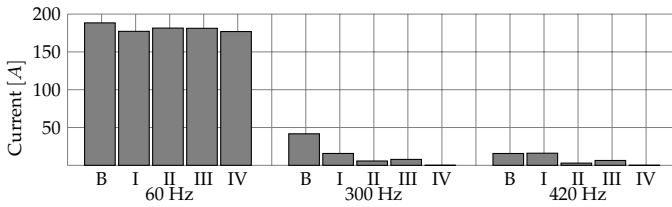
Figure A.15: Main frequency spectrum for the considered cases (I,II,III and IV) and base load current (B)

presents the optimal solution from the losses point of view. However, from the point of view of protections and power quality the best solution is achieved with the pure sinusoidal objective.

Table A.3: Losses in the line

Case	Losses in $[kW]$	Decrease in $[\%]$
Base	6.980421	0.00
Case I	5.896077	15.53
Case II	5.811034	16.75
Case III	5.794854	16.98
Case IV	5.804201	16.85

The maximum energy storage required for each compensation objective are shown in Figure A.16. There is a trade off between the harmonic distortion and the energy storage requirement.
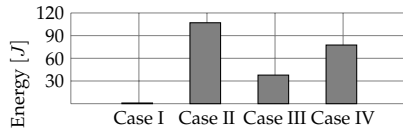
Figure A.16: Maximum energy storage requirement in the compensator for each objective

A.6   Experimental results

An experimental investigation was carried out to demonstrate the practical applicability and simplicity of implementation of the proposed power compensation theory. A picture of the set-up is shown in Figure A.17(a). The voltage is supplied by a programmable three-phase voltage source in order to generate harmonic distortion and unbalance condition. Three independent programmable non linear loads are used. The converter was modulated using hysteresis control. The control algorithm was implemented with a DSPace board.

Figure A.17(b) shows the voltages and currents without compensation. Three-phase nominal voltage was set to $50[V]$ with 5% of harmonic distorsion with the harmonics 2, 5 and 7. Phase A current is $45[A]$ with a maximum crest factor $CF_{max} = 2$ and 0.7 power factor.

The results obtained from the experimental work for each case are also presented in Figures A.17. In all cases, compensation objectives are achieved. For example, in case III, as expected, the compensated current becomes proportional to the voltage and the neutral current is completely eliminated.

For case IV (sinusoidal waveform), the fundamental component of the voltage must be determined. Various methods could be used to calculate it, in this case a Fast Fourier Transformation (FFT) was used, but a PLL can also be used. The proposed control algorithm requires low computational effort therefore it is possible to afford the high computational resources required by an FFT.

There was a significant difference between the current waveforms with and without compensation. It is important to note is that similar objectives could be obtained with other type of compensation strategies. The clear benefit of the proposed strategy is the generalized optimization approach by a single formulation and the simple implementation of the compensation algorithm. An optimization approach permits a customized solution according to the particular conditions of the load and the system. In addition, the compensation equations are very similar for different compensation objectives. Therefore, the algorithm is flexible to easy changes of control objectives and thus allows the implementation of a multi-modes control algorithm according to the compensation needs of the system.
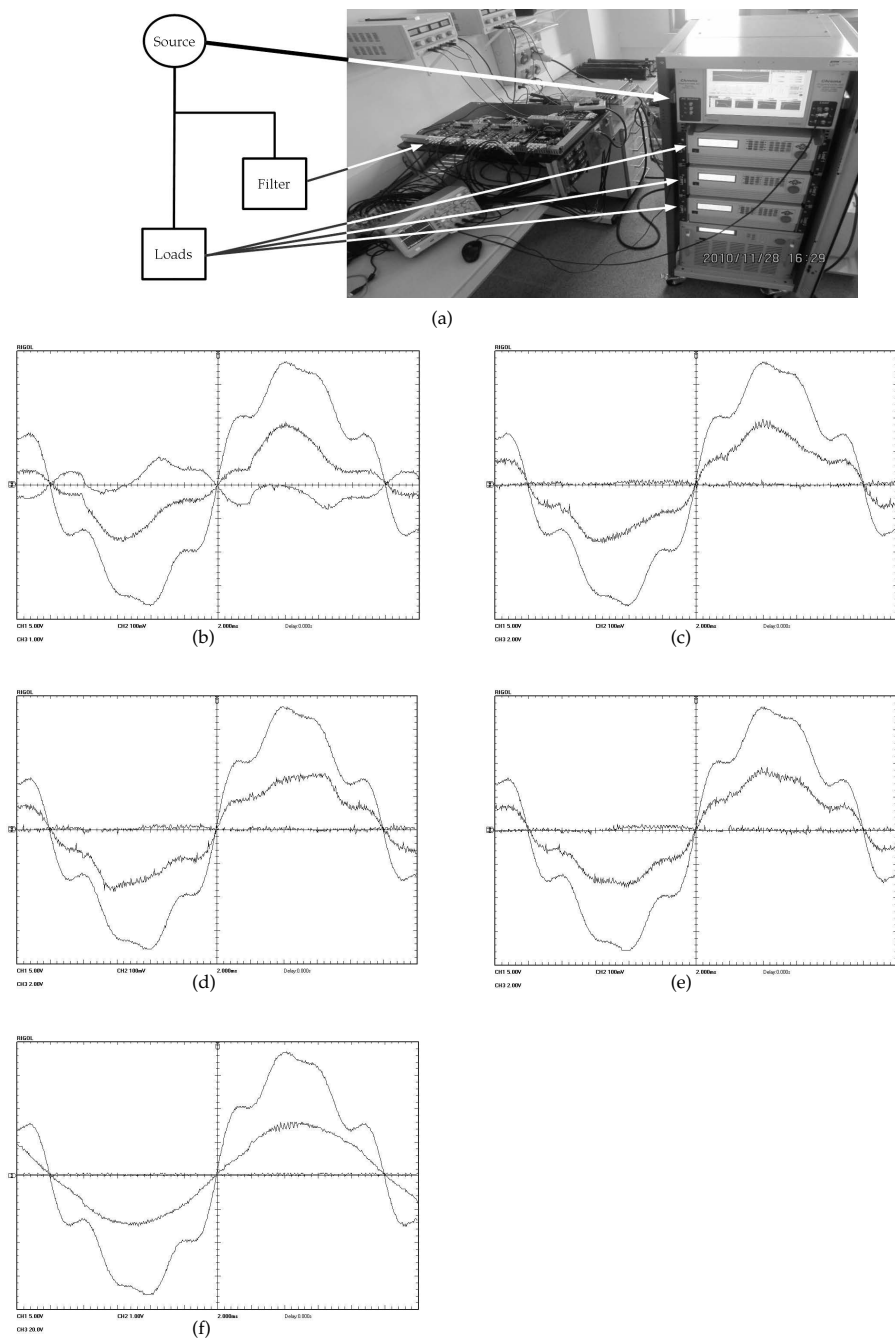
Figure A.17: Experimental results for the four cases studied. (a) Experimental set-up, (b) Case base, (c) Case I, (d) Case II, (e) Case III,(f) Case IV

B

Parameters for Simulation Studies and Experimental Set-Up

This appendix presents the parameters used in the simulations as well as in the experimental set-up.

Parameters of the permanent magnet synchronous generator are presented in Table B.1. They are based on the work presented by Perdana in [70].

Table B.1: Parameters of the PMSG

Parameter	Value	Unit
Nominal power	2	MVA
Nominal AC voltage	690	V
AC Frequency	50	Hz
X_{sd}	0.8	pu
X_{sq}	0.5	pu
R_s	0.1	pu
Permanent magnet flux	1.4	pu
Nominal DC voltage	2.00	kV
Nominal DC current	1.00	kA

The model of the wind turbine was taken from [71] for a 2 MW wind turbine. Its Parameters are shown in Table B.2. The number of pairs of poles of the machine

are calculated using the electrical speed of the generator and the rotor speed of the turbine. It is also possible to use either a 40 poles machine and a gear box 1:8 or a 320 poles machine. Both alternatives are equivalent in the simulations since the dynamic of the gear box were not modeled (according to [71] one mass model is enough for electrical analysis).

Table B.2: Parameters of the wind turbine

Parameter	Value	Unit
Nominal power	2	MW
Nominal wind velocity	10	m/s
Rotor diameter	75	m
Minimum rotor speed	9	rpm
Nominal rotor speed	18.75	rpm
Total inertia constant	3	s

Parameters of the cable (R_t, L_t, C_t) are given in Table B.3. The resistance were calculated using Equation B.1

$$R_t = \frac{\rho}{A} \tag{B.1}$$

where $\rho = 1.68 \times 10^{-8}$ is the resistivity of the copper and $A = 2500mm^2$ is the cross section area. The length of the offshore wind farm to the shore is 40 km but the equivalent resistance is $2 \cdot R_t \cdot Length = 0.5376\Omega$ in order to consider the returning cable. For 10 series connected wind turbines operated at nominal power the transmission losses are 2.7%. This was the main criteria to select the cross section area.

The equivalent inductance is calculated using Equation B.2

$$L_t = \frac{\mu_o}{\pi}\left(\frac{1}{4} + ln\left(\frac{d}{r}\right)\right) \tag{B.2}$$

were d is the distance between the centers of the two conductors and r is the radius of the conductors as depicted in Figure B.1. In this case $d = 93.06 \; mm$.

Table B.3: Parameters of the DC cable

Parameter	Value	Unit
R_t	6.76	$m\Omega/km$
L_t	0.5774	mH/km
C_t	128	μF
Length	40	nF/km
Switching frequency	2	kHz
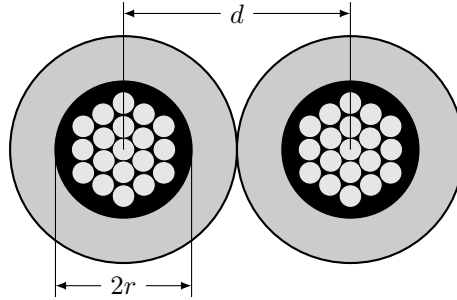
Figure B.1: Simplified representation of an HVDC cable

Table B.4: Parameters of the on-land CSC

Parameter	Value	Unit
L_s	2.985	mH
R_s	0.093	Ω
C_s	95.34	μF
V_s	22.00	kV
L_{DC}	64.00	mH
Switching frequency	3	kHz

Table B.4 presents the parameters of the PWM-CSC. These were calculated using typical values of this type of converter presented in [113]. The three-phase inductance is typically 15% while the DC choke is typically 80%. Resistance was asumed $1/10$ of the inductance. The capacitance was calculated using Equation B.3 for a cut-off frequency half of the switching frequency.

$$(2\pi f) = \frac{1}{\sqrt{L_s C_s}} \tag{B.3}$$

Parameters of the experimental set-up are given in Table B.5. The criteria for their calculation are also presented in the same table.

133

Table B.5: Parameters of the experimental set-up

Parameter	Symbol	Value	Note
Nominal Power	S_{nom}	10 kVA	
Nominal voltage	V_{nom}	200 V	line-line rms
Switching frequency	f	10 kHz	
Maximal voltage	V_{max}	300 V	50% overvoltage
Nominal current	I_{nom}	30 A	$S_{nom}/(\sqrt{3}V_{nom})$
Maximal current	I_{max}	50 A	60% over current
$Imax$ diodes in clamp circuit	I_d	10 A	$20\%I_{max}$
Voltage in clamp circuit	V_d	400 V	$3\sqrt{2}/\pi V_{max}$
Maximum voltage clamp circuit	V_{dmax}	450 V	50 V safety margin
Power in clamp circuit	P_c	50 W	$0.5\%S_{nom}$
Resistance in clamp circuit	R_c	3200Ω	V_{d2}/P_c
Nominal DC voltage	V_{dc}	326 V	$V_{nom}\sqrt{2/3}$
Maximal DC voltage	V_{dcmax}	450 V	V_{dmax}
Cut off frequency for DC filter	f_{dc}	1kHz	$10\%f$
Capacitance in DC filter	C_f	50 μF	
Inductance in DC filter	L_f	0.5 mH	$\omega_o = 1/\sqrt{LsCr}$
Capacitance in AC filter	C_r	50 μF	

<div align="right">

C

</div>

Models of the Wind

This chapter describes the models of the wind in short and long term. The short term model was used for dynamic simulations while the long term model was used for the Montecarlo simulation.

THERE are mainly two models of the wind according to the type of study. For dynamic simulations, it is necessary to model the possible behaviour of the wind and turbulence. This is named short-term model. For long-term simulations, specially power and energy planning, it is necessary to have a long-term model. These two models are presented in this appendix.

C.1   Wind velocities (short-term model)

There are two models for the wind according to the type of simulation. For transient analysis it is required a detail model which considers the fast changes in the wind during a short period of time (for example 1 minute). The model for this type of simulation was taken from [126] and [127]. This model considers four elements as follow:

- Average velocity ($V_{w(mean)}$): it is the expected nominal speed, its value is constant in the simulation.

- Ramp ($V_{w(ramp)}$) models a linear increase or decrease of the wind velocity.

- Gust ($V_{w(gust)}$) models some very low frequency turbulences in the wind

- Noise ($V_{w(noise)}$) is a random turbulence modelled as a stationary process:

The wind applied to the turbine is the sum of these four elements:

$$V_\omega = V_{w(mean)} + V_{w(ramp)} + V_{w(gust)} + V_{w(noise)} \tag{C.1}$$

The deterministic terms (mean,ramp,gust) can appear at the same time or in different instants, but the control must take into account all the possibilities. The noise is model as a stationary proses with a spectral density equal to:

$$S(f) = \frac{600 \cdot V_{mean}}{ln(h/z_o)^2} \cdot \left(1 + 900\frac{f}{V_w}\right)^{5/3} \tag{C.2}$$

with f the frequency in Hz, h the height of the turbine, and z_o the roughness length. This factor depends of the landscape type, but for open sea is in the interval $[1 \times 10^4 - 1^3]$.

C.2   Wind velocities (long-term model)

For long-term analysis the wind is modelled with a Weibull probability function. The Weibull probability density function f and cumulative distribution function F are respectively expressed as:

$$f(V_{pu}) = V_{pu}\left(\frac{k}{\alpha}\right)^{\beta-1} e^{-V_{pu}^\beta} \tag{C.3}$$

$$F(V_{pu}) = 1 - e^{-V_{pu}^\beta} \tag{C.4}$$

where α is the scale factor and β is the shape factor. Per-unit wind velocity is defined over the scale factor basis:

$$V_{pu} = \frac{V_w}{\beta} \tag{C.5}$$

Parameters of the Weibull distribution are particular to the place where the wind park is located [128]. Usually a shape constant of $\beta = 2$ and scale constant of $\alpha = 10[m/s]$ is a good approximation to model the stochastic behaviour of the wind velocity as shown in Figure C.1.
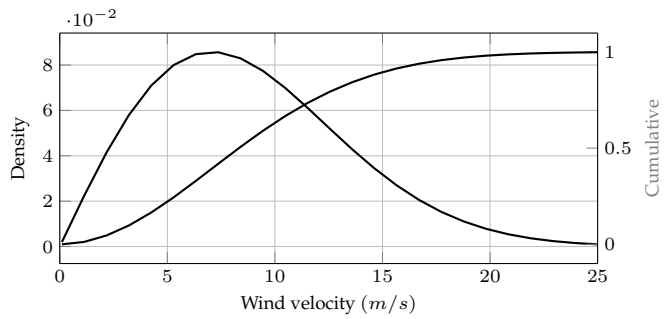
Figure C.1: Curves of Weibull probability density function (left axis) and cumulative distribution function (right axis)

References

[1] WWEA, *World Wind Energy Report 2009*. Bonn. Germany: WWEA, March. 2010.

[2] P. Bresesti, W. Kling, R. Hendriks, and R. Vailati, "Hvdc connection of offshore wind farms to the transmission system," *IEEE Trans. Energy Conversion*, vol. 22, no. 1, pp. 37–43, March 2007.

[3] N. Negra, J. Todorovic, and T. Ackermann, "Loss evaluation of hvac and hvdc transmission solutions for large offshore wind farms," *Electric Power System Research. Elsevier*, vol. 1, no. 76, pp. 916–927, 2005.

[4] S. Meier and P. Kjaer, "Benchmark of annual energy production for different wind farm topologies," in *proc. of IEEE Power Electronics Specialists Conference PESC*, 2005.

[5] P. Steimer, "Medium voltage power conversion technology for efficient wind park power collection grids," in *Proc. 2nd IEEE International Symposium on Power Electronics for Distributed Generation Systems*, China, June 2010.

[6] R. M. Dermott, "Investigation of use of higher ac voltage on offshore wind farms," in *Proc. Of European Wind Energy Conference*, France, March 2009.

[7] C. Meyer, "Key components for future offshore dc grids," Ph.D. dissertation, Rheinisch-Westfallischen Technischen Hochschule Aachen, Germany, 2007.

[8] S. Lundberg, "Evaluation of wind farm layouts," in *Proc. of Nordic workshop on power and industrial electronics*. Norway: Proc. of Nordic workshop on power and industrial electronics, 2004.

[9] L. Max, "Design and control of a dc collection grid for a wind farm," PhD. thesis, Chalmers University of technology, Goteborg, Sweden, 2009.

[10] J. Robinson, D. Jovcic, and G. Joo ands, "Analysis and design of an offshore wind farm using a mv dc grid," *IEEE Trans. Power Delivery*, vol. 25, no. 4, pp. 2164 –2173, oct. 2010.

[11] A. B. Mogstad, "New switching pattern for ac/ac converters with rbigbts for offshore wind parks," M. Eng. thesis, Norwegian University of Science and Technology (NTNU), Trondheim, Norway, 2008.

[12] R. Candrdenas, R. Pe anda, J. Clare, and P. Wheeler, "Analytical and experimental evaluation of a wecs based on a cage induction generator fed by a matrix converter," *IEEE Trans. Energy Conversion*, vol. 26, no. 1, pp. 204 –215, 2011.

[13] J. A. Baroudi, V. Dinavahi, and A. M. Knight, "A review of power converter topologies for wind generators," *Renewable Energy*, vol. 32, no. 14, pp. 2369 – 2385, 2007.

[14] Z. Chen, J. Guerrero, and F. Blaabjerg, "A review of the state of the art of power electronics for wind turbines," *Power Electronics, IEEE Transactions on*, vol. 24, no. 8, pp. 1859 –1875, aug. 2009.

[15] Y. Tamai, Y. Abe, A. Odaka, I. Sato, and A. Sakuma, "A high performance 1 mva matrix converter suitable for wind power systems," in *Proc of. China wind power conference. Beijing*, Oct 2009.

[16] E. P. Cha, H.J., "A three-phase ac/ac high-frequency link matrix converter for vscf applications," in *Proc. of Power Electronics Specialist Conference, 2003. PESC '03. 2003 IEEE 34th Annual*, vol. 4, June 2003, pp. 1971 – 1976 vol.4.

[17] T. N. Yamato, I., "Power loss reduction techniques for three phase high frequency link dc-ac converter," in *Power Electronics Specialists Conference, 1993. PESC '93 Record., 24th Annual IEEE*, Jun 1993, pp. 663 –668.

[18] P. Drabek, Z. Peroutka, M. Pittermann, and M. Cedl, "New configuration of traction converter with medium-frequency transformer using matrix converters," *Industrial Electronics, IEEE Transactions on*, vol. 58, no. 11, pp. 5041 –5048, nov. 2011.

[19] S. Meier, "Novel voltage source converter based hvdc transmission system for off-shore wind farms," Master thesis, KTH Royal Institute of Technology, 2005.

[20] J. Wang, B. Wu, D. Xu, and N. Zargari, "Multi-modular matrix converters with sinusoidal input and output waveforms," *IEEE Trans. Industrial Electronics*, vol. PP, no. 99, p. 1, 2011.

[21] M. Kazerani, "A direct ac/ac converter based on current-source converter modules," in *Power Electronics Specialists Conference, 2001. PESC. 2001 IEEE 32nd Annual*, vol. 2, 2001, pp. 1115 –1121 vol.2.

[22] R. Cardenas, R. Pena, P. Wheeler, and J. Clare, "Experimental validation of a space-vector-modulation algorithm for four-leg matrix converters," *IEEE Trans. Industrial Electronics*, vol. 58, no. 4, pp. 1282 –1293, 2011.

[23] S. Ahmed, A. Iqbal, H. Abu-Rub, J. Rodriguez, C. Rojas, and M. Saleh, "Simple carrier-based pwm technique for a three-to-nine-phase direct ac/ac converter," *Industrial Electronics, IEEE Transactions on*, vol. 58, no. 11, pp. 5014 –5023, nov. 2011.

[24] J. Kang, E. Yamamoto, M. Ikeda, and E. Watanabe, "Medium-voltage matrix converter design using cascaded single-phase power cell modules," *Industrial Electronics, IEEE Transactions on*, vol. 58, no. 11, pp. 5007 –5013, nov. 2011.

[25] P. Wheeler, X. Lie, M. Y. Lee, L. Empringham, C. Klumpner, and J. Clare, "A review of multi-level matrix converter topologies," in *Power Electronics, Machines and Drives, 2008. PEMD 2008. 4th IET Conference on*, april 2008, pp. 286 –290.

[26] S. A. R. Erickson and K. Almazeedi, "A new family of multilevel matrix converters for wind power applications: Final report," NREL National renewable energy laboratory US., Tech. Rep., 2006.

[27] M. Y. Lee, P. Wheeler, and C. Klumpner, "Space-vector modulated multilevel matrix converter," *IEEE Trans. Industrial Electronics*, vol. 57, no. 10, pp. 3385 –3394, 2010.

[28] Y. Shi, X. Yang, Q. He, and Z. Wang, "Research on a novel capacitor clamped multilevel matrix converter," *IEEE Trans. Power Electronics*, vol. 20, no. 5, pp. 1055 – 1065, sept. 2005.

[29] M. Y. Lee, P. Wheeler, and C. Klumpner, "Space-vector modulated multilevel matrix converter," *IEEE Trans. Industrial Electronics*, vol. 57, no. 10, pp. 3385 –3394, oct. 2010.

[30] S. Muyeen, R. Takahashi, and J. Tamura, "Operation and control of hvdc-connected offshore wind farm," *IEEE Trans. Sustainable Energy*, vol. 1, no. 1, pp. 30 –37, april 2010.

[31] M. Popat, B. Wu, and N. Zargari, "A novel decoupled interconnecting method for current source converter based offshore wind farms," in *Electric Machines Drives Conference (IEMDC), 2011 IEEE International*, may 2011, pp. 711 –716.

[32] A. Garces and M. Molinas, "Coordinated control of series-connected offshore wind park based on matrix converters," *Wind Energy*, pp. n/a–n/a, 2011. [Online]. Available: http://dx.doi.org/10.1002/we.507

[33] ——, "A study of efficiency in a reduced matrix converter for offshore wind farms," *IEEE Transactions on Industrial Electronics*, vol. 59, no. 1, 2012.

[34] ——, "Optimal control for pwm-csc based hvdc with series connected offshore wind turbines," *submitted to IEEE Transactions on Industrial Electronics*.

[35] ——, "Optimal operation of series connected turbines for offshore wind parks," in *IEEE 12th conference on probabilistic methods applied to power systems PMAPS*, Turkey, 2012.

[36] ——, "A generalized compensation theory for active filters based on mathematical optimization in abc frame," *submitted to Power Systems Research*, vol. 90, 2012.

[37] ——, "Electrical conversion system for offshore wind turbines based on high frequency ac link," in *Proc of IX International Conference and Exhibition of Renewal Energy and Ecological Vehicles EVER2009*, March 2009.

[38] A. Mogstad and M. Molinas, "Power collection and integration on the electric grid from offshore wind parks," in *Proc. Nordic Workshop on Power and Industrial Electronics*, 2008.

[39] A. Garces and M. Molinas, "Cluster interconnection of offshore wind farms using a direct high frequency link," in *Proc of 8th International Workshop on Large-Scale Integration of Wind Power into Power Systems as well as on Transmission Networks for Offshore Wind Farms*, October 2009.

[40] ——, "Comparative investigation of losses in a reduced matrix converter for off-shore wind turbines," in *Proc. of 5th IET International Conference on Power Electronics, Machines and Drives, PEMD*, April 2010.

[41] ——, "Reduced matrix converter operated as current source converter for offshore wind farms," in *Proc of 14th International Power Electronics and Motion Control Conference PEDM 2010*, Sep 2010.

[42] ——, "Impact of operation principle on the losses of a reduced matrix converter for offshore wind parks," in *Proc of IEEE International symposium on industrial electronics ISIE 2010*, July 2010.

[43] M. Roed, A. Garces, and M. Molinas, "Operation features of a reduced matrix converter for offshore wind power'," in *Proc. of IEEE International Symposium on Industrial Electronics ISIE 2010*, 2010.

[44] A. Garces and M. Molinas, "High frequency wind energy conversion from the ocean," in *Proc of IEEE International power electronics conference ECCE ASIE IPEC 2010*, June 2010.

[45] ——, "Optimal control of a reduced matrix converter for offshore wind parks'," in *Proc. of Powertech 2011*, 2011.

[46] E. Carpaneto, G. Chicco, P. Mancarella, and A. Russo, "Cogeneration planning under uncertainty: Part i: Multiple time frame approach," *Applied Energy*, vol. 88, no. 4, pp. 1059 – 1067, 2011. [Online]. Available: http://www.sciencedirect.com/science/article/pii/S0306261910004162

[47] A. Garces and M. Molinas, "A flexible and optimal power theory for reactive power compensation in abc frame," in *Power Tech 2011. Trondheim Norway*, 2011.

[48] A. Garces, E. Tedeschi, G. Verez, and M. Molinas, "Power collection array for improved wave farm output based on reduced matrix converters," in *Control and Modeling for Power Electronics (COMPEL), 2010 IEEE 12th Workshop on*, june 2010, pp. 1 –6.

[49] A. Garces and A. Trejos, "A voltage regulator based on matrix converter for smart grid applications," in *2011 IEEE PES Coference on innovative smart grid technologies Latin America.* IEEE, 2011.

[50] S. Sanchez, A. Garces, M. Molinas, and T. Underland, "A current-coupled topology for grid integration of wind turbines in micro-grids," in *Accepted in IEEE Power and Energy Society Transmission and Distribution Conference and Exposition, Orlando-Florida USA*, oct. 2012, pp. 1 –6.

[51] A. Garces and M. Molinas, "A control strategy for series connected offshore wind turbines," in *Proc. of 9th IEEE International Conference on Power Electronics and Drives Systems*, 2011.

[52] R. Torres, A. Garces, M. Molinas, and T. Underland, "Hybrid hvdc based on pwm current-sourced converter and line-commutated converter for offshore wind farm integration," in *Accepted in IEEE Asia-Pacific Power and Energy Engineering Conference APPEEC2012, Changai China*, oct. 2012, pp. 1 –6.

[53] B. Snyder and M. J. Kaiser, "Ecological and economic cost-benefit analysis of offshore wind energy," *Renewable Energy*, vol. 34, no. 6, pp. 1567 – 1578, 2009.

[54] J. B. S Pryor, "Comparison of potential power production at on- and offshore sites," *Wind Energy*, vol. 4, no. 4, pp. 173–181, dec. 2002.

[55] T. W. power database, "List of offshore wind farms," Nov 2010. [Online]. Available: http://www.thewindpower.net/offshore_wind_farms_list.php

[56] H.-J. Lee and S.-K. Sul, "Wind power collection and transmission with series connected current source converters," in *Proc. of EPE Wind Chapter Trodheim*, 2011.

[57] D. Jovcic, "Offshore wind farm with a series multiterminal csi hvdc," *Electric Power Systems Research*, vol. 78, no. 4, pp. 747 – 755, 2008.

[58] P. L. E. Veilleux, "Interconnection of direct-drive wind turbines using dc grid," in *proc of. 8th International Workshop on Large-Scale Integration of Wind Power into Power Systems as well as on Transmission Networks for Offshore Wind Farms*, Bremen, Germany, Oct 2009.

[59] E. Veilleux and P. Lehn, "Interconnection of direct-drive wind turbines using a distributed hvdc converter station," in *Industrial Electronics, 2009. IECON '09. 35th Annual Conference of IEEE*, nov. 2009, pp. 584 –589.

[60] L. Heinemann, "An actively cooled high power, high frequency transformer with high insulation capability," *Applied Power Electronics Conference and Exposition, 2002. APEC 2002. Seventeenth Annual IEEE*, vol. 1, pp. 352–357 vol.1, 2002.

[61] W.-J. Gu and R. Liu, "A study of volume and weight vs. frequency for high-frequency transformers," *Power Electronics Specialists Conference, 1993. PESC '93 Record., 24th Annual IEEE*, vol. 1, pp. 1123–1129, Jun 1993.

[62] W. Shen, F. Wang, D. Boroyevich, and C. Tipton, "High-density nanocrys-talline core transformer for high-power high-frequency resonant converter," *IEEE Trans. Industry Applications*, vol. 44, no. 1, pp. 213–222, Jan.-feb. 2008.

[63] ——, "Loss characterization and calculation of nanocrystalline cores for high-frequency magnetics applications," *IEEE Trans. Power Electronics*, vol. 23, no. 1, pp. 475–484, Jan. 2008.

[64] M. Kheraluwala, D. Novotny, and D. Divan, "Coaxially wound transformers for high-power high-frequency applications," *IEEE Trans. Power Electronics*, vol. 7, no. 1, pp. 54–62, Jan 1992.

[65] W. Reass, D. Baca, R. Gribble, D. Anderson, J. Przybyla, R. Richard-son, J. Clare, M. Bland, and P. Wheeler, "High-frequency multimegawatt polyphase resonant power conditioning," *IEEE Trans. Plasma Science*, vol. 33, no. 4, pp. 1210 – 1219, 2005.

[66] X. Jing, "Single-phase vs. three-phase high power high frequency transform-ers," Master thesis, Virginia Polytechnic Institute and State University, Vir-ginia, USA, 2010.

[67] W. Hurley, W. Wolfle, and J. Breslin, "Optimized transformer design: inclusive of high-frequency effects," *IEEE Trans. Power Electronics*, vol. 13, no. 4, pp. 651–659, Jul 1998.

[68] S. Wei, "Design of high-density transformers for high-frequency high-power converters," PhD. thesis, Virginia Polytechnic Institute and State University, Virginia USA, 2006.

[69] C. Bhende, S. Mishra, and S. Malla, "Permanent magnet synchronous generator-based standalone wind energy supply system," *IEEE Trans. Sustain-able Energy*, vol. 2, no. 4, pp. 361 –373, oct. 2011.

[70] A. Perdana, "Dynamic models of wind turbines: a contribution towards the establishment of standardized models of wind turbines for power system sta-bility studies," Ph.D. dissertation, Chalmers University of Technology, Gote-borg, Sweden, 2008.

[71] J. Slootweg, S. de Haan, H. Polinder, and W. Kling, "General model for rep-resenting variable speed wind turbines in power system dynamics simula-tions," *IEEE Trans. Power Systems*, vol. 18, no. 1, pp. 144–151, Feb 2003.

[72] J. Cotrell, "Preliminary evaluation of a multiple-generator drive-train config-uration for wind turbines," in *Proc. of 21st American Society of Mechanical Engi-neers (ASME) Wind Energy Symposium*, 2002.

[73] A. Mikhail, *Distributed generation drivetrain for high torque wind turbine applica-tions (Final project report)*. California Energy Commission and Clipper Wind-power Technology Inc, 2011.

[74] T. Kanemoto and A. Galal, "Development of intelligent wind turbine genera-tor with tandem wind rotors and double rotational armatures," *JSME Interna-tional Journal Series B Fluids and Thermal Engineering*, vol. 49, no. 2, pp. 450–457, 2006.

[75] F. Deng and Z. Chen, "Variable speed wind turbine based on multiple genera-tors drive-train configuration," in *Innovative Smart Grid Technologies Conference Europe (ISGT Europe), 2010 IEEE PES*, oct. 2010, pp. 1 –8.

[76] N. Stretch, M. Kazerani, and R. El Shatshat, "A current-sourced converter-based hvdc light transmission system," in *Industrial Electronics, 2006 IEEE In-ternational Symposium on*, vol. 3, july 2006, pp. 2001 –2006.

[77] J. Espinoza and G. Joos, "A current-source-inverter-fed induction motor drive system with reduced losses," *IEEE Trans. Industry Applications*, vol. 34, no. 4, pp. 796–805, Jul/Aug 1998.

[78] H. Bilgin and M. Ermis and, "Design and implementation of a current-source converter for use in industry applications of d-statcom," *IEEE Trans. Power Electronics*, vol. 25, no. 8, pp. 1943 –1957, aug. 2010.

[79] M. Bierhoff and F. Fuchs, "Loss minimized pulse width modulation of igbt current source converters," in *IEEE Industrial Electronics, IECON 2006 - 32nd Annual Conference on*, nov. 2006, pp. 1739 –1744.

[80] Y. W. Li, B. Wu, D. Xu, and N. Zargari, "Space vector sequence investigation and synchronization methods for pwm modulation of a high power current source rectifier," in *Power Electronics Specialists Conference, 2007. PESC 2007. IEEE*, june 2007, pp. 2841 –2847.

[81] H. Bilgin and M. Ermis, "Current source converter based statcom: Operat-ing principles, design and field performance," *Electric Power Systems Research*, vol. 81, no. 2, pp. 478 – 487, 2011.

[82] K. Nielsen and M. Molinas, "Superconducting magnetic energy storage (smes) in power systems with renewable energy sources," in *Industrial Elec-tronics (ISIE), 2010 IEEE International Symposium on*, july 2010, pp. 2487 –2492.

[83] J.-M. Meyer and A. Rufer, "A dc hybrid circuit breaker with ultra-fast con-tact opening and integrated gate-commutated thyristors (igcts)," *IEEE Trans. Power Delivery*, vol. 21, no. 2, pp. 646 – 651, april 2006.

[84] C. Franck, "Hvdc circuit breakers: A review identifying future research needs," *IEEE Trans. Power Delivery*, vol. 26, no. 2, pp. 998 –1007, april 2011.

[85] J. Mahlein, M. Bruckmann, and M. Braun, "Passive protection strategy for a drive system with a matrix converter and an induction machine," *IEEE Trans. Industrial Electronics*, vol. 49, no. 2, pp. 297 –303, apr 2002.

[86] K. You and F. Rahman, "Over voltage protection using power zener diode for matrix converter and matrix z source converter," *Proc of Power Electronics and Drive Systems, 2009. PEDS 2009. International Conference on*, vol. 1, pp. 193 –197, jan 2009.

[87] J. ichi Itoh, I. Sato, A. Odaka, H. Ohguchi, H. Kodachi, and N. Eguchi, "A novel approach to practical matrix converter motor drive system with reverse blocking igbt," *IEEE Trans. Power Electronics*, vol. 20, no. 6, pp. 1356 – 1363, nov. 2005.

[88] S. Lundberg, "Wind farm configuration and energy efficiency studies - series dc versus ac layouts," Lic. of Eng. thesis, Chalmers University of technology, Goteborg, Sweden, 2006.

[89] A. B. Mogstad and M. Molinas, "Power collection and integration on the electric grid from offshore wind parks," in *Proc. of the Nordic Workshop on Power and Industrial Electronics*, Finland, Jun 2008.

[90] P. Wheeler, J. Rodriguez, J. Clare, L. Empringham, and A. Weinstein, "Matrix converters: a technology review," *IEEE Trans. Industrial Electronics*, vol. 49, no. 2, pp. 276–288, Apr 2002.

[91] J. Itoh, T. Iida, and A. Odaka, "Realization of high efficiency ac link converter system based on ac/ac direct conversion techniques with rb-igbt," in *Proc. of IEEE Industrial Electronics, IECON 2006 - 32nd Annual Conference*, Nov. 2006, pp. 1703–1708.

[92] M. Bland, P. Wheeler, J. Clare, and L. Empringham, "Comparison of bi-directional switch components for direct ac-ac converters," *Power Electronics Specialists Conference, 2004. PESC 04. 2004 IEEE 35th Annual*, vol. 4, pp. 2905–2909 Vol.4, 2004.

[93] J. Kolar, T. Friedli, J. Rodriguez, and P. Wheeler, "Review of three-phase pwm ac-ac converter topologies," *Industrial Electronics, IEEE Transactions on*, vol. 58, no. 11, pp. 4988 –5006, nov. 2011.

[94] R. Gupta, K. Mohapatra, A. Somani, and N. Mohan, "Direct-matrix-converter-based drive for a three-phase open-end-winding ac machine with advanced features," *IEEE Trans. Industrial Electronics*, vol. 57, no. 12, pp. 4032 –4042, 2010.

[95] S. Lopez Arevalo, P. Zanchetta, P. Wheeler, A. Trentin, and L. Empringham, "Control and implementation of a matrix-converter-based ac ground power-supply unit for aircraft servicing," *IEEE Trans. Industrial Electronics*, vol. 57, no. 6, pp. 2076 –2084, jun. 2010.

[96] R. Bucknall and K. Ciaramella, "On the conceptual design and performance of a matrix converter for marine electric propulsion," *IEEE Trans. Power Electronics*, vol. 25, no. 6, pp. 1497 –1508, jun. 2010.

[97] J. Monteiro, J. Silva, S. Pinto, and J. Palma, "Matrix converter-based unified power-flow controllers: Advanced direct power control method," *IEEE Trans. Power Delivery*, vol. 26, no. 1, pp. 420 –430, jan. 2011.

[98] R. Cardenas, R. Pena, P. Wheeler, J. Clare, and G. Asher, "Control of the reactive power supplied by a wecs based on an induction generator fed by a matrix converter," *IEEE Trans. Industrial Electronics*, vol. 56, no. 2, pp. 429–438, Feb. 2009.

[99] N. Holtsmark and M. Molinas, "Reactive power compensation using an indirectly space vector-modulated matrix converter," in *Industrial Electronics (ISIE), 2010 IEEE International Symposium on*, july 2010, pp. 2455 –2460.

[100] P. C. Loh, F. Blaabjerg, F. Gao, A. Baby, and D. Tan, "Pulsewidth modulation of neutral-point-clamped indirect matrix converter," *IEEE Trans. Industry Applications*, vol. 44, no. 6, pp. 1805 –1814, nov.-dec. 2008.

[101] P. Correa, J. Rodriguez, M. Rivera, J. Espinoza, and J. Kolar, "Predictive control of an indirect matrix converter," *IEEE Trans. Industrial Electronics*, vol. 56, no. 6, pp. 1847 –1853, june 2009.

[102] R. Garcia-Gil, J. Espi, E. Dede, and E. Sanchis-Kilders, "A bidirectional and isolated three-phase rectifier with soft-switching operation," *IEEE Trans. Industrial Electronics*, vol. 52, no. 3, pp. 765–773, June 2005.

[103] C. Klumpner and F. Blaabjerg, "Using reverse blocking igbts in power converters for adjustable speed drives," *IEEE Trans. Industry Applications*, vol. 42, no. 3, pp. 807–816, 2006.

[104] P. Steimer, O. Apeldoorn, B. Odegard, S. Bernet, and T. Bruckner, "Very high power igct pebb technology," in *Power Electronics Specialists Conference, 2005. PESC '05. IEEE 36th*, june 2005, pp. 1 –7.

[105] Y. Suh, J. Steinke, and P. Steimer, "Efficiency comparison of voltage-source and current-source drive systems for medium-voltage applications," *IEEE Trans. Industrial Electronics*, vol. 54, no. 5, pp. 2521 –2531, oct. 2007.

[106] Y. Suh and P. Steimer, "Application of igct in high-power rectifiers," *IEEE Trans. Industry Applications*, vol. 45, no. 5, pp. 1628 –1636, sept.-oct. 2009.

[107] A. Trentin, P. Zanchetta, P. Wheeler, and J. Clare, "Automated optimal design of input filters for direct ac/ac matrix converters," *IEEE Trans. Industrial Electronics*, vol. PP, no. 99, p. 1, 2011.

[108] A. Odaka, J. Itoh, I. Sato, H. Ohguchi, H. Kodachi, N. Eguchi, and H. Umida, "Analysis of loss and junction temperature in power semiconductors of the matrix converter using simple simulation methods," in *Industry Applications Conference, 2004. 39th IAS Annual Meeting. Conference Record of the 2004 IEEE*, vol. 2, Oct. 2004, pp. 850–855 vol.2.

147

[109] D. Xu, H. Lu, L. Huang, S. Azuma, M. Kimata, and R. Uchida, "Power loss and junction temperature analysis of power semiconductor devices," *IEEE Trans. Industry Applications*, vol. 38, no. 5, pp. 1426–1431, Sep/Oct 2002.

[110] R. Stengel, *Optimal control and estimation*. Dover publications, 1994.

[111] D. E. Kirk, *Optimal control theory: an introduction*. Dover publications, 1998.

[112] B. Anderson and J. More, *Linear Optimal Control*. Prentice Hall, 1971.

[113] B. Wu, *High-Power Converters and AC drives*, J. W. . Sons., Ed. IEEE PRESS, 2006.

[114] K. Astergaard, P. Brath, and J. Stoustrup, "Estimation of effective wind speed," *Journal of Physics: Conf. Series*, vol. 75, no. 1, p. 012082, 2007.

[115] A. Peña, C. Hasager, S. Gryning, M. Courtney, A. Ioannis, and T. Mikkelsen, "Offshore wind profiling using light detection and ranging measurements," *Wind Energy*, vol. 12, no. 2, pp. 105–124, Sep. 2008.

[116] C. Hasager, A. Peña, T. Mikkelsen, M. Courtney, I. Antoniou, S.-E. Gryning, P. Hansen, and P. B. Srensen, *12MW Horns Rev Experiment*. Riso National Laboratory, 2007.

[117] H. Akagi, Y. Kanazawa, and A. Nabae, "Instantaneous reactive power compensators comprising switching devices without energy storage components," *IEEE Trans. Industry Applications*, vol. IA-20, no. 3, pp. 625 –630, may 1984.

[118] R. S. Herrera and P. Salmeron, "Instantaneous reactive power theory: A comparative evaluation of different formulations," *IEEE Trans. Power Delivery*, vol. 22, no. 1, pp. 595 –604, jan. 2007.

[119] H. Kim, F. Blaabjerg, B. Bak-Jensen, and J. Choi, "Instantaneous power compensation in three-phase systems by using p-q-r theory," *IEEE Trans. Power Electronics*, vol. 17, no. 5, pp. 701 – 710, sep 2002.

[120] F. Z. Peng and J.-S. Lai, "Generalized instantaneous reactive power theory for three-phase power systems," *IEEE Trans. Instrumentation and Measurement*, vol. 45, no. 1, pp. 293 –297, feb 1996.

[121] F. Z. Peng, J. Ott, G.W., and D. Adams, "Harmonic and reactive power compensation based on the generalized instantaneous reactive power theory for three-phase four-wire systems," *IEEE Trans. Power Electronics*, vol. 13, no. 6, pp. 1174 –1181, Nov. 1998.

[122] H. Akagi, E. H. Watanabe, and M. Aredes, *Instantaneous Power Theory and Applications to power Conditioning*. IEEE Press, 2007.

[123] L. S. Czarnecki, "Budeanu and fryze: Two frameworks for interpreting power properties of circuits with nonsinusoidal voltages and currents," *Electrical Engineering (Archiv fur Elektrotechnik)*, vol. 80, no. 6, pp. 359–367, dic 1997.

[124] W. Kersting, "Radial distribution test feeders," in *IEEE Power Engineering Society Winter Meeting, 2001*, vol. 2, 2001, pp. 908 –912 vol.2.

[125] M. Depenbrock, "The fbd-method, a generally applicable tool for analyzing power relations," *IEEE Trans. Power Systems*, vol. 8, no. 2, pp. 381 –387, may 1993.

[126] P. Anderson and A. Bose, "Stability simulation of wind turbine systems," *IEEE Trans. Power Apparatus and Systems*, vol. PAS-102, no. 12, pp. 3791 –3795, dec. 1983.

[127] M. Shinozuka and C. M. Jan, "Digital simulation of random processes and its applications," *Journal of Sound and Vibration*, vol. 25, no. 1, pp. 111 – 128, 1972.

[128] T. P. Chang, "Wind energy assessment incorporating particle swarm optimization method," *Energy Conversion and Management*, vol. 52, no. 3, pp. 1630 – 1637, 2011. [Online]. Available: http://www.sciencedirect.com/science/article/pii/S0196890410004735